UNIVERSIDADE FEDERAL DE PERNAMBUCO
CENTRO DE TECNOLOGIA E GEOCIÊNCIAS
DEPARTAMENTO DE GEOLOGIA
PROGRAMA DE PÓS-GRADUAÇÃO EM GEOCIÊNCIAS

MÁRCIO LIMA ALENCAR

MODELAGEM DE REDE DE FRATURAS E ANÁLISE ESTRUTURAL DE SISMITOS DOS CALCÁRIOS LAMINADOS DA FORMAÇÃO CRATO, BACIA DO ARARIPE, NE BRASIL

Recife
2023

MÁRCIO LIMA ALENCAR

MODELAGEM DE REDE DE FRATURAS E ANÁLISE ESTRUTURAL DE SISMITOS DOS CALCÁRIOS LAMINADOS DA FORMAÇÃO CRATO, BACIA DO ARARIPE, NE BRASIL

Tese apresentada ao Programa de Pós-Graduação em Geociências da Universidade Federal de Pernambuco como parte dos requisitos para obtenção do título de Doutor em Geociências.

Área de Concentração: Geologia Sedimentar e Ambiental

Orientador: Profº. Dr. Tiago Siqueira de Miranda.
Coorientador: Profº. Dr. José Antonio Barbosa.
Coorientador: Profº Dr. Igor Fernandes Gomes

Recife
2023

Catalogação na fonte:

Bibliotecário Carlos Moura, CRB-4/1502

A368m Alencar, Márcio Lima.

Modelagem de rede de fraturas e análise estrutural de sismitos dos calcários laminados da Formação Crato, Bacia do Araripe, NE Brasil. / Márcio Lima Alencar. – 2023.

149 f.: il.

Orientador: Prof. Dr. Tiago Siqueira de Miranda.

Coorientador: Prof. Dr. José Antonio Barbosa.

Coorientador: Prof. Dr. Igor Fernandes Gomes.

Tese (doutorado) – Universidade Federal de Pernambuco. CTG. Programa de Pós-Graduação em Geociências. Recife, 2023.

Inclui referências.

1. Geociências. 2. Sismitos. 3. Fraturas verticais. 4. Laminitos. 5. DFN. 6. Permeabilidade equivalente. 7. Porosidade de fratura. 8. Pseudopoços. I. Miranda, Tiago Siqueira de (orientador). II. Barbosa, José Antonio (coorientador). III. Gomes, Igor Fernandes (coorientador). IV. Título.

UFPE

551 CDD (22. ed.) BCTG/2024-10

MÁRCIO LIMA ALENCAR

MODELAGEM DE REDE DE FRATURAS E ANÁLISE ESTRUTURAL DE SISMITOS DOS CALCÁRIOS LAMINADOS DA FORMAÇÃO CRATO, BACIA DO ARARIPE, NE BRASIL

Tese apresentada ao Programa Pós-Graduação em Geociências do Centro de Tecnologia e Geociências da Universidade Federal de Pernambuco como parte dos requisitos para obtenção do título de Doutor em Geociências. Área de Concentração: Geologia Sedimentar e Ambiental

Aprovado em 05 de Setembro de 2023

BANCA EXAMINADORA

Participação por videoconferência
Profº. Drº. Virgínio Henrique de Miranda Lopes Neumann (Examinador Interno)
Universidade Federal de Pernambuco

Participação por videoconferência
Profª. Drª. Debora Cristina Almeida Assis (Examinador externo)
Universidade Federal de Pernambuco

Participação por videoconferência
Profº. Drº. Gorki Mariano (Examinador Interno)
Universidade Federal de Pernambuco

Participação por videoconferência
Profº. Drº. Francisco Manoel Wohnrath Tognoli (Examinador Externo)
Universidade Federal do Rio de Janeiro

Participação por videoconferência
Profº. Drº. José Ricardo Gonçalves Magalhães (Examinador Externo)
Universidade Federal do Recôncavo da Bahia

AGRADECIMENTOS

Primeiramente, eu quero agradecer aos meus pais, José e Margarida, por acreditarem em mim, pelo apoio incondicional que sempre me deram nas decisões difíceis e nas horas de desânimo.

Gostaria de agradecer igualmente ao meu filho Gabriel. Tão pequeno e responsável por grandes mudanças no meu universo.

Gostaria de agradecer aos meus irmãos, Natália e Marcelo, com os quais fortaleci nossos elos familiares ao longo desses anos de trabalho.

Agradeço aos Professores Tiago e Antonio pela paciência e zelo durante sua orientação.

Um agradecimento especial aos colegas que fazem parte da minha rotina do dia a dia: Osvaldo, Alcione, Elídio e Daniel. O que seria dos meus dias na UFPE sem a contribuição de cada um desses camaradas?

Agradeço também à PETROBRAS pelo financiamento deste trabalho por meio de um projeto de cooperação em P&D FADE/UFPE/PETROBRAS.

“Ser resiliente é acreditar em si mesmo.” (Autor Desconhecido)

RESUMO

Modelos discretos de fratura (MDF) representam uma ferramenta chave na caracterização de reservatórios fraturados. Sistemas de fraturas possuem um importante papel na distribuição de permeabilidade e porosidade secundárias de reservatórios carbonáticos que normalmente apresentam baixa permeabilidade. Este trabalho investiga a distribuição espacial de heterogeneidades geológicas (estruturas rúpteis e sedimentares) nos calcários laminados, lacustres, de idade Aptiana da Formação Crato, Bacia do Araripe, NE Brasil. Essas rochas possuem a mesma idade e características sedimentológicas/geomecânicas dos reservatórios carbonáticos do intervalo pré-sal das bacias sedimentares da margem sudeste brasileira. Portanto, a Formação Crato é considerada como uma unidade litoestratigráfica chave para estudar, em escala subsísmica, a geologia de reservatórios carbonáticos naturalmente fraturados. Este trabalho tem como objetivo principal modelar a variação da rede permoporosa de laminitos de baixa permeabilidade considerando a segmentação vertical de fraturas em diferentes escalas. Além disso, este trabalho teve como foco a análise estrutural dos sismitos e dos laminitos da Formação Crato e sua relação com reativações tectônicas de estruturas dúcteis. Para observar o efeito de escala, foram elaborados modelos tridimensionais de fraturas (DFNs) em duas escalas: reservatório (1:15.000) e afloramento (1:1). Os DFNs foram construídos a partir de técnicas tradicionais de aquisição de dados (scanlines, resistência mecânica, modelos digitais de afloramento) e pseudopoços. As estruturas sin-deposicionais foram formadas por abalos sísmicos de magnitudes maiores que 6. Esses terremotos estão possivelmente relacionados com a deformação rúptil da Zona de Cisalhamento Patos. A modelagem de fraturas mostrou que a permeabilidade equivalente das fraturas horizontais apresentou valores semelhantes em ambas as escalas para as direções Kxx e Kyy. A permeabilidade equivalente das fraturas verticais (Kzz) mostrou que estas estruturas desempenham um papel importante no fluxo de fluido. Os resultados deste trabalho contribuem para a parametrização de modelos discretos de fratura relacionados a reservatórios carbonáticos de baixa permeabilidade.

Palavras-chave: sismitos; fraturas verticais; laminitos; DFN; permeabilidade equivalente; porosidade de fratura; pseudopoços

ABSTRACT

Discrete fracture models (DFMs) serve as a key tool in characterizing fractured reservoirs. Fracture systems play a role in the distribution of permeability and secondary porosity in carbonate reservoirs, which typically exhibit low permeability. This study investigates the spatial distribution of geological heterogeneities (brittle and sedimentary structures) in laminated lacustrine limestones of Aptian age from the Crato Formation, Araripe Basin, NE Brazil. These rocks share the same age and sedimentological/geomechanical characteristics as the carbonate reservoirs in the pre-salt interval of sedimentary basins on the southeastern Brazilian margin. Thus, the Crato Formation is considered a key lithostratigraphic unit for studying, on a subsismic scale, the geology of naturally fractured carbonate reservoirs. The main objective of this study is to model the variation in the permoporosity network of low-permeability laminites considering the vertical segmentation of fractures at different scales. Additionally, the focus of this work was on the structural analysis of seismite and laminites in the Crato Formation and their relation to tectonic reactivations of ductile structures. To observe the scale effect, three-dimensional fracture models (DFNs) were developed at two scales: reservoir (1:15,000) and outcrop (1:1). DFNs were built using traditional data acquisition techniques (scanlines, mechanical resistance, digital outcrop models) and pseudo-wells. Sin-depositional structures were formed by seismic events with magnitudes greater than 6. These earthquakes are possibly related to the brittle deformation of the Patos Shear Zone. Fracture modeling showed that the equivalent permeability of horizontal fractures exhibited similar values at both scales for the Kxx and Kyy directions. The equivalent permeability of vertical fractures (Kzz) demonstrated that these structures play a significant role in fluid flow. The results of this study contribute to the parameterization of discrete fracture models related to low-permeability carbonate reservoirs.

Keywords: seismite; vertical fractures; laminites; DFN; equivalent permeability; fracture porosity; pseudowells.

SUMÁRIO

1 INTRODUÇÃO

Esta Tese apresenta e discute os resultados obtidos durante a realização da pesquisa de Doutorado de Márcio Lima Alencar, desenvolvida sob a orientação do professor Tiago Siqueira de Miranda e co-orientação dos professores José Antonio Barbosa e Igor Gomes. Este documento é item fundamental para o atendimento dos requisitos necessários para a obtenção do Título de Doutor em Geociências pelo Programa de Pós-graduação em Geociências da Universidade Federal de Pernambuco (UFPE).

A presente pesquisa obteve suporte financeiro e logístico de dois projetos de pesquisa intitulados: a) Análise Comparativa entre Modelos Geológicos de Sistemas Fraturados (Calcários Laminados), executado com base nos Métodos de Levantamento de Pseudopoços e de Varredura de Superfícies em Afloramentos Análogos - “Projeto Pseudopoços”, coordenado pelo Professor José Antonio Barbosa; e b) Caracterização estrutural e modelagem numérica de zonas de falha, coordenado pelo Professor Tiago Siqueira de Miranda. Ambos os projetos foram financiados pela Petrobras em cooperação com a Fundação de Apoio ao Desenvolvimento da UFPE. Vale destacar que o projeto a já foi encerrado enquanto que o projeto ainda b está em fase de execução

Este estudo envolveu uma investigação com o objetivo de avaliar a influência exercida pela segmentação de fraturas verticais sobre os parâmetros permoporosos em modelos discretos de fraturas pertencentes a reservatórios carbonáticos de permeabilidade baixa. Para além desse escopo, a pesquisa também envolveu uma análise das estruturas sin-sedimentares dos depósitos de calcários laminados no topo da Formação Crato, Bacia do Araripe (NEUMANN, 1999; ASSINE, 1994, 2007; ASSINE et al., 2014). O estudo foi executado através de pesquisa in loco, com observações e coleta de dados realizadas em exposições naturais de calcários laminados que se encontram em áreas de extração a céu aberto localizadas na região das cidades de Santana do Cariri e Nova Olinda, ambas localizadas no Estado do Ceará.

1.2 Objetivos

1.2.1 Objetivo Geral

Esta pesquisa tem como objetivo principal elaborar modelos geológicos 3D da rede de fraturas, a partir de dados de afloramentos, e analisar a porosidade e permeabilidade de fraturas considerando sua segmentação vertical em diferentes escalas. O estudo também se concentra em classificar as estruturas sin-sedimentares e a sua origem, procurando entender os mecanismos associados ao desenvolvimento das mesmas durante os efeitos rúpteis da fase pós-rifte na Formação Crato.

1.2.3 Objetivos Específicos

1. Descrever as estruturas sin-sedimentares dos laminitos da Formação Crato;
2. Interpretar as forças condutoras e os mecanismos de deformação atuantes no desenvolvimento das *Soft sediment deformation structures* (SSDS);
3. Interpretar a relação das SSDS com as reativações das estruturas do embasamento cristalino durante a fase pós-rifte da Bacia do Araripe;
4. Construir modelos geológicos tridimensionais da rede de fraturas (DFN), a partir da aquisição de dados de fraturas dos afloramentos de calcários laminados da Formação Crato.
5. Demonstrar por meio de análises quantitativas, com base na comparação dos modelos, a variação na distribuição da rede de fraturas e dos parâmetros hidrodinâmicos; e
6. Avaliar o efeito da segmentação das fraturas verticais na rede de fraturas em diferentes escalas.

1.3 Justificativa e Relevância

Nos últimos anos, as pesquisas voltadas para a exploração de óleo e gás em reservatórios carbonáticos naturalmente fraturados têm se intensificado

devido ao grande volume de hidrocarbonetos associado a este tipo de reservatório (e.g., bacias de Campos e Santos) (LAVENU et al., 2015; WENNBERG et al., 2016). O estudo proposto permitirá obter uma avaliação do efeito da segmentação das fraturas verticais para a construção de modelos geológicos de reservatórios fraturados em rochas calcárias. O estudo também mostra relevância por apresentar um conjunto de heterogeneidades sedimentares (SSDSs) responsáveis por variações nas propriedades petrofísicas, de fluxo de fluido e que também atuam como barreiras (NOVAK AND EGENHOFF, 2019; SHANMUGAM, 2016). Reservatórios formados por rochas carbonáticas abrigam cerca de 60% das reservas convencionais de petróleo e gás conhecidas (BURCHETTE, 2012; ELSHERIF et al., 2016, MAZZULLO, 2006). O estudo é focado nos calcários laminados da Formação Crato, que são depósitos carbonáticos considerados análogos aos carbonatos do intervalo pré-sal das Bacias de Santos e Campos, situados da margem sudeste do Brasil (CATTO *et al*., 2016; MIRANDA, 2015; SANTOS *et al.,* 2016; ZIHMS, 2017). Desta maneira, esta pesquisa se justifica pela potencialidade de contribuição ao tema e também pela possibilidade de fornecer informações que serão utilizadas para a construção de modelos análogos, tais como os reservatórios da Formação Barra Velha, na Bacia de Santos, localizados na margem sudeste do Brasil. A pesquisa também se destaca pelo seu potencial de contribuição com o armazenamento de CO_2 em rede de fraturas. Um tema que tem se tornado objeto de pesquisa nos últimos tempos (IDING & RINGROSE, 2010; MOTIE & ASSAREH, 2020; VALLE et al., 2020). Além disso, este trabalho apresenta relevância tanto acadêmica quanto econômica.

1.4 Localização da Área de Estudo

A área de estudo está situada na região do nordeste brasileiro, na microrregião do Cariri, entre os municípios de Santana do Cariri e Nova Olinda, ambos no estado do Ceará (Fig.1). Estes dois municípios estão localizados a uma distância de aproximadamente 540 km da cidade de Fortaleza, Capital do Ceará, e aproximadamente 650 km de Recife, Capital do estado de Pernambuco. Esta área foi escolhida para a realização do estudo devido à existência de

minerações a céu aberto onde ocorrem excelentes afloramentos, que chegam a atingir até 20 metros de altura e continuidade lateral de centenas de metros.

Figura 1 – Mapa de localização da Bacia do Araripe com destaque para a área de estudo (retângulo vermelho) localizada na borda norte desta bacia.

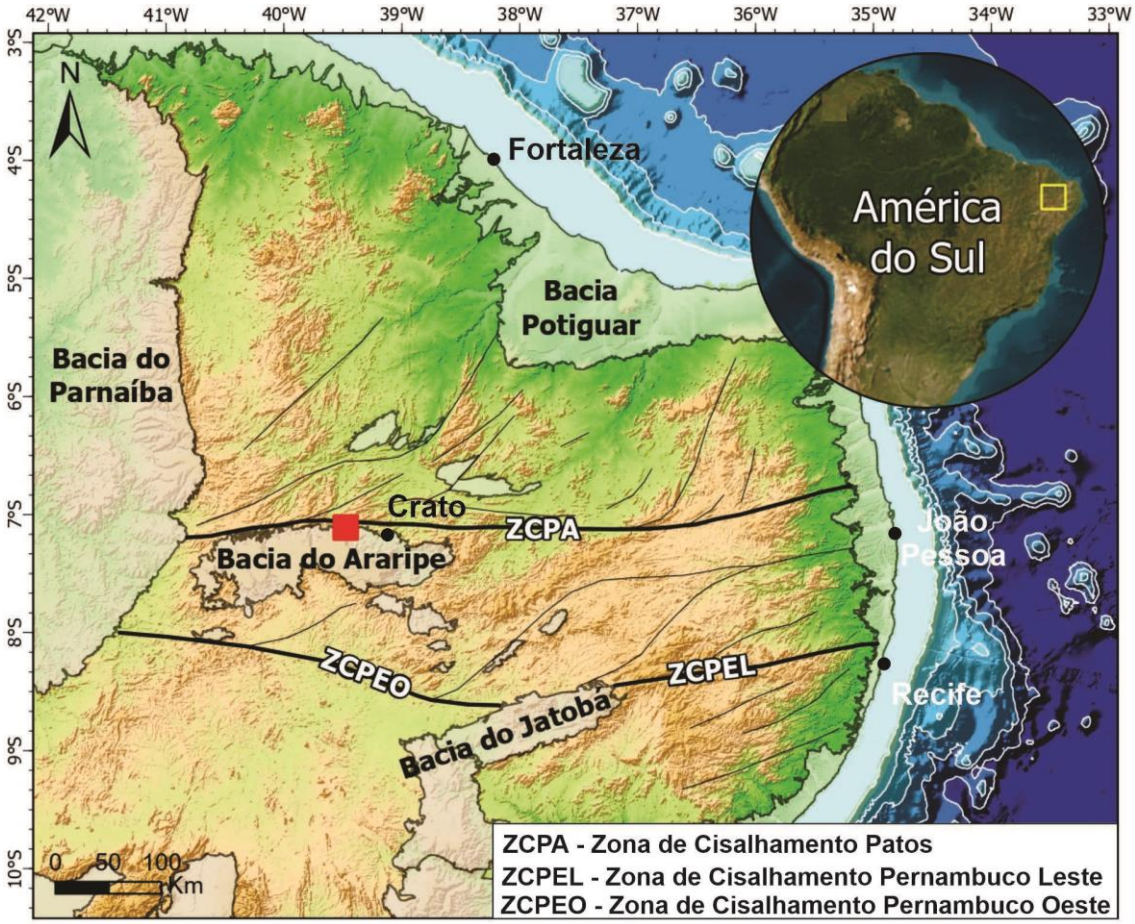

Fonte: O Autor (2023)

1.5 Estrutura da Tese

O presente estudo está organizado em cinco capítulos. O capítulo 1, chamado de introdução, é onde a pesquisa é apresentada e os detalhes dos objetivos da pesquisa são expostos. Também neste capítulo aborda-se a justificativa da escolha da área em estudo.

No capítulo 2, denominado de Revisão Bibliográfica do Contexto Geológico, é abordado os aspectos geológicos da Bacia da Bacia do Araripe com foco na Formação Crato, destacando-se características importantes e que contribuem com a pesquisa.

No capítulo 3, Materiais e Métodos, serão abordadas as técnicas utilizadas na abordagem do tema desta pesquisa.

No capítulo 4 são expostos os resultados da pesquisa, nos quais encontram-se expostos as produções cientificas submetidas as revistas. O item 4.1 corresponde ao artigo submetido para publicação na revista Journal of South American Earth Sciences: “Soft-sediment deformation structures in Aptian lacustrine laminites: Evidence of post-rift paleoseismicity in the Araripe basin, NE Brazil”. Neste artigo, são apresentadas as estruturas sin-sedimentares dos calcários laminados da Formação Crato, abordando os processos de liquefação e fluidização e sua origem causada por eventos sísmicos. O item 4.2 corresponde ao artigo submetido para publicação na revista Marine and Petroleum Geology: “The effect of fracture networks on the vertical permeability of a tight carbonate reservoir analog: a case study from the Crato Formation, NE Brazil”. Este artigo analisa a permoporosidade da rede de fraturas em diferentes escalas, considerando a segmentação vertical das fraturas.

No capítulo 5 apresenta-se as conclusões sobre todos os resultados da pesquisa.

2 REVISÃO BIBLIOGRÁFICA DO CONTEXTO GEOLÓGICO

2.1 Província Borborema

A Província Borborema (PB) está situada na região Nordeste do Brasil e possui uma área com aproximadamente 450.000 km² (Fig. 2). Esta província se destaca por ser um domínio geotectônico onde fenômenos tectônicos e magmáticos se desenvolveram com atividade intensa. Durante a formação da PB, é necessário reconhecer o papel exercido pelo ciclo orogênico Neoproterozoico Brasiliano, sendo o principal agente na deformação das rochas, até culminar na configuração geológica atualmente observada. (ALMEIDA, 1977; BRITO NEVES, 2000; OLIVEIRA, 2008). Os estudos sobre a atual configuração da PB vêm sido desenvolvidos ao longo de décadas, e os debates e hipóteses sobre sua gênese sugerem que as deformações e metamorfismo foram resultados da colisão entre os crátons Amazônico, Oeste Africano e São Francisco (SANTOS et al., 2008; OLIVEIRA et al 2010; ARAÚJO et al., 2014). Por outro lado, existem hipóteses de que a PB era um único bloco continental (NEVES, 2003; Neves et al., 2009), sendo que não existe ainda um consenso no que diz respeito às estas teorias (NEVES *et al.,* 2015).

A PB é limitada ao Norte e ao Leste pelas bacias sedimentares marginais, cuja origem retrata a abertura do Oceano Atlântico Sul. O Cráton de São Francisco limita a mesma província ao Sul, enquanto que a Bacia do Parnaíba a limita ao Oeste (MATOS, 1992, 1999). De acordo com BRITO NEVES *et al* (2000), a PB é dividida em três grandes Domínios, denominados: Domínio Norte, Domínio da Zona Transversal e Domínio Sul. Estes três Domínios são limitados por duas zonas de cisalhamento de escala continental, são elas: a Zona de Cisalhamento Patos (ZCPA), e a Zona de Cisalhamento Pernambuco (ZCPE). As zonas de cisalhamentos, aqui citadas, formam um sistema de estruturas formadas em diferentes estágios, cada uma com seus próprios sistemas de zonas de cisalhamento (VAUCHEZ, 1995). A ZCPA é dividida em dois segmentos, a zona de cisalhamento Patos (segmento Oeste) e a zona de cisalhamento Campina Grande (segmento Leste) (NEVES, 2003). Da mesma forma, a ZCPE também é dividida em dois segmentos, a zona de cisalhamento

Pernambuco Oeste e a zona de cisalhamento Pernambuco Leste (VAUCHEZ, 1995; NEVES & MARIANO, 1999).

A partir do Fanerozoico ocorreram importantes eventos geotectônicos que marcaram o desenvolvimento da PB. Durante a Era Paleozoica, ocorreu à formação das bacias sedimentares intracratônicas, por exemplo os depósitos da Bacia do Parnaíba, formado pelo desenvolvimento de sinéclises, ou seja, depressões instaladas em zonas tectonicamente instáveis na crosta (BALLY & SNELSON, 1980). Os depósitos sedimentares relacionados a estas bacias paleozoicas recobriam a PB antes mesmo da separação do Gondwana. Durante a E ra Mesozoica, ocorreu a fragmentação do supercontinente e a divisão entre as placas Sulamericana e Africana, dando origem às bacias marginais ao longo de toda a plataforma continental (MATOS, 1992). A era Cenozoica é representada por eventos relevantes marcados por mecanismos de soerguimento e posteriores denudações (MORAIS NETO, 1999; JARDIM DE SÁ *et al.,* 2005; OLIVEIRA & MEDEIROS, 2012; PEAULVAST & BÉTARD, 2015), que modelaram a morfologia de bacias interiores, como por exemplo a bacia do Araripe, destacada por sua extensa chapada.

Figura 2 – Mapa geológico simplificado da Província Borborema destacando a localização das principais bacias intracratônicas e faixa costeira das bacias marginais. Os Domínios da PB são: Domínio Norte (DN), Domínio da Zona Transversal (DTZ) e Domínio Sul. Os domínios são limitados pelas principais Zonas de Cisalhamento ZCPE e ZCPA. O polígono vermelho assinala o local da Bacia do Araripe na PB.

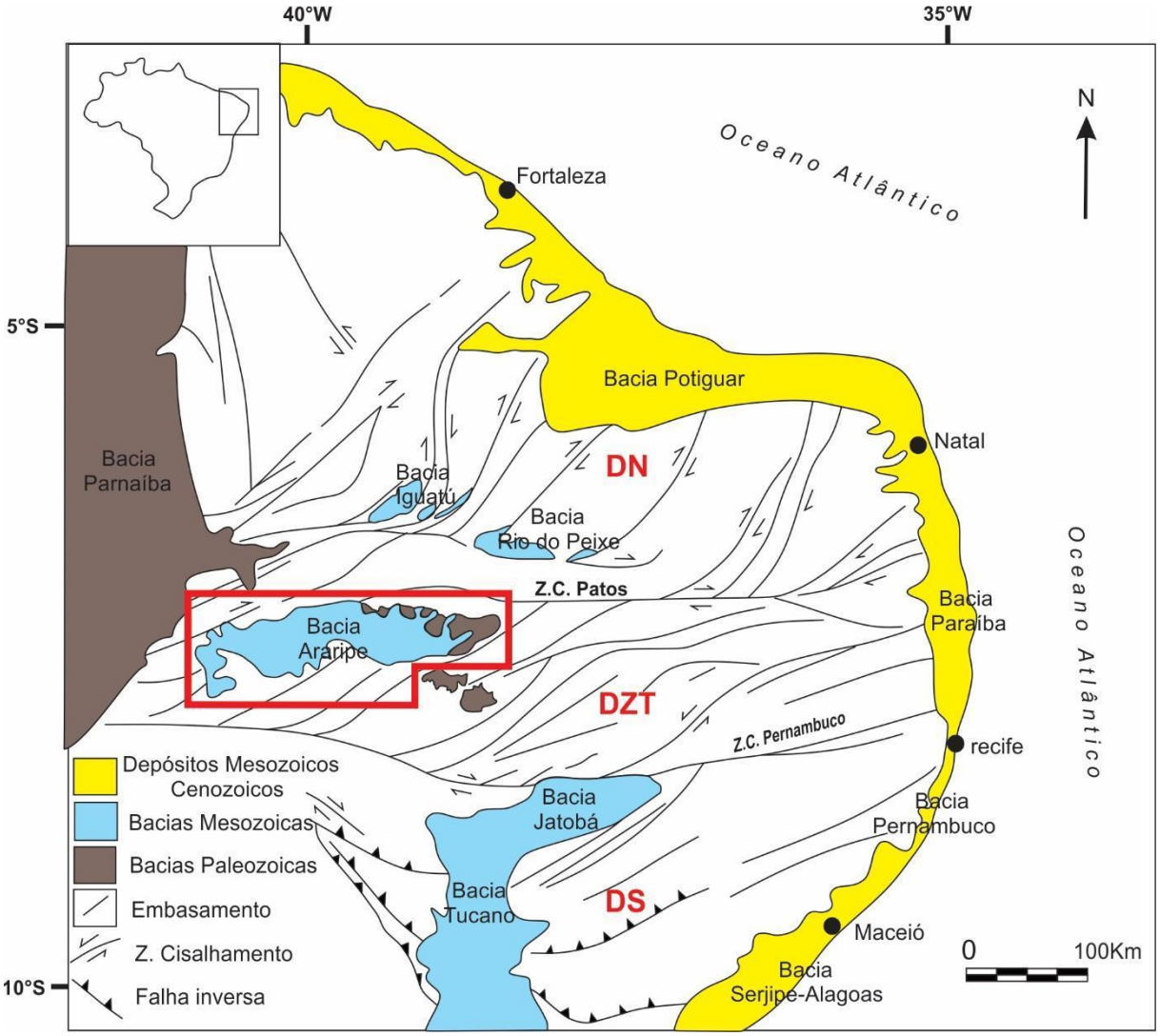

Fonte: Modificado de Matos (1992).

2.2 Bacia do Araripe

A Bacia do Araripe é a mais extensa das bacias intracratônicas do Nordeste do Brasil, com área de aproximadamente 9.000 km², e está localizada no Domínio da Zona Transversal, ao Sul da Zona de Cisalhamento Patos (Fig. 2). Os depósitos sedimentares desta bacia são compostos por sucessões de rochas com idades que variam desde o Paleozoico Inferior até o Mesozoico Superior, e seu embasamento cristalino é composto por rochas de idade Pré-Cambrianas (ALMEIDA, 1977; ASSINE 1992, 2007; BRITO NEVES *et al.,* 2000).

Na região em que está localizada a Bacia do Araripe destaca-se por sua geomorfologia devido à feição em forma de Chapada que a mesma apresenta. Esta feição é denominada Chapada do Araripe e apresenta características com um relevo positivo, tabular e em forma de *cuesta*, com um eixo maior na direção E-W e com mergulho suave para oeste (ASSINE, 2007; PEAULVAST, 2015). A Chapada do Araripe é composta por formações de idades correspondentes ao Cretáceo Superior (ASSINE, 1992, 1994).

De maneira geral, a Bacia do Araripe é compartimentada em duas sub-bacias: a) Sub-bacia Feitoria, a Oeste e b) Sub-bacia Cariri, a Leste. Esses dois depocentros são divididos por um conjunto de *horsts* e *grábens, sendo o horst de* Dom Leme o divisor principal entre essas duas sub-bacias (PONTE & PONTE FILHO, 1996; CASTRO & CASTELO BRANCO, 1999). Vale destacar que na sub-bacia Feitoria existe um poço (2-AP-1-CE) que foi perfurado pela PETROBRAS e foi executado no ano de 1986. O poço tem aproximadamente 1.500 metros de profundidade e contém todo o registro da coluna estratigráfica da Bacia (ASSINE, 2007).

Em relação ao contexto tectonoestratigráfico, a Bacia do Araripe passou por várias proposições ao longo do histórico de estudos realizados (PONTE & API, 1990; ASSINE, 1992;). Neumann (1999) e Neumann & Cabrera (1999) dividiram a Bacia do Araripe em cinco tectonosequencias: Beta (Paleozoico), Pré-rifte (Jurássico) Rifte (Cretáceo Inferior), Pós-rifte (Cretáceo Superior) e Zeta (Cenozóico). A sequência Beta é representada pela Formação Cariri; a sequência pré-rifte corresponde às formações Brejo Santo e Missão Velha; a sequência rifte é formada pela Formação Abaiara; a sequência pós-rifte é representada pelas formações Barbalha (Rio da Batateira), Crato, Ipubi, Romualdo, Araripina e Exu; e a sequência Zeta são as coberturas recentes representadas pelos depósitos aluvio-coluvionares.

A sucessão pós-rifte foi dividida em duas sequências (Assine, 2007): Pós-rifte I e pós-rifte II. A sequência pós-rifte I é constituída pelas Formações Barbalha (Rio da Batateira), Membro Crato, Camadas Ipubi e Membro Romualdo. Enquanto que a sequência pós-rifte II seria constituída pelas formações Araripina e Exu. A sequência pós-rifte I passou por uma nova interpretação na qual o Membro Crato, as Camadas Ipubi e o Membro Romualdo

foram elevados para a condição de Formação (ASSINE *et al.,* 2014). A Figura 3 exibe a carta litoestratigráfica da Bacia do Araripe destacando a sequência pós-rifte I.

Os eventos tectônicos vinculados à evolução da Bacia do Araripe também vêm sendo debatidos ao longo dos últimos anos. Uma das propostas sugere que na Era P aleozoica, período em que a fase tectônica era de uma sinéclise, a Bacia pode ter sido sobreposta por uma fase de regime *pull-apart (*MIRANDA *et al.,* 2014; MIRANDA, 2015). Durante o Mesozoico, a bacia foi submetida a um processo de afinamento crustal relacionado a esforços extensionais causando a ascensão de material astenosférico que contribuiu para a formação do relevo positivo da chapada (GARCIA et al., 2019). Durante o Cenozoico, as hipóteses para a evolução tectônica da Bacia do Araripe sugerem um processo de inversão tectônica, representado pelo relevo positivo da Chapada do Araripe. Essa proposta é assunto de debates entre alguns autores da atualidade. Marques *et al* (2014) atribui a inversão topográfica da Chapada a processos tectônicos rúpteis, evidenciados por dados de campo. Por outro lado, Peaulvast & Bétard (2015) sugeriram que um evento de arqueamento regional da PB seguido por um processo de denudação periférica foi o responsável pela configuração atual da Chapada.

Figura 3 - Carta litoestratigráfica simplificada da Bacia do Araripe. Em destaque a Formação Crato na sequência Pós-rifte I.

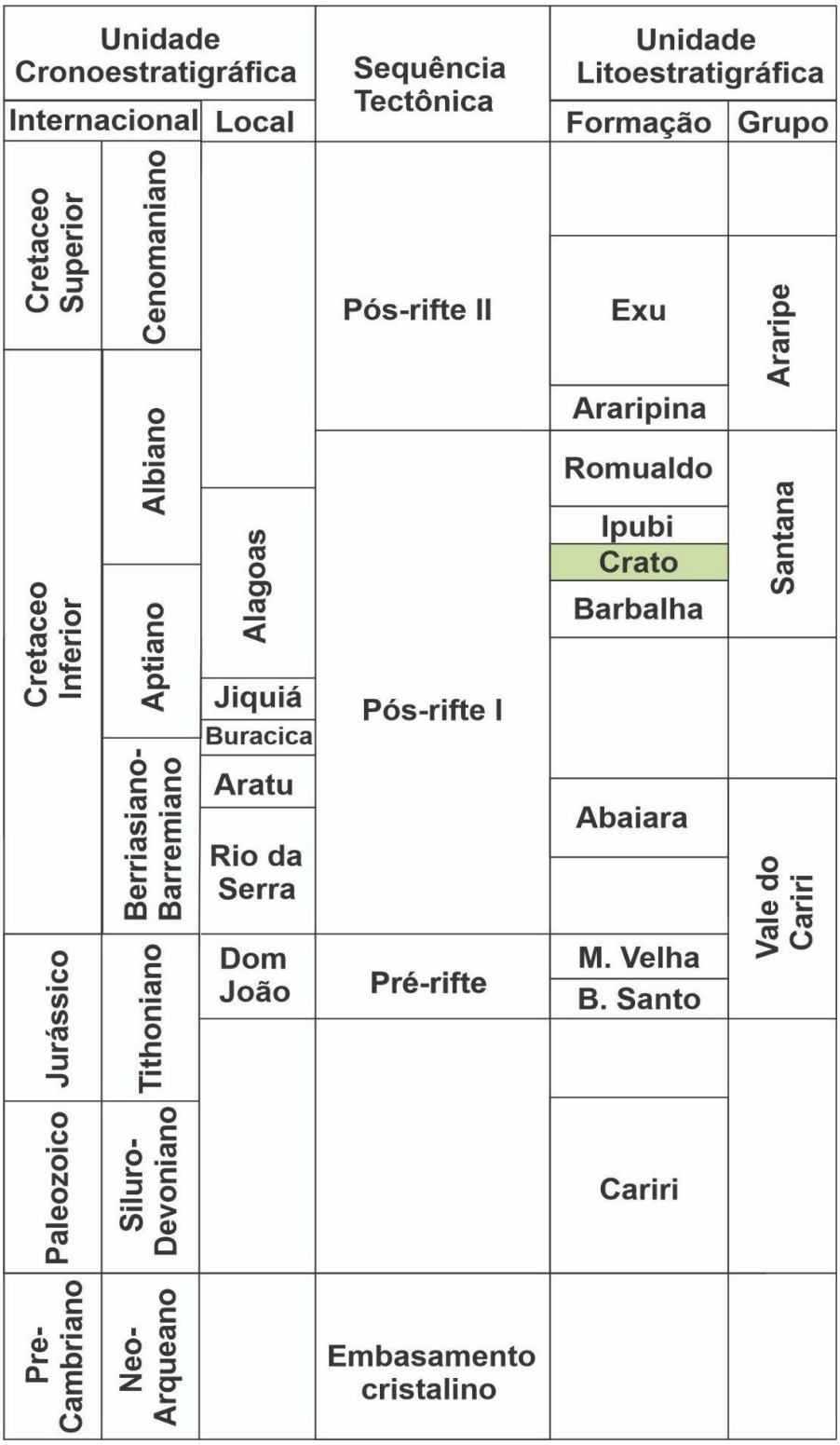

Fonte: Autor (2023)

2.2.1 Formação Crato

A Formação Crato vem sendo estudada desde o início do século XX onde a mesma era denominada como Calcário de Santana (SMALL, 1913). A partir da década de 60, conforme os estudos sobre esta unidade foram se intensificando, estes depósitos carbonáticos receberam a denominação de Formação Crato (BEURLEN, 1962, 1963, 1971). A unidade foi motivo de debates sobre a sua hierarquia estratigráfica, sendo que alguns autores a classificam como Membro Crato (ASSINE, 2007). Para este trabalho, o termo Formação Crato será mantido para os depósitos carbonáticos estudados conforme proposto por Neumann (1999) e por Neumann & Assine (2015). A Figura 4 apresenta o mapa geológico da área e aponta a localização da mina na qual foi realizado o estudo.

Figura 4 – Mapa geológico de detalhe da área de estudo destacando os depósitos da Formação Crato na borda norte da Bacia, o conjunto de falhas associadas a ZCPa (Celestino et al., 2020) e a localização da Pedreira do Willians.

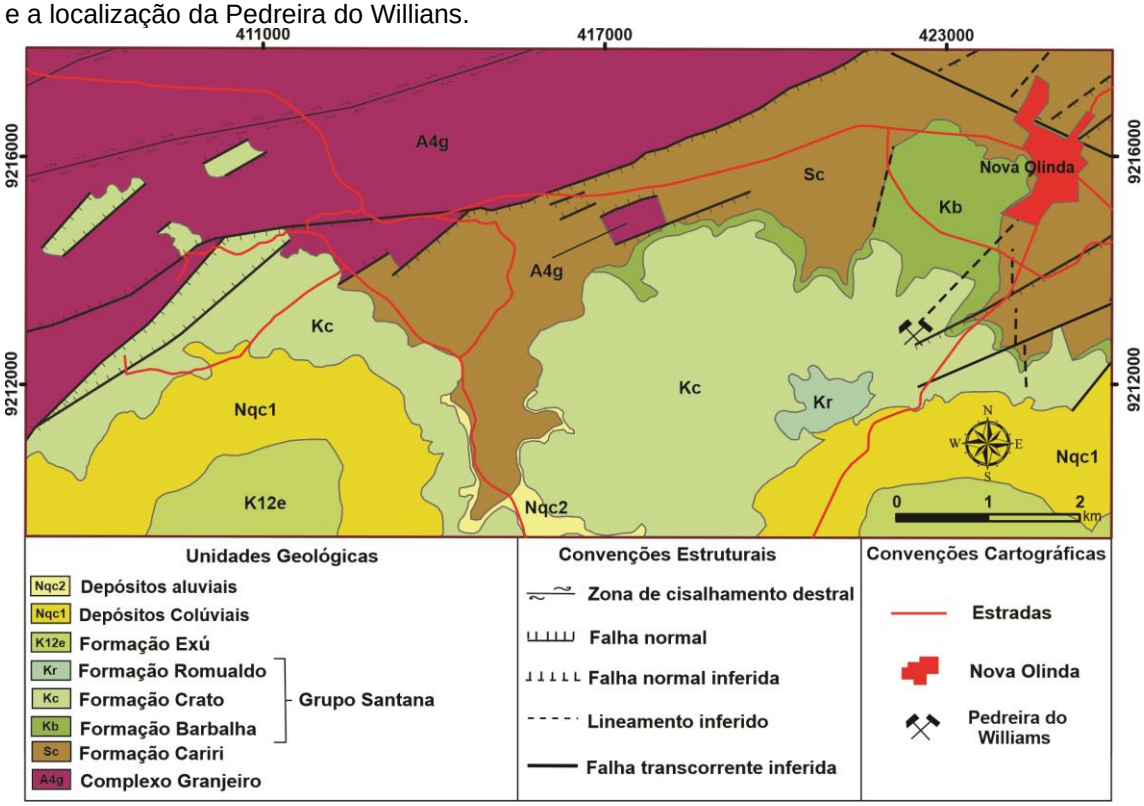

Fonte: autor (2023)

A Formação Crato é constituída por depósitos formados em um sistema flúvio-lacustre, de idade Aptiano-Albiano, situada na fase pós-rifte da Bacia do Araripe onde predominou as regiões proximais dos grandes paleolagos (COIMBRA *et al.,* 2002; ASSINE, 2007). Esta unidade é composta por depósitos de calcários laminados intercalados com margas, arenitos, siltitos e folhelhos

(NEUMANN, 1999; NEUMANN & CABRERA, 1999; SILVA et al., 2002; SILVA & NEUMANN, 2002). De acordo com estes autores, os intervalos compostos por calcários laminados são divididos em seis níveis, da base para o topo denominados de C1 até C6. A Formação Crato é recoberta pela Formação Ipubi, uma unidade composta por camadas de folhelhos e rochas evaporitícas (gipsita e anidrita) (ASSINE, 2007; ASSINE et al., 2014; FABIN et al., 2018). Por sua vez, a Formação Crato está depositada sobre os arenitos e folhelhos da Formação Barbalha (ASSINE, 2007).

Os calcários laminados da Formação Crato são compostos por calcita de baixo teor de magnésio e apresentam coloração cinza e bege. Também se destaca uma notável ritmicidade nos calcários laminados (NEUMANN, 1999). De acordo com Heimhofer *et al* (2010), a ritmicidade dos calcários laminados, caracterizado pela alternância de cores, está ligada à sua composição química. Desta maneira, as lâminas de coloração mais escuras apresentam concentrações maiores de Fe e S, enquanto que as laminações de coloração mais claras apresentam menores concentrações de Fe e S.

Este estudo tem como foco o nível C6, que é o nível de maior expressão na área de estudo. Este nível apresenta em sua porção basal laminitos de cores cinzas enquanto que na porção superior os laminitos apresentam cores amarelas e beges. A origem da variação das cores apresentadas pelo calcário laminado tem sido motivo de debates ao longo das décadas. Alguns autores sugerem que a cor amarelada na porção superior pode estar associada à alteração meteórica devido à exposição dos depósitos nas cavas das minas (NEUMANN, 1999; MIRANDA, 2015). Por outro lado, a diferenciação das cores dos laminitos podem estar associados a questões deposicionais e na preservação do conteúdo fossilífero. Os laminitos de cor cinza apresentam uma taxa de sedimentação maior do que os calcários de cor amarela, afetando dessa maneira as condições de anoxia e consequentemente a preservação dos fósseis (OSÉS *et al.,* 2017).

Em relação aos parâmetros hidrodinâmicos, é pertinente notar que os laminitos em questão manifestam uma característica marcante de baixa permeabilidade, apresentando-se em uma faixa de valores que varia de um mínimo de 0,0 mD a um máximo de 0,09 mD (MIRANDA et al., 2016, 2018). Juntamente, vale ressaltar que a porosidade exibe uma gama de flutuações que

compreende desde valores tão baixos quanto 4% até níveis mais substanciais, alcançando até 22% (MIRANDA et al., 2016, 2018). Ademais, é digno de nota que estudos anteriores, nos quais ensaios de resistência mecânica foram conduzidos, corroboram a notável distinção entre os dois tipos de calcário em estudo, demonstrando que o calcário amarelo se revela substancialmente mais rígido em comparação ao calcário cinzento (TORRES *et al.,* 2016).

Alguns estudos foram desenvolvidos ao longo dos anos e tiveram como produto a caracterização das micro*fácies* dos laminitos Formação Crato. Neumann (1999) e Silva *et al* (2002) diferenciam cinco micro*fácies*: Sm1 – caracterizada por lâminas de espessuras centimétricas, planas ou plano onduladas, com ou sem presença de concreções; Sm2 – caracterizada por lâminas centimétricas, planas ou plano-onduladas, com ocorrência frequente de *loop beddings*; Sm3 – caracterizada por calcarenitos peloidais e esteiras algálicas; Sm4 – diferenciada pela ocorrência de lâminas onduladas e plano-onduladas e pela presença de *slumps*; Sm5 – diferenciada por apresentar lâminas centimétricas, planas ou plano-ondulada, com presença de concreções, convoluções e microfalhas; e, Sm6 – distinguida por lâminas centimétricas, planas e plano-onduladas, com microfósseis e ostracodes.

Catto (2015) e Catto *et al* (2016), também estudaram esses depósitos de laminito através dos testemunhos do poço 1-PS-11-CE, e caracterizaram quatro micro*fácies*: laminar, rítmica, nodular e drusiforme.

Araújo (2020) estudou os laminitos do nível C6 através de painéis de alta resolução e diferenciou tipos de micro*fácies* tanto para o laminitos de cor cinza quanto para os laminitos de cor amarela.

Os laminitos amarelos se dividem nas seguintes micro*fácies*:

- CLA - Calcário Laminado Amarelo;
- CLALB - Calcário Laminado Amarelo com *Loop beddings* tipo simples;
- CLACV - Calcário Laminado Amarelo com Convolução;
- CLAD - Calcário Laminado Amarelo com Dissolução;
- CLAVUG - Calcário Laminado Amarelo com *Vugs;*
- CLAGP - Calcário Laminado Amarelo com Veio de Gipsita; e
- CLACON- Calcário Laminado Amarelo com Concreção.

Nos laminitos de cor cinza foram diferenciadas as seguintes micro*fácies*:

- CLC- Calcário Laminado Cinza maciço;
- CLCLB- Calcário Laminado Cinza com *Loop beddings*;
- CLCCV- Calcário Laminado Cinza com Convolução;
- CLCD- Calcário Laminado Cinza com Dissolução;
- CLCVUG- Calcário Laminado Cinza com *Vugs*; e
- CLCCON- Calcário Laminado Cinza com Concreção.

Quanto à origem, os estudos dos calcários laminados da Formação Crato têm sido motivo de debate ao longo dos anos. O trabalho pioneiro, realizado por Neumann (1999), propôs que a origem destes laminitos estava associada com precipitação química, sugerindo que a taxa de evaporação nos paleolagos era elevada, enquanto que o aporte de água nestes mesmos corpos lacustres eram baixas. Por outro lado, Heimhofer (2010) sugeriu que o mineral calcita teve sua origem causada pela precipitação induzida pela atividade de micro-organismos (algas e bactérias). Catto (2016) sugeriu que a origem dos laminitos está associada à precipitação bioinduzida de carbonato de cálcio. Este autor ainda destacou a existência de estruturas precipitadas a partir de substâncias poliméricas extracelulares (EPS), e também sugeriu o envolvimento de cianobactérias, cocoides e bactérias filamentosas.

A Formação Crato é conhecida por amplo e variado conteúdo fossilífero, do qual fazem parte peixes, crustáceos, aracnídeos, ostracodes, pterossauros, lagartos e plantas (ASSINE, 2007). Este autor destaca que a ausência de fósseis marinhos implica em uma predominância de um sistema continental. Devido à preservação de uma grande quantidade de fósseis, inclusive de partes moles, a Formação Crato é classificada como uma jazida fossilífera Lagerstätte (MARTILL & FREY, 1998; MARTILL *et al.,* 2007, 2008;).

3 MATERIAIS E MÉTODOS

O produto desta pesquisa representa a integração do conjunto de dados coletados a partir de afloramentos localizados em pedreiras de calcários laminados localizados entre as cidades de Nova Olinda e Santana do Cariri, Ceará, Brasil.

3.1 Caracterização geológica

Para o estudo das Soft-Sediment Deformation Structure (SSDS) foi realizada uma coleta sistemática focada na identificação dessas estruturas, a qual levou em consideração afloramentos com centenas de metros de extensão e que chegam a atingir até 8 metros de altura. Os principais aspectos considerados para a identificação e caracterização das SSDS foram as forças condutoras e os mecanismos de deformação. As forças condutoras estão relacionadas com as instabilidades causadas pela interação entre os fluidos dentro dos poros e a coesão da rocha. Sendo essas instabilidades causadas por *stress, slumping* ou por contraste de densidade. Já os mecanismos de deformação estão relacionados com os processos de liquefação e fluidização (ANKETEL et al., 1970; ALLEN, 1977; NEUWERTH et al., 2006; OWEN et al., 2011).

3.2 Painel de alta resolução

O painel de alta resolução foi executado em uma bancada de frente de lavra em uma pedreira de calcário laminado na região entre as cidades de Santana do Cariri e Nova Olinda. A pedreira onde este trabalho foi realizado é denominada Mina do William e apresenta um conjunto de cavas e bancadas, das quais foi selecionado um afloramento com boa acessibilidade e uma boa exposição tanto lateral quanto vertical. Também foi levado em consideração o afloramento com menor grau de alteração e que também apresentava um bom número de superfícies tridimensionais. O afloramento escolhido possui uma base com dimensões que medem 23,5 m x 5 m, e uma altura que atinge até 5 metros (Fig. 5a).

Após a seleção da superfície que melhor representa as heterogeneidades do bloco tridimensional foi executada uma descrição detalhada do afloramento. Esta descrição contou com uma vistoria visual e marcação das heterogeneidades da rocha, levando em consideração seus atributos (Fig. 5b-e). A descrição detalhada do afloramento foi realizada em escala 1:1. Para as fraturas foram coletados dados, como: direção, intensidade, sentido de mergulho e abertura. Para o restante das heterogeneidades, a indicação com símbolos e siglas foi utilizada para discretizá-las. Desta maneira, todas as estruturas e heterogeneidades diagenéticas e deposicionais foram registradas. Para auxiliar esta coleta de dados detalhada foram usadas lupas de bolso, bússola, pincel, escada, réguas, comparadores, borrifadores e marcadores permanentes.

Após a preparação e marcação dos afloramentos, foram construídos painéis de alta resolução a partir do registro fotográfico terrestre com câmeras de alta resolução. O registro fotográfico terrestre foi executado usando uma câmera modelo Sony Alfa 77, com uma lente 28/75 SAM, seguindo um procedimento onde as fotos adquiridas tinham um recobrimento parcial de uma foto em relação a outra, mas um recobrimento total da face principal do afloramento (Tavani et al., 2014). As imagens processadas resultaram em um ortofotomosaico construído pelo *software Agisoft Metashape 1.5.2*.. Os detalhes das etapas serão descritas mais adiante.

Figura 5 – Imagem destacando a frente da bancada dos calcários laminados da Formação Crato. A imagem também apresenta algumas feições discretizadas diretamente no afloramento. a) Imagem geral dos calcários laminados, destacando a face principal que foi escolhida para a sua descrição. b) e c) Veios verticais discretizados no painel. d) Nível convoluto (CV) e *loopbedding* (LB). e) Fraturas de cisalhamento sin-deposicionais (setas vermelhas) e concreções carbonáticas (CON).

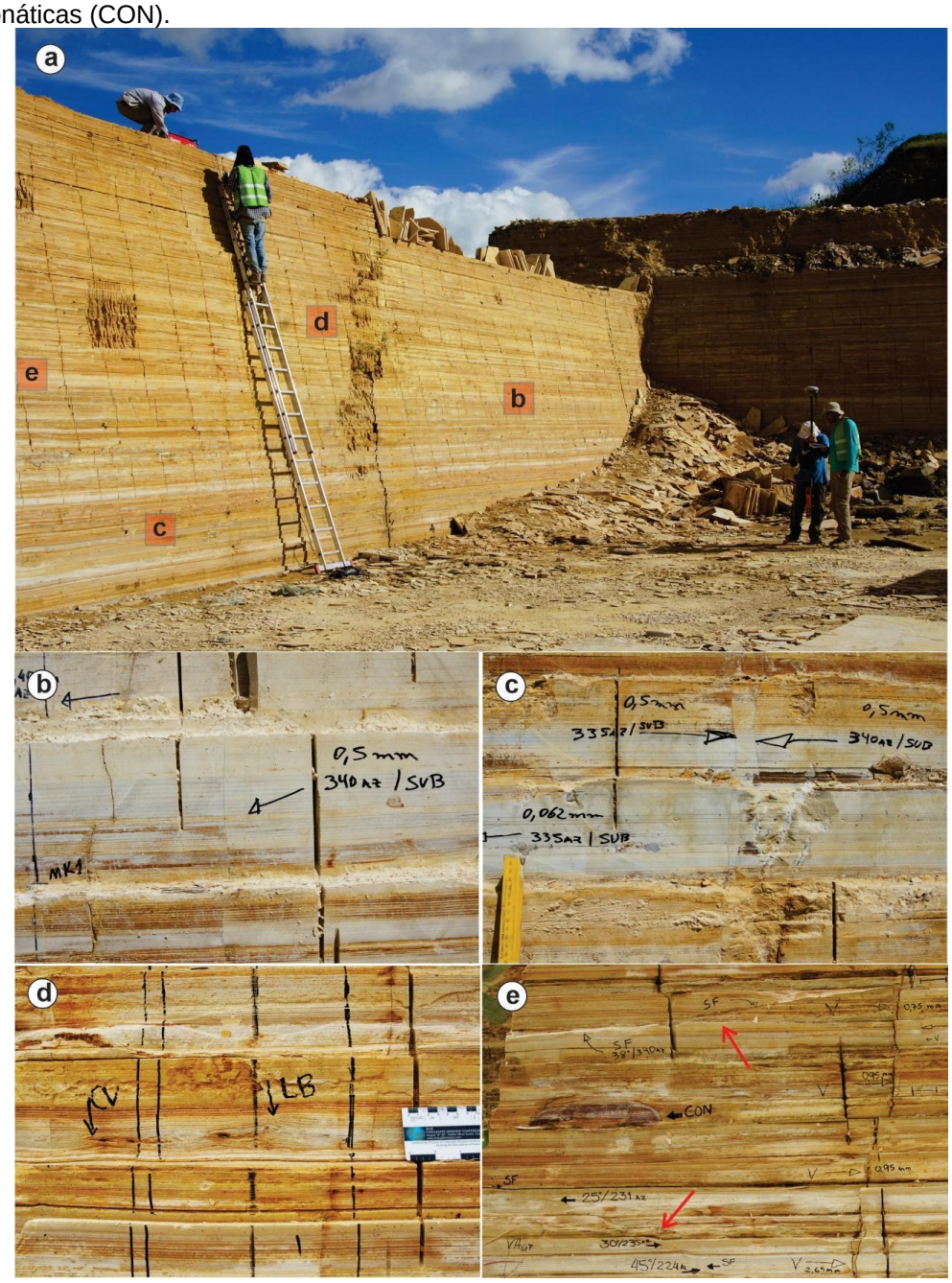

Fonte: Autor (2023)

Para a aquisição de imagens também foi utilizado um veículo aéreo não tripulado (VANT) da marca Phantom 4 Advanced, o qual possui uma câmera acoplada com resolução máxima de 4K. (Fig. 6a).

3.3 Modelo Digital de Afloramento e Aquisição de Imagens com Drone

Além dos painéis de alta resolução, também foram construídos modelos digitais de afloramentos (MDA). MDAs são ferramentas que possuem uma vasta aplicação nas geociências, em destaque na sedimentologia, na estratigrafia e na geologia estrutural. A construção de um MDA utiliza técnicas nas quais a aquisição e o posterior processamento dos dados permite a reconstrução, em meio digital, das rochas e dos afloramentos em estudo (BISDOM et al., 2014; VOLLGER & CRUDEN, 2016; SAVASTANO et al., 2016; TAVANI, 2016). De acordo com estes autores, a construção de um painel de alta resolução e dos MDA facilita a observação da distribuição das geometrias laterais das heterogeneidades e também facilita a observação do empilhamento estratigráfico.

A aquisição das fotografias aéreas foi executada durante as etapas de campo, onde foram realizados voos híbridos que recobrem a área do afloramento em estudo. Voos híbridos, no contexto de drones, são voos nos quais são combinadas operações manuais de voo com a aquisição automática de fotos. Essa abordagem híbrida é frequentemente utilizada em missões de mapeamento, inspeção e vigilância, permitindo que o operador tenha controle sobre a aeronave quando necessário, mas também aproveite os recursos de automação para tarefas específicas, como tirar fotos em intervalos regulares ou percorrer áreas predefinidas. As etapas foram realizadas de 23 até 25 de abril de 2019 e 08 até 10 de Agosto. Ao todo foram adquiridas 198 imagens para cobrir a região do afloramento em estudo. De toda a extensão da área, foram selecionadas as imagens focando a superfície de interesse do afloramento, totalizando um número de 56 fotografias (Fig. 6c). Com o objetivo de assegurar que a coleta de imagens fosse realizada seguindo critérios rigorosamente estabelecidos, optou-se pelo emprego do aplicativo de aerolevantamento conhecido como Pix4D Capture. Esse software viabiliza a concepção e execução de missões de voo de forma completamente autônoma. Importante ressaltar que o Pix4D Capture está disponível para as plataformas Android e iOS, abrangendo assim um amplo espectro de dispositivos móveis. Ele também é capaz de estabelecer uma comunicação eficaz com o hardware do equipamento de voo e,

com base nos parâmetros predefinidos para a captura de imagens e nas delimitações geográficas da área a ser mapeada, calcular a trajetória ideal para a aquisição das imagens.

Figura 6 – a) Fotografia de um drone modelo Phantom 4 Advanced. A imagem ilustra um modelo do equipamento utilizado para a aquisição de imagens aéreas. b) Figura mostrando os parâmetros associados em uma visualização estereoscópica. Considera-se P como um objeto fotografado por duas câmeras (C1 e C2), sua posição será determinada pela distância focal e orientação da câmera (modificado de Tavani et al., 2014). c) Exemplo de alinhamento de fotomosaico da superfície de um afloramento.

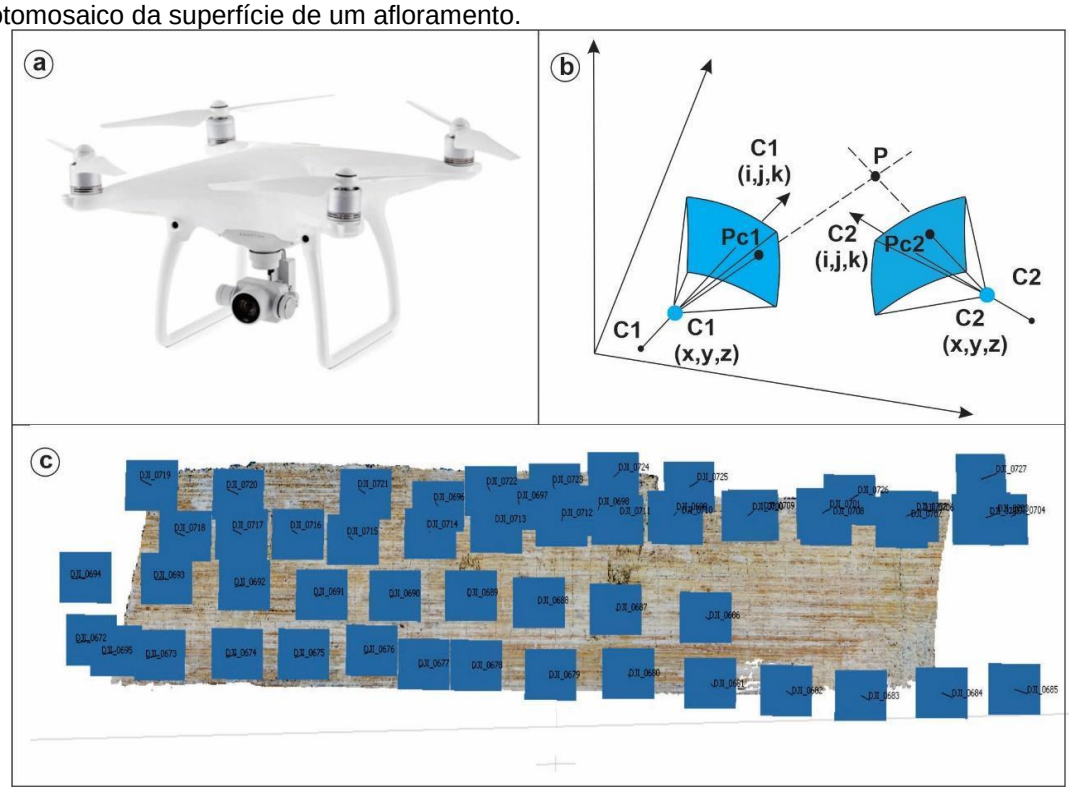

Fonte: Autor (2023)

O VANT utilizado na aquisição das imagens possui um sensor RGB SONY EXMOR 1” CMOS que possibilita a aquisição de imagens com resolução de 20 megapixels, construindo imagens com 4864 x 3648 pixels.

A próxima etapa, após a aquisição das imagens, foi o processamento das mesmas. O processamento das imagens foi realizado através da técnica *Structure from Motion* (SfM), utilizando o algoritmo Scale Invariant Feature (SIFT) e do *software Agisoft Metashape 1.5.2..* Para este procedimento, o processamento consiste na sobreposição de pelo menos três imagens do mesmo objeto tiradas de pontos diferentes Figura 6b (TAVANI et al., 2014).

Primeiramente, o algoritmo realiza um alinhamento das imagens de acordo com suas respectivas coordenadas, de maneira a manter a sobreposição original da aquisição. Na etapa seguinte, o algoritmo cria uma nuvem densa de pontos, que consiste no aumento da quantidade de pontos e a consequente diminuição de espaços vazios. A partir da nuvem densa de pontos pode-se construir uma superfície triangular (*mesh*). O algoritmo gera uma superfície de texturização, que é aplicada no modelo e tem como objetivo melhorar o aspecto visual da imagem (LARSSEN et al, 2020; MARTINELLI et al, 2020; VILARREAL et al, 2020). Com a superfície de texturização pode-se obter ortofotomosaicos do modelo construído. A Figura 7 mostra as etapas do processamento de imagens. Seguindo estes passos, foram gerados modelos com resolução de 6 mm/pixel e ortomosaicos com 3 mm/pixel.

Figura 7 – Imagem destacando o processamento de um modelo digital de afloramento. a) imagem aérea do afloramento destacando a face onde foram coletados os dados para o painel de alta resolução. b) nuvem densa de pontos. C) superfície de triangulação conectando os pontos da nuvem densa. d) superfície de triangulação em detalhe. e) superfície de texturização aplicada no mosaico.

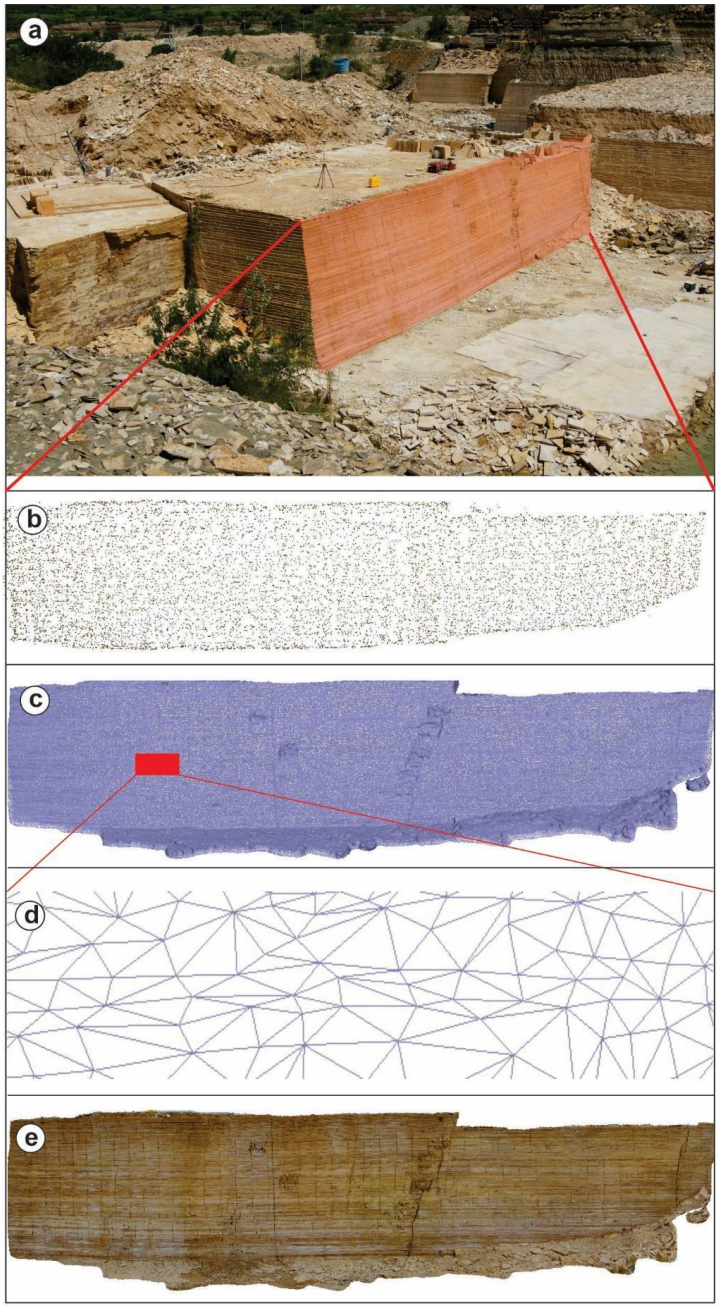

Fonte: Autor (2023)

Por fim, o painel de alta resolução e o MDA foram exportados e vetorizados no COREL DRAW, onde tiveram os seus elementos discretizados e tratados na mesma proporção de escala real. Desta maneira, os dados foram integrados em um único bloco facilitando a interpretação dos padrões existentes tanto nas estruturas rúpteis quanto nas feições diagenéticas (Fig. 8).

Figura 8 – a) Ortomosaico derivado de um MDA destacando a interpretação das estruturas rúpteis e feições diagenéticas. Também estão localizados pseudopoços verticais e horizontais b) Bloco diagrama destacando o afloramento estudado, vetorizado em ambiente CAD, onde os elementos de fraturas foram discretizados mantendo a proporção de sua escala real. As linhas vermelhas representam os veios verticais do afloramento enquanto que as linhas amarelas representam a extensão dos planos dos mesmos veios para a parte interna do bloco.

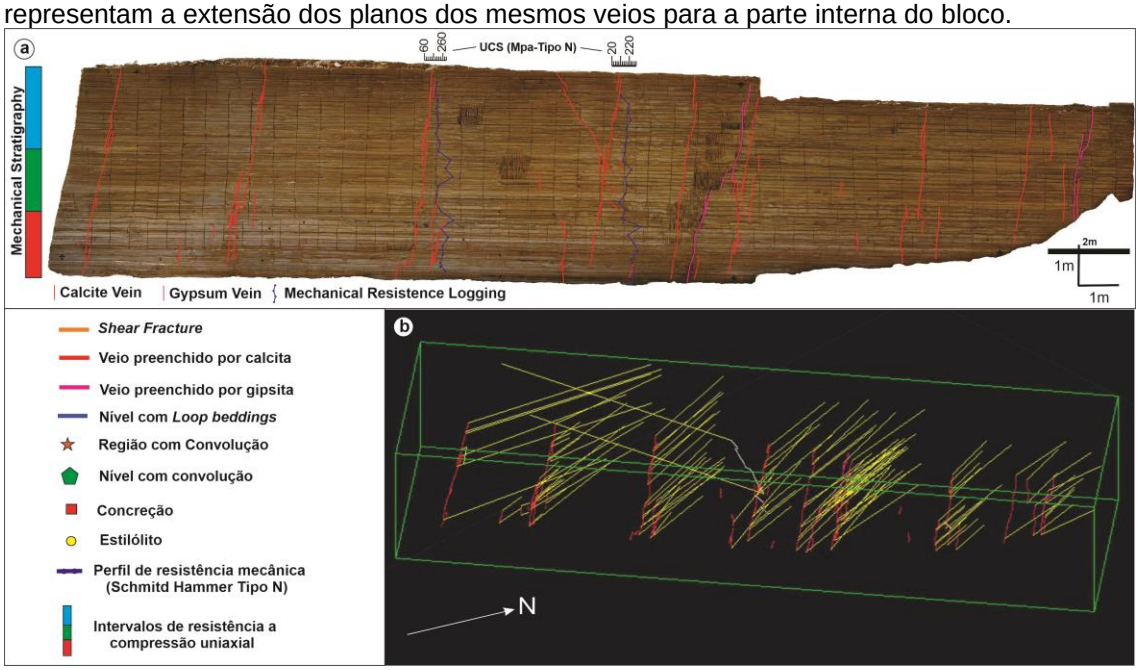

Fonte: Autor (2023)

3.4 Pseudopoços

Para a integração das informações dos dados de afloramento nos modelos tridimensionais foi feito o uso de perfis estratigráficos, considerados aqui como pseudopoços (Fig. 8a). Os pseudopoços desempenharam o papel de poços virtuais cujas informações representam os atributos dos elementos estudados. De acordo com Nilsen et al. (1999), um pseudopoço é um ponto de informação compilada dentro de uma área específica. A aplicação de pseudopoços permitiu a inserção de dados de diferentes atributos das fraturas, criando uma relação direta entre os dados e possibilitando a delimitação da geometria da rede de fraturas (KRAFT, 2004).

Para fins de controle, foram designados nomes, inseridas coordenadas de localização e também a profundidade dos poços. Desta maneira, os pseudopoços foram elaborados. Utilizamos tanto pseudopoços horizontais quanto verticais. Zakirov e Zakirov (1996) discutiram a importância da

sensibilidade de poços verticais e horizontais em relação às heterogeneidades existentes em um reservatório, que podem variar com base na relação espacial entre os poços e essas características. Isso significa que a orientação e posicionamento dos poços em relação a estruturas geológicas, como fraturas, falhas, camadas e outros tipos de heterogeneidades, podem afetar sua capacidade de detectar e medir propriedades do reservatório, como porosidade, permeabilidade e saturação de fluidos.

Neste trabalho, pseudoços horizontais foram usados tanto em planta quanto em seções transversais, desempenhando um papel como scanlines virtuais (P10), que nos permitiram acesso eficiente aos dados de atributos necessários para nossa análise (Fig. 9). Utilizamos pseudopoços horizontais nas seções transversais devido ao fato da rede de fraturas estudada ser predominantemente vertical (Zakirov e Zakirov, 1996). Consequentemente, uma representação adequada destas características geológicas foi obtida por meio do uso de pseudopoços horizontais. Por outro lado, é importante destacar que os pseudopoços verticais foram empregados em seções transversais com o propósito específico de representar os registros de resistência mecânica das rochas em estudo. Como resultado, obteve-se um banco de dados a partir dos quais tornou-se possível a modelagem tridimensional da rede de fraturas, também conhecida como *Discret Fractured Network* (DFN).

Figura 9 – Bloco diagrama destacando a relação dos pseudopoços com algumas heterogeneidades nos calcários laminados da Formação Crato. Observar que para as feições horizontais os pseudopoços verticais são mais representativos enquanto que para as estruturas verticais os pseudopoços horizontais são mais representativos.

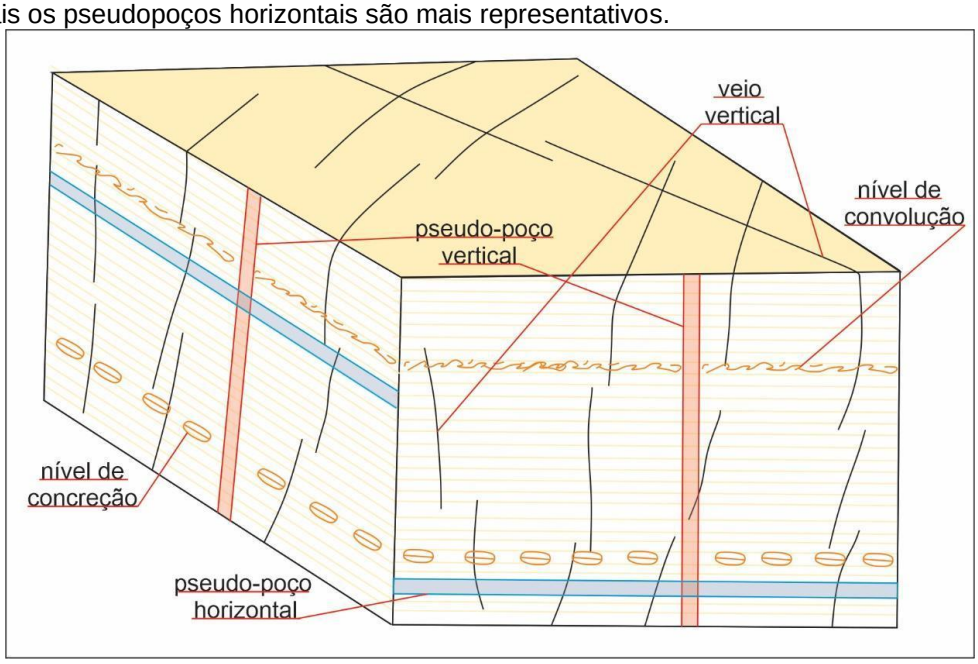

Fonte: Autor (2023)

3.5 Modelagem de fraturas

A partir da integração dos dados adquiridos pelos métodos expostos acima, obteve-se um banco de dados por onde foram extraídos os parâmetros para a construção dos modelos DFN. Para a construção dos modelos foi utilizado o software MOVE. O fluxograma da Figura 10 ilustra as etapas seguidas para a execução da modelagem dos DFNs apresentados neste trabalho.

Figura 10 – Desenho esquemático ilustrando o fluxograma das etapas da modelagem de um DFN. O fluxo de trabalho começa com a etapa de aquisição de imagens e finaliza com a construção do DFN.

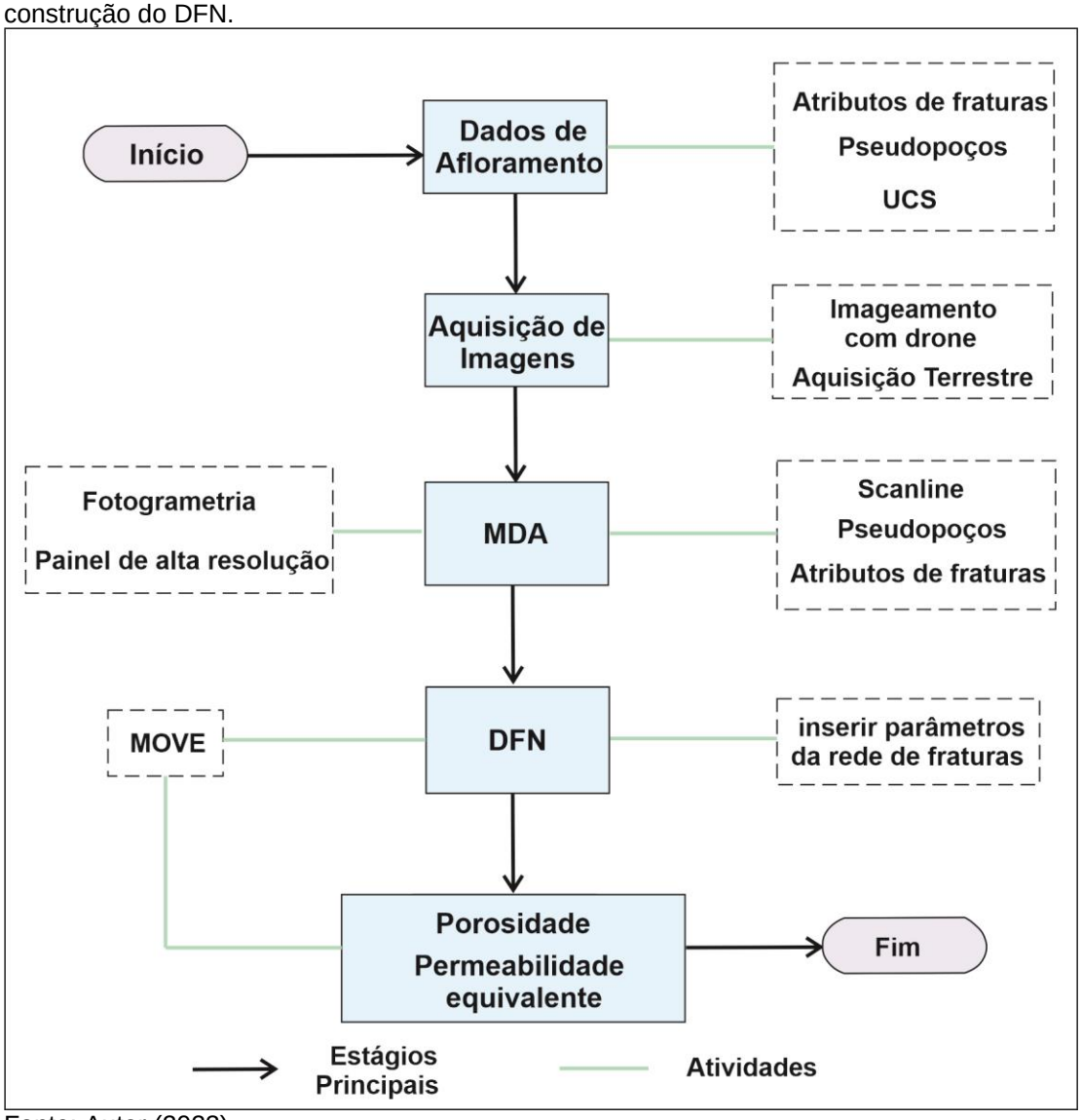

Fonte: Autor (2023)

O DFN é um modelo computacional que representa as propriedades geométricas e os atributos de cada fratura dentro de um maciço rochoso. O objetivo de um DFN é representar numericamente a rede de fraturas de um determinado afloramento, baseando-se nas estatísticas envolvidas nos atributos das fraturas (MIYOSHI et al., 2018; NYBERG et al., 2018; RACOLTE, 2021). Os modelos de fraturas podem ser construídos a partir do cálculo dos seguintes parâmetros estruturais: direção, ângulo de mergulho, sentido de mergulho, abertura, altura, comprimento, forma e interseção com outras fraturas da rede (LEI et al., 2017).

De acordo com Lei et al. (2017), uma rede de fraturas pode ser construída a partir de um mapeamento geológico (modelo determinístico) e também através de uma abordagem estocástica.

O mapeamento geológico (modelo determinístico) permite que a rede de fraturas seja observada a partir da exposição das rochas em afloramentos naturais, cavas de minas e em cortes de estrada. Sendo esta estratégia amplamente usada para o entendimento da origem, formação e arranjo populacional das fraturas (SEGALL & POLLARD, 1983; POLLARD & SEGALL, 1987; LA POINTE, 1988; BOUR et al., 2002; LEI & WANG, 2016). A técnica de mapeamento estrutural também é utilizada para o estudo de campos de *stress* de uma determinada área (ENGELDER & GEISER, 1980; OLSON & POLLARD, 1989; PETIT & MATTAUER, 1995). Por exemplo, um estudo envolvendo aquisição de dados clássicos de mapeamento estrutural foi realizado nos calcários da Bacia de Bristol, UK, e teve como produto a conectividade da rede de fraturas (BELAYNEH & COSGROVE, 2004; MASIHI & KING, 2008). Esta técnica tem a vantagem de preservar as características originais da rede de fraturas, entretanto é limitada a análises bidimensionais (Lei et al., 2017). A Figura 11 destaca um afloramento onde foi realizado o mapeamento das veios/juntas dos laminitos da Formação Crato, borda norte da Bacia do Araripe. Posteriormente, esses dados foram carregados dentro de um volume (modelo) obedecendo o posicionamento espacial real das fraturas.

Figura 11 – Imagem mostrando a relação do afloramento real e o modelo determinístico da rede de fraturas do mesmo. a) Afloramento onde foi realizado a aquisição de dados através dos métodos clássicos. b) Volume de Rede de fraturas construída a partir dos dados coletados em a.

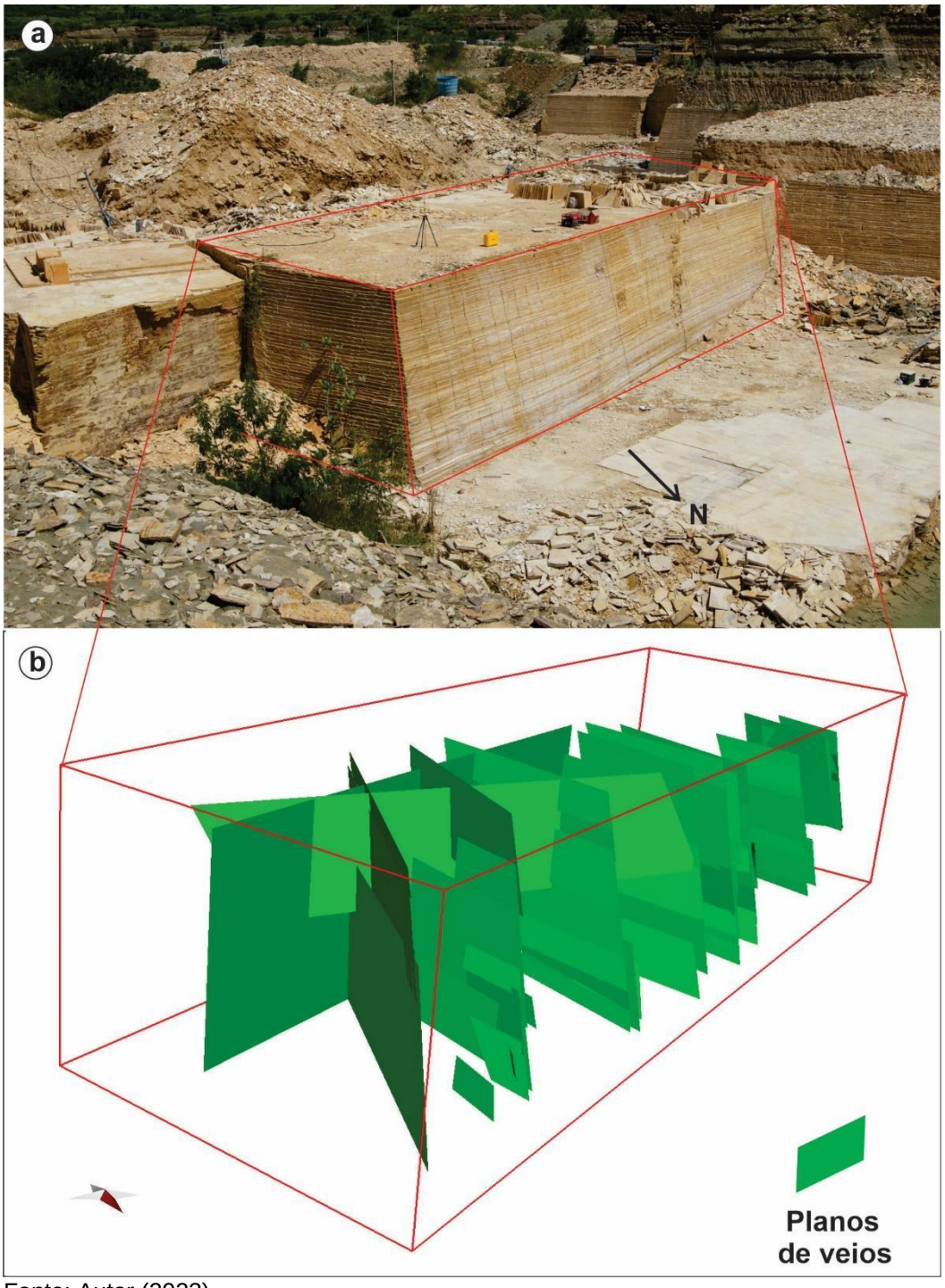

Fonte: Autor (2023)

A construção de um DFN baseado na abordagem estocástica (Fig. 12) faz uso das variações estatísticas dos atributos da rede de fraturas para gerar cenários hipotéticos onde a amostragem é limitada (LEI et al., 2007). O método

de DFN estocástico foi criado nos anos 80 e já era aplicado em estudos associados ao fluxo de fluidos em rede de fraturas (ANDERSON & DVERSTORP, 1987; LONG et al., 1985).

Figura 12 – DFN estocástico construído a partir de dados hipotéticos. Trata-se de uma rede de fratura composta por duas famílias. A conexão entre as famílias gera uma trama permoporosa que possibilita a armazenagem e um fluxo de fluido.

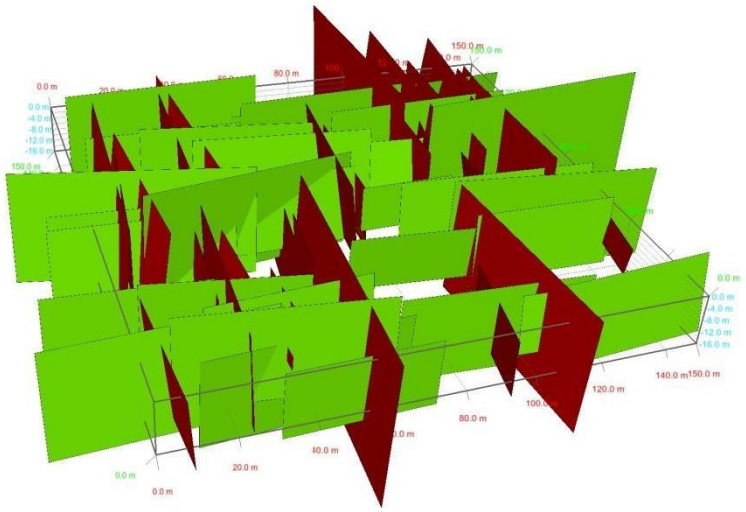

Fonte: Autor (2023)

O DFN estocástico apresenta fraturas geradas de acordo com as dimensões euclidiana na qual estão inseridas. Em modelos 2D, as fraturas são consideradas linhas ou traços, enquanto que nos modelos 3D são tratadas como polígonos planares. Os atributos dos traços ou dos polígonos são considerados variáveis independentes derivadas da aquisição de dados de campo através de técnicas tradicionais de *scanlines (*PRIEST & HUDSON, 1981; BAECHER, 1983; MIRANDA et al., 2018) e recentemente através de modelos digitais de afloramento (GIUFFRIDA et al., 2019; 2020; SMERAGLIA et al., 2021). A atitude dos planos nas redes de fraturas, parâmetro fundamental para a construção de um DFN, pode ser estimado através de estereogramas, nos quais as famílias de fraturas são agrupadas em diferentes conjuntos e posteriormente caracterizados pela respectiva distribuição (uniforme, normal e Fisher) (EINSTEIN & BAECHER, 1983; LEI et al., 2017; GIUFFRIDA et al., 2019; 2020; SMERAGLIA et al., 2021). Destacamos aqui a distribuição de Fisher (FISHER, 1953) para o controle das atitudes do grupo de fraturas de uma mesma

família, visto que a distribuição das atitudes não são homogêneas e podem ser caracterizadas em funções esféricas.

Apesar do desenvolvimento de uma família de fraturas obedecer a direção preferencial de um campo de tensão, as atitudes das fraturas de uma família não são uniformes e, desta maneira, apresentam-se de forma que as direções ocorrem espalhadas em torno de uma direção média (KHAMFOROUSH et al., 2008). A distribuição de Fisher se deduz em um parâmetro estatístico (conhecido como constante de Fisher ou número de Fisher, representada pela letra K) que corresponde à dispersão da orientação das fraturas dentro de um *cluster* (FISHER, 1953; SMERAGLIA et al., 2021). Quanto maior o número da constante de Fisher maior será o agrupamento da rede de fraturas.

Outro parâmetro intrínseco para a construção de DFN estocástico é a frequência das fraturas, que está diretamente relacionado com a densidade e a intensidade da rede de fraturas. Esses dados são amostrados nos MDA (e também diretamente no afloramento) de acordo com a padronização do sistema P_{ij}, onde i implica a dimensão da amostragem e j remete a dimensão da medida (DERSHOWITZ & HERDA, 1992; ZEEB et al., 2013; ANDREWS, 2019; MARTINELLI et al., (2020)). Segundo estes autores, a densidade de fraturas se traduz no número de fraturas por unidade, sendo P_{30} para o volume, P_{20} para a área e P_{10} para o comprimento. Ainda segundo estes autores, a intensidade de fraturas se traduz no número de fraturas persistentes por unidade de volume, sendo P_{32} para o volume, P_{21} para a área e P_{10} para o comprimento. Ainda temos os índices P_{11}, P_{21} e P_{33} que corresponde a porosidade da rede de fraturas de acordo com as dimensões. A Figura 13 simplifica o sistema P_{ij} em um diagrama. Atributos como a abertura e o comprimento individual das fraturas podem ser coletados de maneiras separadas e também terem suas distribuições estatísticas definidas para posteriormente compor o modelo.

Figura 13 – Tabela relacionando a dimensão da medida e a dimensão da amostragem com o sistema de aquisição P_{ij}. A tabela destaca os sistemas correspondentes às aquisições da densidade, intensidade e porosidade de fraturas.

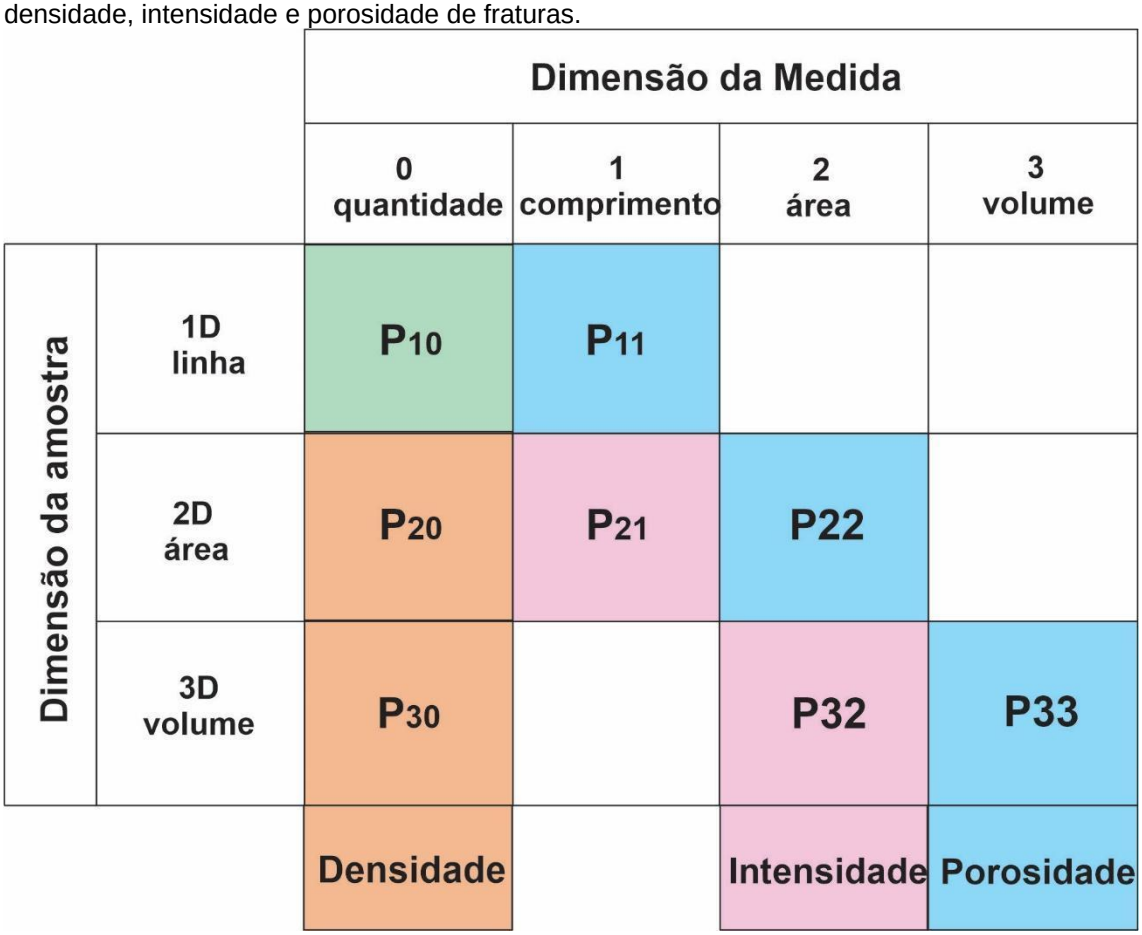

Fonte: Modificado de ZEEB et al. (2013) e ANDREWS et al. (2019)

A vantagem de usar um MDA (e ortomosaicos) para a construção de um modelo DFN estocástico é a utilização das estatísticas tridimensionais da rede de fraturas para realizar uma extrapolação a partir das amostragens uni e bidimensionais (1D e 2D) (WANG, 2005; PARRINO et al., 2019; GIUFFRIDA et al., 2019; 2020; MARTINELLI et al., 2020;) e gerar modelos tridimensionais (3D). As modelagens tridimensionais geralmente são derivadas da aquisição P_{10} e P_{21} e são associadas através das constantes C_{13} e C_{23} (WANG, 2005), respectivamente, levando em consideração os critérios da amostragem, como: a orientação da linha de varredura, dimensão da janela de varredura e orientação das fraturas.

3.6 *Scanlines* e MDA

A *scanline* consiste de uma técnica de varredura que tem como objetivo o estudo dos atributos e a frequência das fraturas que ocorrem em afloramentos. Conforme a metodologia proposta por Ortega et al (2006) as aquisições de medidas na rede de fraturas são executadas a partir de linhas ou janelas aleatórias onde são registrados os atributos das fraturas. Este método fornece uma abordagem de baixo custo e vem sendo utilizado para aquisição dos parâmetros para serem utilizados na modelagem de reservatórios naturalmente fraturados (MIRANDA et al., 2012; BISDOM et al., 2014; WATKINS et al., 2015). Através da *scanline* são coletados os atributos das fraturas, como: orientação, comprimento, abertura, espaçamento entre as fraturas, o preenchimento dos veios (ORTEGA et al., 2006; GUERRIERO et al., 2010; HOOKER et al., 2012, 2013; MIRANDA et al., 2012) e, para o caso de quando a aquisição é realizada por área, é observada a relação topológica através dos padrões de interseção das fraturas (SANDERSON & NIXON, 2015; 2018; MIRANDA et al., 2018). Quando a aquisição é realizada diretamente no campo faz-se uso de trena métrica, lupa de bolso, bússola e régua comparadora (Fig. 14 c). A régua comparadora apresenta valores com espaçamento em escala logarítmica que varia entre 0,05 e 5mm. Geralmente, é utilizada para aquisição de dados de abertura de fraturas. O objetivo de se usar uma escala logarítmica baseia-se no melhor tratamento estatístico dos dados (ORTEGA *et al.,* 2006; SANTOS *et al.,* 2015). A Figura 14 mostra um desenho esquemático de um processo de varredura em área.

Figura 14 – a) Desenho esquemático de uma aquisição de dados através de um *scanline* linear. b) desenho esquemático destacando os elementos anatômicos de um plano de fratura: altura, comprimento, abertura e atitude. c) régua comparadora utilizada na aquisição de dados de abertura das fraturas de acordo com Ortega et al (2006).

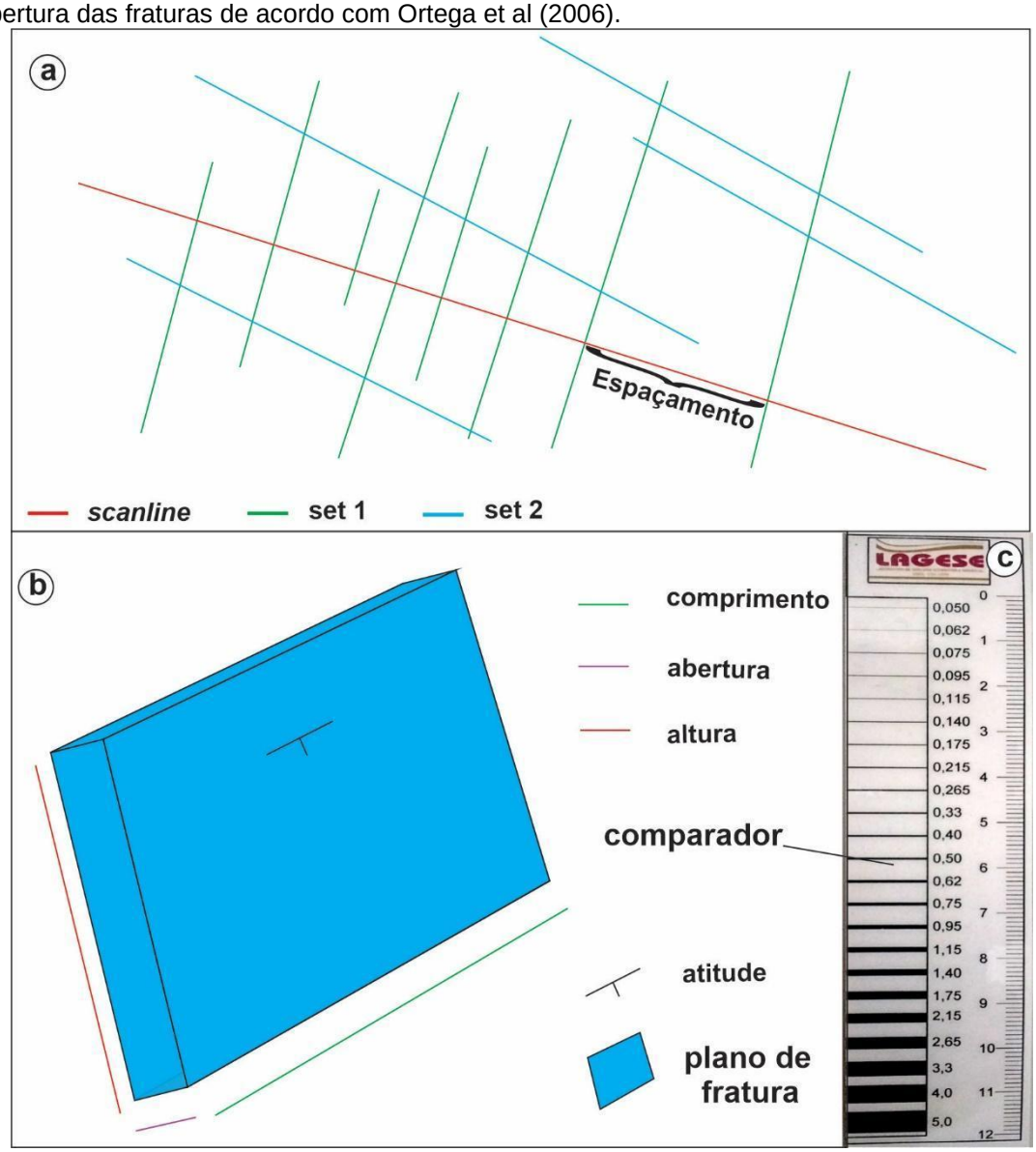

Fonte: Autor (2023)

De maneira geral, a técnica de *scanline* executada em MDA é vista como método que apresenta tendências quando a amostragem se dá em fraturas de grande comprimento, que muitas vezes estão acima dos limites da área de varredura; e também quando as fraturas são pequenas e as abertura não são observáveis devido estarem abaixo da resolução do sensor de aquisição (WATKINS et al., 2015; AKARA et al., 2020;). Mesmo assim, as aquisições feitas desta maneira ainda tem um amplo uso nos estudos (BISDOM et al., 2017; SALVINI et al. (2017)

3.7 Geomecânica

A caracterização geomecânica, compressão uniaxial, foi realizada *in situ* com o uso de um esclerômetro da marca PROCEQ, modelo *Rockshmidt,* tipo L, de baixa energia de impacto (0,735Nm) (Fig. 15). Este equipamento, inicialmente desenvolvido para testes de resistência em concretos, passou a ser bastante utilizado para estimar valores dos parâmetros mecânicos da elasticidade das rochas diante do efeito de compressão uniaxial (AYDIN & BASU, 2005; VILES et al., 2011; STEER et al., 2011). A amostragem da resistência mecânica foi realizada através da média de 10 leituras realizadas no mesmo ponto (AYDIN & BASU, 2005), sendo que os valores de rigidez são fornecidos pelo esclerômetro como rebote (Q), onde posteriormente são convertidos em Mpa (MegaPascal). A Figura 16 mostra um gráfico de correlação entre o coeficiente de rebote (Q) e os valores de resistência mecânica em UCS (*Unconfined Compressive Strength*).

Figura 15 – Fotografia mostrando momento de aquisição de dados de resistência mecânica. a) aquisição de dados na parte superior do afloramento. b) aquisição de dados na parte inferior do afloramento.

Fonte: autor (2023)

Figura 16 – Gráfico mostrando a correlação entre o coeficiente de rebote (Q) e os valores de resistência mecânica em UCS (MPa).

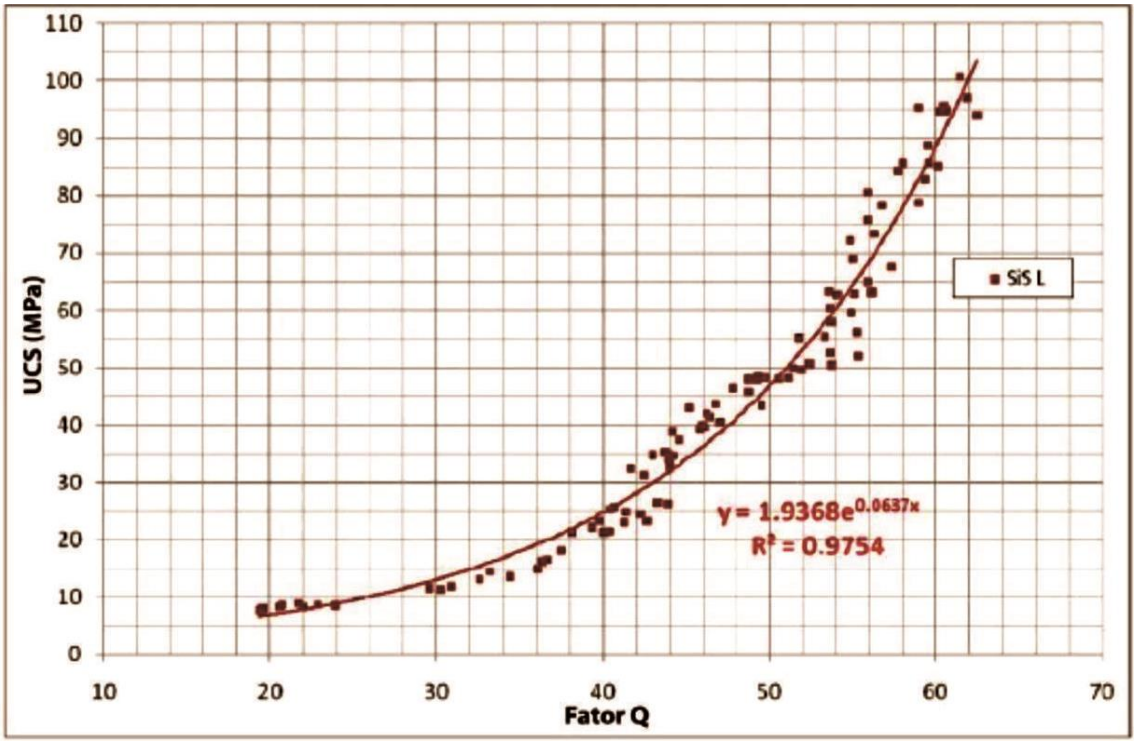

Fonte: Proceq

4 RESULTADOS

4.1 ARTIGO 1 – SOFT-SEDIMENT DEFORMATION STRUCTURES IN APTIAN LACUSTRINE LAMINITES: EVIDENCE OF POST-RIFT PALEOSEISMICITY IN THE ARARIPE BASIN, NE BRAZIL

Soft-Sediment Deformation Structures In Aptian Lacustrine Laminites: Evidence Of Post-Rift Paleoseismicity In The Araripe Basin, Ne Brazil

Márcio Lima Alencar[1]*, Osvaldo José Correia Filho[1], Tiago Siqueira de Miranda[2], José Antonio Barbosa[1], Maria Alcione Lima Celestino[2], Germano Mário Silva Ramos[1], Araly Fabiana Lima de Araújo[1], Virginio Henrique Neumann[2], João Gabriel de Oliveira Topan[1], Eduardo Roemers-Oliveira[3]

[1] GEOQUANTT, Pesquisa em Geociências, Departamento de Geologia - UFPE. Av da Arquitetura, s/n, Cid. Universitária, Recife, PE, Brazil - 50740550. mlimaalencar@gmail.com, osv.correia@gmail.com, jose.antoniob@ufpe.br, nonogermano@gmail.com, aralyfabiana23@gmail.com, gabrieltopan@gmail.com

[2] Departamento de Geologia, Universidade Federal de Pernambuco, Recife, PE, 50740-530, Brazil. tiago.smiranda@ufpe.br; alcionelimma22@gmail.com; neumann@ufpe.br;
*Corresponding author: e-mail: mlimaalencar@gmail.com; telephone: +55 81 2126-8240; postal address: Av. da Arquitetura, 953-995 - Cidade Universitária, Recife - PE, 50740-540, Brazil.
[3]Petrobras Research Center, Av. Horácio de Macedo, 950, Cidade Universitária. Ilha do Fundão, Rio de Janeiro, 21941-915, Brazil. roemers@petrobras.com.br

Abstract

Soft-sediment deformation structures (SSDS) represent synsedimentary structures that can be formed under different tectonic regimes and are considered of great importance for studies associated with the paleoseismic activity. SSDS represent depositional heterogeneities and play an important role in fluid flow, thus influencing hydrocarbon or groundwater reservoirs. This paper describes the SSDS in Aptian lacustrine finely laminated limestones of Crato Formation, the post-rift sequence of Araripe Basin, NE Brazil. SSDS occur in laterally continuous beds, with an average thickness of 5 cm. The set of studied structures comprises loop beddings, convolute laminations, micro faults, fluid escape structures, simple and pendulous load cast, and detached pseudonodules.

We interpreted that these structures resulted from seismic activity associated with brittle reactivation of the Patos shear zone, a major structure that borders the Araripe Basin. This interpretation points to a long history of post-rift tectonic activity of the Borborema Province (NE, Brazil). The diversity and abundance of these structures in these post-rift deposits show that this type of heterogeneities can be formed in tectonic-sedimentary sequences otherwise considered less, or non-affected, by seismic activities.

Keywords: Crato Formation, Tectonic Reactivation, Soft-sediment Deformation, Post-rift phase, Araripe Basin

1. Introduction

Soft-sediment deformation structures (SSDS) are ubiquitous in sedimentary deposits affected by liquefaction and fluidization processes (Singh and Jain 2007; Beck, 2011; Shangman, 2017). These processes occur when the sediment is unconsolidated, during deposition or immediately after that, under little influence of compaction, and are normally triggered by an increase in pore pressure (Mills, 1983; Neuwerth et al., 2006; Owen et al., 2011; Araújo-Gomes, 2013). Liquefaction processes can be caused by several natural mechanisms, the most important of which are earthquakes, tsunamis, and glaciations. Other mechanisms can also be implied as local variation in pore pressure, density contrast, and slope instability (Feng et al., 2016, 2017; Shanmugan, 2016, 2017). The term liquefaction is used, in general terms, to describe a process by which there is a change from solid to liquid state of a sedimentary body or layer (Allen, 1986). Liquefaction is produced by the sudden loss of cohesion, after which the grains become temporarily suspended in the fluid until grains become cohesive again (Lowe, 1975). The result of liquefaction is the fluidization of the unstable mass of sediments and the deformation of the sedimentary fabric (Frey et al., 2009; Owen et al., 2011). SSDS are quite common in both siliciclastics (Singh and Jain, 2007; Beck, 2011; Owen et al., 2011; Gao et al., 2019) and carbonate deposits (Ettensohn et al., 2011; Martin-Chivilet, 2011; Wallace and Eyles, 2015). SSDS occur in sedimentary rocks formed in a wide range of depositional environments such as lacustrine (Alfaro et al., 1997; Rodriguez-Pascua et al., 2000; Beck, 2011; Gladkov et al., 2016; Törő and Pratt, 2016), marine (Martín-Chivillet, 2011; Ettersohn et al., 2015; Wallace And Eyles, 2015), and fluvial (Obermeier, 2005; Owen et al., 2011; Santos et al., 2010). The study of SSDS is important because they represent sedimentary heterogeneities, which cause changes in petrophysical properties of the rock fabric and influence fluid flow in hydrocarbon

reservoirs as they can act as conduits or hydraulic barriers (Shanmugam, 2016; Gao et al., 2019; Liang et al., 2019; Novak and Egenhoff, 2019).

This paper is a sedimentological and structural study of SSDS in Aptian, lacustrine, finely laminated limestone (laminites) deposits of the Crato Formation, a post-rift sedimentary unit of the Araripe Basin in northeast Brazil (Assine et al., 2014; Miranda et al., 2018). The main objective of this study is to classify SSDS structures and define the possible mechanisms involved in their origin. The obtained results improve our understanding of the reactivation of basement structures that postdate the Cretaceous rifting that created the Araripe Basin. The opening of the South Atlantic rift is associated with the reactivation of Pre-Cambrian shear zones in the Borborema Province, NE Brazil, like the Patos Shear Zone that formed the northern border of Araripe Basin (Matos, 1999; Assine et al., 2014; Marques et al., 2014; Nogueira et al., 2015; Celestino et al., 2020).

Laminites of the Crato Formation have been investigated as an analog for some lithofacies found in large oil reservoirs of the pre-salt sequence of the Brazilian marginal basins (Catto et al., 2016; Santos et al., 2015; Zihms, 2017; Miranda et al., 2018). Thus, the research presented here also is important because it provides information about SSDS in reservoir rocks.

2. Geological Setting

The Araripe Basin represents the largest intracratonic basin of north-eastern Brazil, with an area of ~ 9,000 km² (Fig. 1a). This basin is located in the Central Domain of the Borborema Province, a tectonic collage of continental terranes that forms the north-eastern part of the South American plate (Santos et al., 2012; Van Schmus et al., 2011; Araújo et al., 2013; Neves et al., 2014; Celestino et al., 2020). The study area is located in the northern border of the Araripe Basin, which is bounded to the north by the PASZ, a regional-scale shear zone formed during the Pre-Cambrian. The stratigraphy of the Araripe Basin has been divided in four tectono-sequences: a) Paleozoic sequence, which includes Silurian-Devonian continental deposits of the Cariri Formation; b) Pre-rift sequence, composed of Tithonian continental deposits of the Brejo Santo and Missão Velha formations; c) Rift sequence, composed of Hauterivian-Berriasian continental deposits of the Abaiara Formation; d) Post-rift Sequence, which is subdivided in a Lower interval, formed by Aptian-Albian continental to transitional deposits of the Barbalha, Crato and Ipubi formations, as well as shallow-marine deposits of Romualdo Formation, and an upper interval formed by Upper Albian alluvial deposits of Araripina Formation and the Albian-Cenomanian fluvial deposits of the Exu Formation (Neumann, 1999; Assine, 2007; Assine et al., 2014). The Crato Formation is composed of Upper Aptian

post-rift lacustrine deposits, formed in the proximal domains of the basin during a period of cyclic lake level expansion events (Assine et al., 2014; Fabin et al., 2018).

According to Neumann (1999) and Neumann and Cabrera (1999), the Crato Formation is composed of Intervals of laminated limestones, with thickness varying from few meters up to 25 m, interbedded with siliciclastic deposits – clayey marls, calcareous siltstones, and claystones. The Crato unit possess six intervals of laminated limestones, named C1 to C6, which increase in thickness and aerial distribution from base to top of the formation (Neumann, 1999). This study focused on the uppermost C6 interval, which is well exposed in quarries and outcrops along the northern border of Araripe Basin (Martill et al., 2008; Assine et al., 2014; Fabin et al 2018) (Fig. 1).

Figure 1 – A) Geological map of the Araripe Basin (modified from Fabin et al., 2017); The red square marks the location of the study area; B) Detailed geological map of the study area showing the occurrence of Crato Formation deposits in the northern border of the basin, the faults associated with the Patos shear zone (Celestino et al., 2020), and studied outcrops; C) General view of exposures of the C6 interval of laminites in a quarry near the Nova Olinda city.

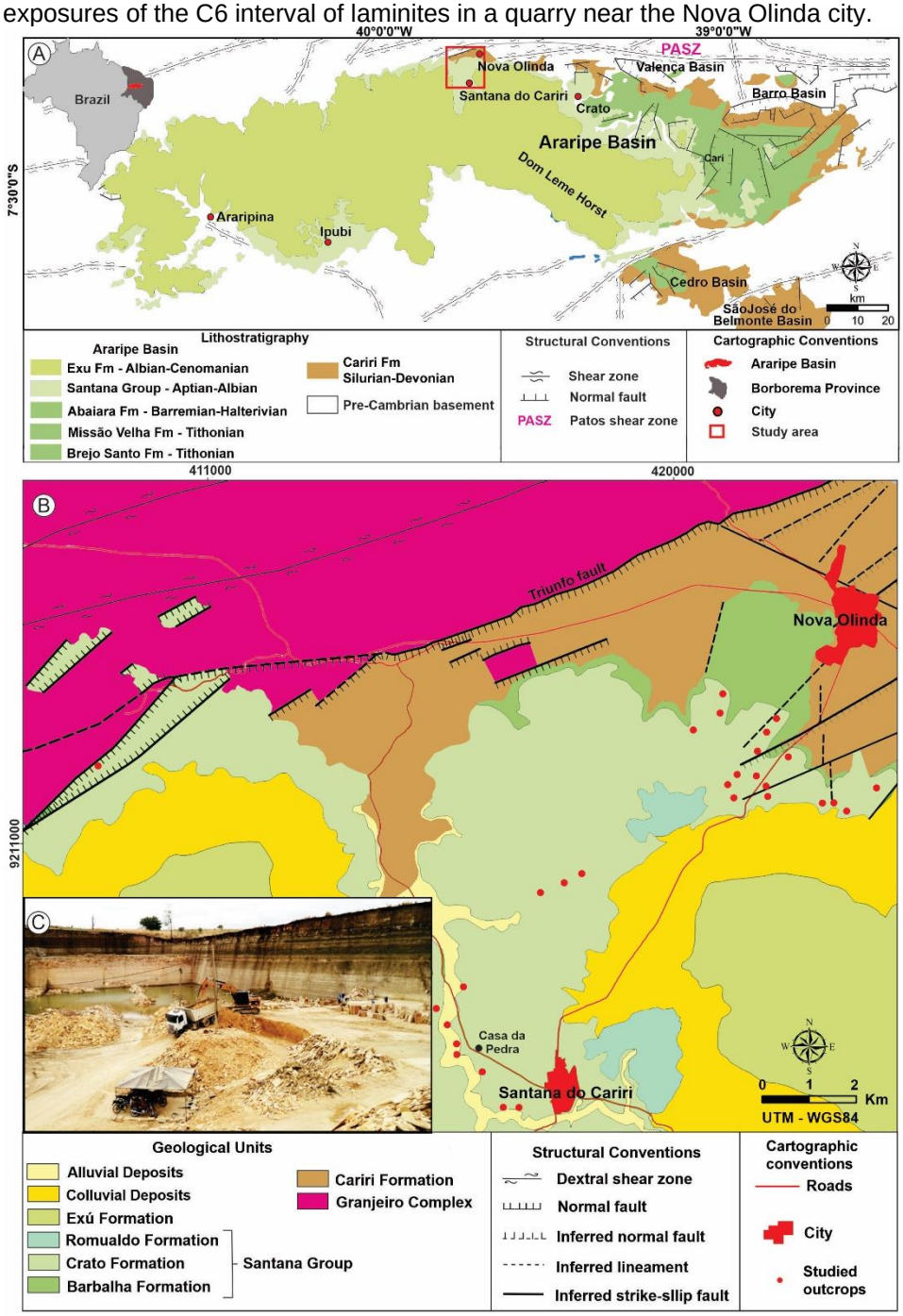

Source: The author

The laminites of the Crato Formation have been considered an analog for low-permeability laminite facies, that occurs in pre-salt reservoirs in the Barra Velha Formation (Gomes et al., 2020), Santos Basin, at the Brazilian southeastern margin. The laminites of studied C6 interval present similar parameters for petrophysical and

mechanical properties of reservoir lithofacies found in reservoirs of the pre-salt succession (Terra et al., 2010; Catto et al., 2016; Menezes et al., 2016; Zihms et al., 2017; Miranda et al., 2018). Interval C6 of the Crato Formation is composed of yellowish to grey laminae, and it varies from 10 to 15 m of thickness. These limestones were exposed during the Cenozoic, and show different levels of alteration due to meteoric weathering (local dissolution and oxidation of pyrite). Laminites of the Crato Formation is composed of micrite with variable content of bioclasts, which mainly consists of pellets, ostracod valves, algal filaments, and amorphous organic matter. Pyrite occurs as very fine euhedral crystals, and as aggregates of framboid pyrite (Neumann et al., 2003). The primary porosity of these rocks is about 4 to 5%, and permeability is very low, about 0,014 mD (Miranda et al., 2018). The limestone is composed of very fine parallel laminae of micritic mudstone, ranging from 0,5 to three millimeters in thickness. The main diagenetic aspects are early precipitation micro quartz and local substitution of calcite by fine crystals of dolomite, and late oxidation of Pyrite crystals (Neumann et al., 2003; Heimhofer et al., 2010), and local dissolution of calcite matrix, which resulted in the formation of secondary porosity. The origin of the fine calcite grains was attributed to the authigenic precipitation induced/mediated by microorganisms (Heimhofer et al., 2010). However, contributions of bottom algal growth also occurred (Warren et al., 2017). The depositional system was dominated by low energy and hypersaline conditions (Neumann et al., 2003; Martill et al., 2007; Heimhofer et al., 2010).

Various types of structures have been described in the laminites deposits: 1) Synsedimentary structures - loop beddings, convolute laminations, shear fractures, and breccias pipes (Fig. 2); 2) Diagenetic structures - centimetric vertical stylolites, millimetric to centimetric pyrite nodules, carbonate concretions, vertical calcite veins, horizontal and vertical gypsum veins (Neumann, 1999; Neumann et al., 2003; Martill et al., 2008; Miranda et al., 2018; Cabral et al., 2019). Previous work has pointed to the influence of seismic activity in the formation of some structures like convolute laminae, loop beddings, and synsedimentary shear fractures (Neumann, 1999; Alencar, 2018; Miranda et al., 2018). Ondulated and domic structures formed by laminations are possibly associated with microbial growth (Catto et al., 2016; Warren et al., 2017) and are not discussed in this research.

Figure 2 – Main structures of the Crato Formation. A) vertical stylolite; B) pyrite nodules; C) concretion; D) vertical calcite vein; E) oblique to vertical gypsum vein; F) horizontal gypsum vein.

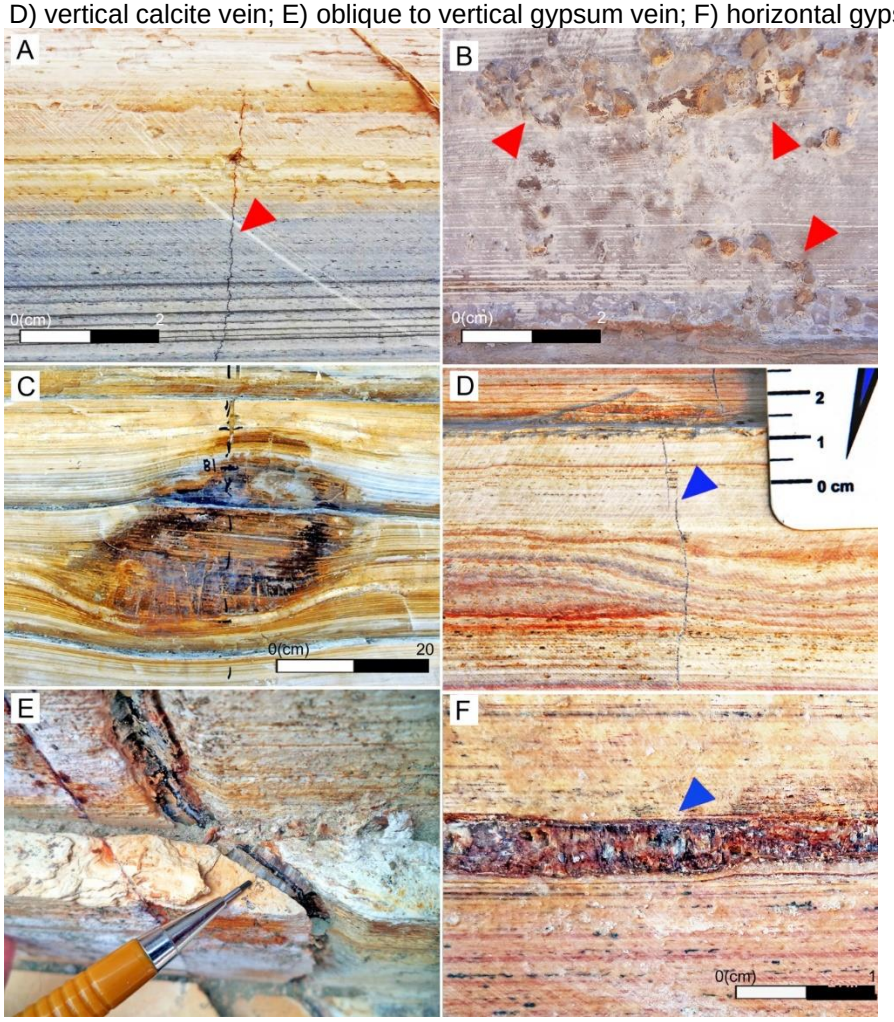

Source: The author.

3. Material and methods

Characterization and classification of SSDS in laminites deposits from the Crato Formation were carried out in 28 selected outcrops located along with the several quarries between the cities of Santana do Cariri and Nova Olinda (Fig. 1b). Outcrops used for the data collection in quarries are typically three-dimensional exposures with hundreds of meters of extension and thickness with up to 8 meters. Data collection has systematically focused on the identification of SSDS, the definition of its temporal relations with other structures indicated by cross-cutting and superposition effects. We have considered two main aspects for the characterization and classification of SSDS: a) the driving forces involved in the deformation, and b) the deformation mechanism (Neuwerth, 2006; Owen et al., 2011). The deformation mechanisms are generally related to liquefaction and fluidization processes. The driving forces are related to the interaction between pore fluid and cohesion of the rock fabric, and instability is caused by reverse density gradient, slumping, or shear stress (Anketel et al., 1970; Allen, 1977). Thus,

based on the characteristics of the SSDS, we have proposed the triggering mechanism and its possible origin.

4. Results

In the C6 interval of the Crato Formation, we identify and describe a variety of SSDS types: 1) loop beddings, 2) convolute laminations, 3) fluid escape structures, 4) Simple and pendulous load casts, 5) detached pseudonodules, 6) shear fractures, and 7) seismic breccia pipes.

4.1 Loop bedding

Loop bedding structures are abundant in the C6 limestone interval. These structures consist of bundles of laminae which exhibit local constriction, which forms a flattened elliptic geometry up to 3 cm wide, and 5 to 10 millimeters of height. Generally, various loop bedding structures occur in the same set of laminae, which forms loop beddings bearing-zones with lateral continuity of a few meters. This structure forms by local constriction, which produces a morphology of loops or links in a chain (Rodríguez-Pascua et al., 2000) (Fig. 3a-b). The high-frequency occurrence of loop bedding structures gives the laminae a boudinaged appearance. The internal part of loop bedding structures shows the rupture of the laminae, and the external area shows smooth undulations, which generates pinch-and-swell morphology (Törő and Pratt, 2016). All the outcrops show a repetition of isolated sets of laminae containing loop beddings, interbedded with undisturbed laminations.

4.2 Convolute laminations

Convolute laminations occur confined in specific sets of laminae across the studied outcrops (Figs. 3C and 3D). Deposits showing convolute bedding are alternating with deposits displaying undisturbed lamination. The thickness of beds formed by convolute laminae varies from 10 to 15 cm, and they present lateral continuity with tens to hundreds of meters. These structures are marked by a range of variable geometries such as domes, asymmetric and symmetric anticlinals, and synclinals folds with horizontal axes (Figs. 3C and 3D). Locally, beds formed by convolute lamination show lateral thickening and thinning, and it commonly shows a top non-parallel contact with overlying sets of laminae (Fig. 3C and 3D). Deposits with convolute laminations occur interbedded with undisturbed laminations.

4.3. Fluid escape structures

Fluid escape structures occur in deposits of laminites of C6 interval and form beds with an average thickness of approximately 12 to 20 cm (Figs. 3E and 3F). These structures show high lateral continuity tens to hundreds of meters in the studied outcrops. Laminites deposits affected by fluid escape show the complete disruption of laminae, and the destruction of parallel lamination by fast transient fluid flow indicates the high plasticity of these deposits at the time of deformation, which includes segmentation of laminations, the intense formation of folds, slumps, and dike-like structures constituted by homogenized sediments. Locally, the deformation caused the upper laminations partially to break and sink in the subjacent deformed horizon (Figs. 3E and 3F). Fluid escape structures occur mainly in the southern region of the study area, at the top of the C6 interval, interbedded with undisturbed deposits.

4.4 Simple and pendulous load casts

Simple and pendulous load casts (e.g., Owen, 2003; Neuwerth et al., 2006) are associated with deposits showing evidence of fluid escape structures. These structures form due to a load of more dense strata (yellowish material) that sink into the lower, less dense strata (brownish material seen in Figs. 3G and 3H). As seen in examples illustrated (Figs. 3G and 3H), the different colors of laminations resulted from variation in concentrations of organic matter and other minerals like pyrite and oxides, which was caused by variation in sedimentation rates, which influenced the pore water saturation and early diagenesis (Heimhofer et al., 2010; Osés et al., 2017). The brownish color observed in these deposits is mainly the result of oxidation of pyrite and oxide deposition due to the circulation of meteoric water in laminae more susceptible to dissolution during diagenesis. The simple load cast structures show beige color and rounded geometries, resembling a pillow-like shape (cm-scale) that occurs in the upper laminations of the fluidized zones (Fig. 3G and 3H). The laminations within the simple load cast show deformation in the border and the interior of the cast (Figs. 3G and 3H). The pendulous load casts display long and narrow geometries, with the longer axis varying from 2 to 7 cm. Some of the pendulous casts still preserve some connection with the overlying laminations (Fig. 3I and 3J). As observed for the simple load cast structures, pendulous load cast also shows deformation in the original laminations, which formed in the border and the interior of the cast.

These structures occur in the southern region of the study area, at the top of the C6 interval of laminites.

4.5 Detached pseudonodules

Detached pseudonodules (e.g., Neuwerth et al., 2006; Rodriguez-Pascua et al., 2000) occur in the form of fragments of laminites that sank into the deformed deposits. The laminae within these fragments are only slightly deformed and show variable dimensions, from 4 to 5 cm (Figs. 3I and 3J). These fragments present a slightly contorted elliptical shape. This type of structure occurs associated with fluid escape structures in deformed strata intervals, which range laterally from tens to hundreds of meters in the outcrops, interbedded with undisturbed deposits.

Figure 3 – Soft-sediment deformation structures formed in laminated limestones of C6 interval of the Crato Formation. Each photograph is accompanied by a schematic drawing that illustrates the structures. A-B) Detail of a loop bedding structure formed in a set of laminations of yellowish-white color, C-D) Convolute lamination with asymmetric and symmetric folds, E-F) Fluid escape structure formed by liquefied sediments of a brownish color injected in the overlying laminites. The injected sediment flowed laterally and formed a load cast, G-H) Simple load cast of beige color with rounded geometries with a pillow-like shape, I-J) Pendulous load cast (blue arrow) and detached pseudonodules (yellow arrow).

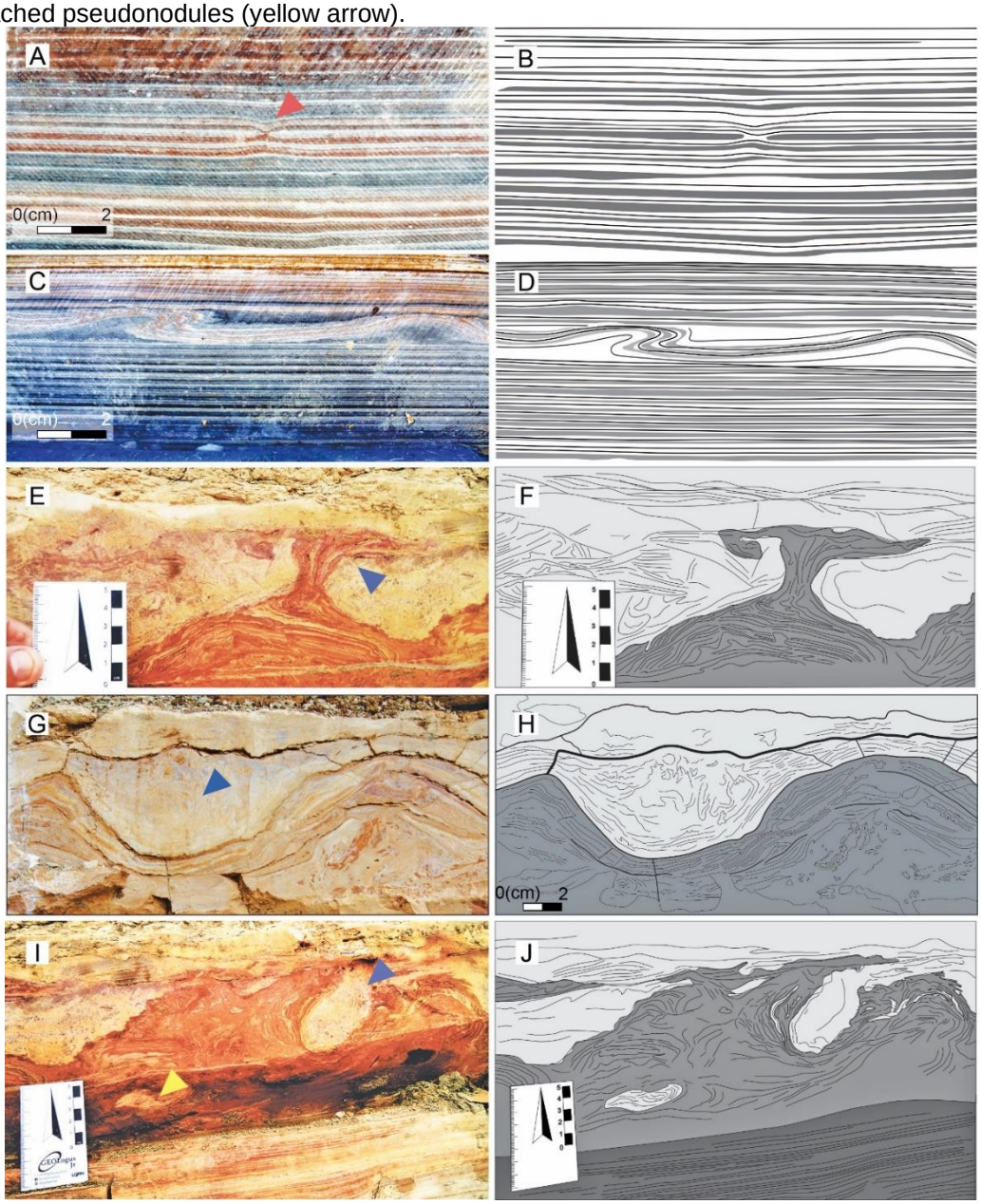

Source: The author.

4.6 Shear fractures

Synsedimentary shear fractures occur in the laminites of C6 interval and present centimeter to meters scale (Miranda et al., 2018). Fault throws ranges from 0,5 mm to 1 cm. Small fault planes show local branching and segmentation, with segments commonly showing an en-echelon pattern (Fig. 4A) (Childs et al., 2003). Shear fractures show

planar and listric planes with high and low dip angles (Figs. 4A and 4B). Larger listric planes are rooted in beds with convolute laminations and high lateral continuity and formed wide gentle rollovers (Figs. 4A, 4B, 6A, and 6B). The folding associated with the accommodation of plastic deformation generated fault planes with reverse displacement. The fault planes exhibit normal and reverse drag folds, which preserve evidence of the local reverse motion due to the plasticity of deposits and different timing of deformation (Figs. 4A and 4B). The brittle-ductile pattern of the faults is linked to the unconsolidated nature of the deposits. The plastic behavior of sediments also influenced the formation of isolated shear-mode fractures with small vertical to sub-vertical planes with 1,5 to 3 cm length. These micro faults cut a small number of laminae, with no evidence of deformation in overlying and underlying laminites (Figs. 4C and 4D). The shear fractures planes present two main trends that form conjugated pairs, with a preferential NNW-SSE direction (Fig. 4e).

Figure 4 – Shear-mode fractures of laminites of C6 interval of the Crato Formation. A-B) Shear fractures with local normal and inverse displacement that was controlled by the plasticity of the deposits during the deformation. The lower termination of the larger fault plane detached in a bed with convoluted laminations, C-D) Example of isolated small shear fracture, which cut a few laminations. The inset in C shows Lower-hemisphere, equal-area stereographic projection showing density contour of pole to normal faults. N, North (n=349).

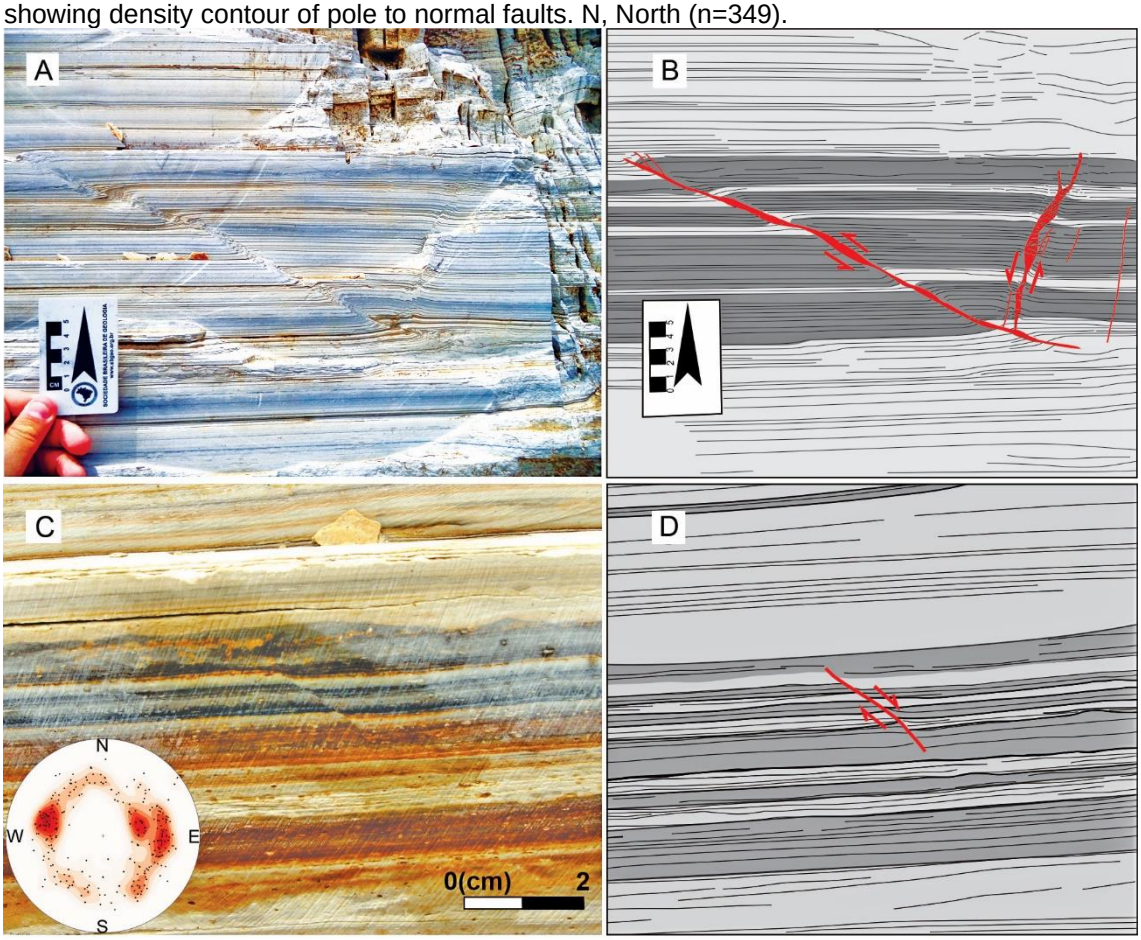

Source: The author.

4.7 Seismic breccia pipes

Seismic breccia pipes represent structures originated by hydro-fracturing or liquefaction processes (e.g., Shukla et al., 2018). Breccia pipe structures occur in the studied laminites in quarries in the northeast sector of the study area, mainly in the Três Irmãos Quarry. These structures are 1 to 2 m in diameter and a few meters height. The structures are filled with a breccia that is composed of a micritic matrix hosting limestone angular clasts of the laminite deposits, which were formed by fluid injection and liquefaction of the sediments. In the outcrops, the breccia pipes are particularly well exposed due to the removal of surrounding less resistant rocks (Figs. 5A and 5B). The structures form a vertical tube-like shape with brownish to dark bluish colors, which creates a clear contrast with the surrounding yellowish to beige laminites (Figs. 5C and 5D). One example (Fig. 5B) presents a circular section with a diameter of about 120 cm, which also exhibits various clusters of calcite veins (marked in yellow). The laminations

around the pipe structure present plastic deformation. They were warped upward due to the passage of the pressurized fluid through the unconsolidated laminite deposits (Figs. 5C and 5D). All the evidence suggests that the fluid injection upward occurred when the limestone was unconsolidated or partially consolidated. The formation of calcite veins concentrated in the pipe indicated that after the lithification these structures probably acted as conduits for the late processes of fracturing and fluid migration. The breccia pipes allowed the late formation of karst in its surrounding strata, due to meteoric processes (Figs. 5C and 5D).

Figure 5 – Examples of breccia pipes of the Crato Formation laminites. A) lateral view of the breccia pipe structure with brownish color exposed by the removal of surrounding rocks. The structure is filled with a breccia containing laminite clasts. B) Plan view of the pipe shown in A and its nucleus with the circular section seen in dark brownish color. The beige-colored rim around the pipe represents a zone of deformed laminations. Yellow lines mark the occurrence of calcite veins that occurs in the nucleus of the breccia. The diameter of the structure is about 1.2 m. C) Shows vertical section of another breccia pipe. The boundary between the breccia and the host rock was also affected by karstification processes. The laminites around the nucleus of the pipe structure are warped upward. D) Schematic draw of the photo shown in C.

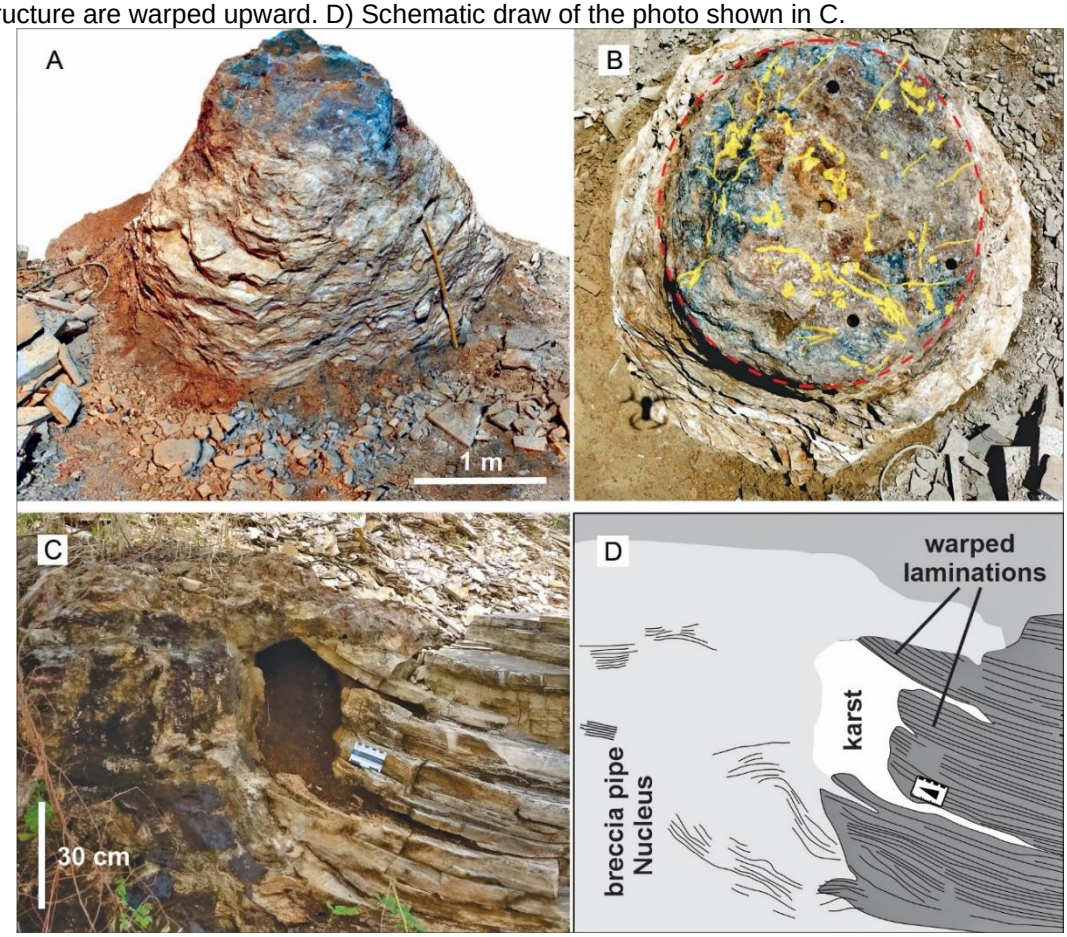

Source: The author

5. Discussion

5.1 Origin of the SSDS of Crato Formation C6 Interval

5.1.1 Loop beddings

Generally, loop bedding structures form in unconsolidated deposits under low-energy events, and the process does not involve liquefaction (Rodriguez-Pascua et al., 2000). The mechanism of deformation involves the extension of laminae caused by local stress (Calvo et al., 1998; Martin-Chivelet et al., 2011). These structures occur in layers that exhibit a contrast in mechanical competence and are common in lacustrine sediments (Calvo et al., 1998; Martin-Chivelet et al., 2011). The formation of these structures does not involve overload processes. In the studied laminite deposits the genesis of loop beddings involved the development of ductile deformation of shallow buried sediments. In the C6 interval of laminite deposits, loop bedding structures occur in specific zones, or intervals, alternating with deposits showing undisturbed laminations, which indicates they formed due to the effect of repeated events of increase in the internal tension. The loop bedding structures in the Crato Formation are quite similar to those described by Martin-Chivelet et al (2011) in the Jurassic microbialites of the Neuquén Basin, Argentina, which formed due to seismic activity under an extensional stress field.

5.1.2 Convolute laminations

According to the literature, there is not a single mechanism to explain the formation of convolute laminations (e.g., Allen, 1977; Neuwerth et al., 2006; Owen et al., 2011; Shanmungan, 2017). The conductive forces involved are related to drag, folding and inner laminations shearing (Owen, 1996; Neuwerth et al., 2006). Wallace and Eyles (2015) described remarkably similar features in Paleozoic deposits located in Southern Ontario, in the Ledgerock Quarry. The authors suggested that liquefaction and fluidization were the main mechanisms involved in the formation of these convolute structures. They also attributed the influence of seismic events on the generation of the convolute-bearing zones. Osés et al (2017) showed that variation in sedimentation rates produced differences in the diagenetic evolution of laminites in the succession of the C6 interval. Those differences, according to these authors, resulted in different amounts of pyrite and organic matter preservation within the cyclic deposition of the micrite laminae. The evidence about the variation in the sedimentation rates and the consequent amount of pore water in the laminae possible resulted in different levels of mechanical behavior in a millimetric to centimetric scale. Consequently, laminations with additional pore water content became more susceptible to the loss of cohesion during events of a sudden increase in energy (hydrostatic pressure). Different levels of internal cohesion were the

probable mechanism of deformation of stratigraphic intervals between undisturbed laminites, which absorbed the increase of internal energy with no deformation. The episodic occurrence of convolute laminations interbedded with undisturbed laminae across the succession points to seismic shocks as the cause of these events. The detachment of some shear fractures in beds with convolute laminations indicates that this type of instability allowed the simultaneous formation of other brittle-ductile structures in the unconsolidated deposits.

5.1.3 Fluid escape structures

Fluid escape structures are associated with the fluidization of specific beds, which creates a cavity and allows the ascension of sediment masses over-saturated with fluids through overlying strata (Owen, 1996). During the liquefaction process, the interstitial water contained in the over-saturated zones move upward, which created convolutions, folds, small faults, and dyke-like structures. According to Neuwerth et al (2006), this type of structure forms due to the transport of fluids to upper regions of the bedding caused by the instability of pore pressure in the unconsolidated sediment. The formation of fluid escape structures contributed to the formation of other types of SSDS as load casts that formed by fragments of unconsolidated limestones, which floated and sank inside of fluidized deposits. In other fine-grained lacustrine deposits, like the case studied here, these types of structures have been associated with the localized liquefaction caused by an increase in pore water pressure induced by seismic shocks (Rodriguez-Pascua et al., 2000; Singh and Jain, 2007). In lacustrine laminated micrites of the Fossil Butte Member, Eocene Green River Formation, localized fluid escape structures formed under the influence of paleo-earthquakes (Törő and Pratt, 2015a).

5.1.4 Simple and pendulous load casts

The occurrence of simple and pendulous load casts is associated with the same mechanisms and driving forces that can create fluid escape structures (Owen, 2003). They can be created by overload processes due to the difference of density/water saturation between sedimentary beds (Owen, 2003; Neuwerth et al., 2006). In these cases, gravitational instability drives the formation of structures in unconsolidated deposits. They can also be created due to the liquefaction and fluidization processes that produce complex deformation (Owen, 2003; Neuwerth et al., 2006) due to the increase in the pore pressure and related fluid flow within unconsolidated deposits (Owen, 2003).

In the laminites of the Crato Formation, these structures occur in intervals composed of laminites deformed by liquefaction. These beds present thickness that varies from 10 to 25 centimeters and lateral extension of tens to hundreds of meters. In these beds, the detachment of limestone fragments that sunk into the intervals of fluidized sediments formed the simple and pendulous load casts structures (Figs. 3E and 3I) (Owen, 2003; Neuwerth et al., 2006). Similar structures occur in Silurian turbidites from Aberystwyth Grits, central Wales (Owen, 2003), in Pleistocene lacustrine deposits of the Sant'Arcangelo Basin (Moretti and Sabato, 2007), as well as in carbonate deposits of the Kolankaya Formation, in the Denizli Basin (Topal And Skul, 2014).

5.1.5 Detached pseudonodules

The occurrence of pseudonodules is associated with the formation of fluid escape structures. The pseudonodules developed from the pendulous load cast structures. Part of the casts evolved due to the plasticity of the laminites and formed detached fragments that sunk into the liquified beds (Owen, 2003, Neuwerth et al., 2006; Topal and Skul, 2014). According to Owen (2003) and Topal and Skul (2014), the transition from load structure to detached pseudonodules is related to the increase in fluidization stages. An important point is a possible variation in terms of water saturation between the top and the base of the liquefied beds. The laminations in the upper part of the liquefied zone remained cohesive, while the lower region presents intense fluidization. The characteristics of the pseudonodules structures depend mainly on the dynamic viscosity contrast of the laminites (Alfaro et al., 2007; Topal and Skul, 2014).

5.1.6 Synsedimentary shear fractures

Investigation showed that the formation of synsedimentary shear fractures of the C6 interval involved the ductile-brittle behavior of the strata (Fig. 4A) (Calvo et al., 1998; Childs et al., 2003; Miranda et al., 2018). The geometries of the shear fractures and deformation of surrounding strata also indicate that they formed under a ductile-brittle regime (e.g., Puy-Alquiza et al., 2015; Yang et al., 2016). Literature shows that shear fractures are relatively abundant in unconsolidated deposits, and their size is generally of cm-scale (e.g., Puy-Alquiza et al., 2015; Yang et al, 2016). This type of fault occurs isolated and present vertical to sub-vertical orientations. Studies performed by Neuwerth et al (2006), in the Zarzal Formation, Western Colombia, suggested that synsedimentary faults may form due increase in pore pressure in unconsolidated sediments that are rigid enough to prevent liquefaction. Isolated shear fractures that occur in other laminated

lacustrine deposits are associated with the sudden increase in the internal pore pressure tension due to seismic shocks (Puy-Alquiza et al., 2015).

The origin of shear fractures in the laminites of Crato formation is associated with beds that undergo liquefaction and plastic deformation (Fig. 6). The formation of meters-scale shear fractures is linked to the development of these beds with convolute laminations that present high lateral continuity. The internal mechanical instability of these planar and continuous beds allowed the creation of the larger faults (Fig. 4A). The creation of unstable horizons and the consequent accommodation of tension in the less plastic interbedded deposits created the low and high angle planes of discontinuity and gentle rollovers structures (Fig. 6) that induced the formation of local reverse faults (Fig. 4). Local folding of strata linked to the formation of wide and gentle rollovers accommodated deformation between the fault planes (Figs. 6A and 6B). The large faults present differences in the amount of throw along the planes. This aspect is common along the fault slip in deposits with plastic and viscous behavior. It is caused by the heterogeneous stress and displacement fields developed in surrounding deposits along the fault plane. Reverse drag (drag is opposite to the sense of fault slip) in normal faults are also related to local deformation along the fault plane. This effect is a function of the angle of the faults, their length, and the competence of the host rocks (Grasemann et al., 2005; Katz and Reches, 2006). Synsedimentary faults generated by tectonic seismic shocks in laminated micrites of the Eocene Green River Formation, Wyoming, show normal, reverse and thrust geometries. In this case, fault-related folds and micro faults were generated by seismic shaking induced by paleo-earthquakes (Törő and Pratt, 2015a, 2015b). They suggest that the coeval occurrence of intrastratal compression and dilation indicates that the chaotic nature of seismic shaking generated variably oriented shear stresses (Törő and Pratt, 2016).

Figure 6 – Relationship between shear fracture and beds with convolute lamination of the Crato Formation. A) Detail of a shear fracture formed from a basal detachment within a bed with convolute laminations. B) A low-angle shear fracture that also formed from a basal interval with convolute bedding, which propagated and cut an upper bed with convolute laminations. C) Schematic diagram detailing geometric aspects seen in B.

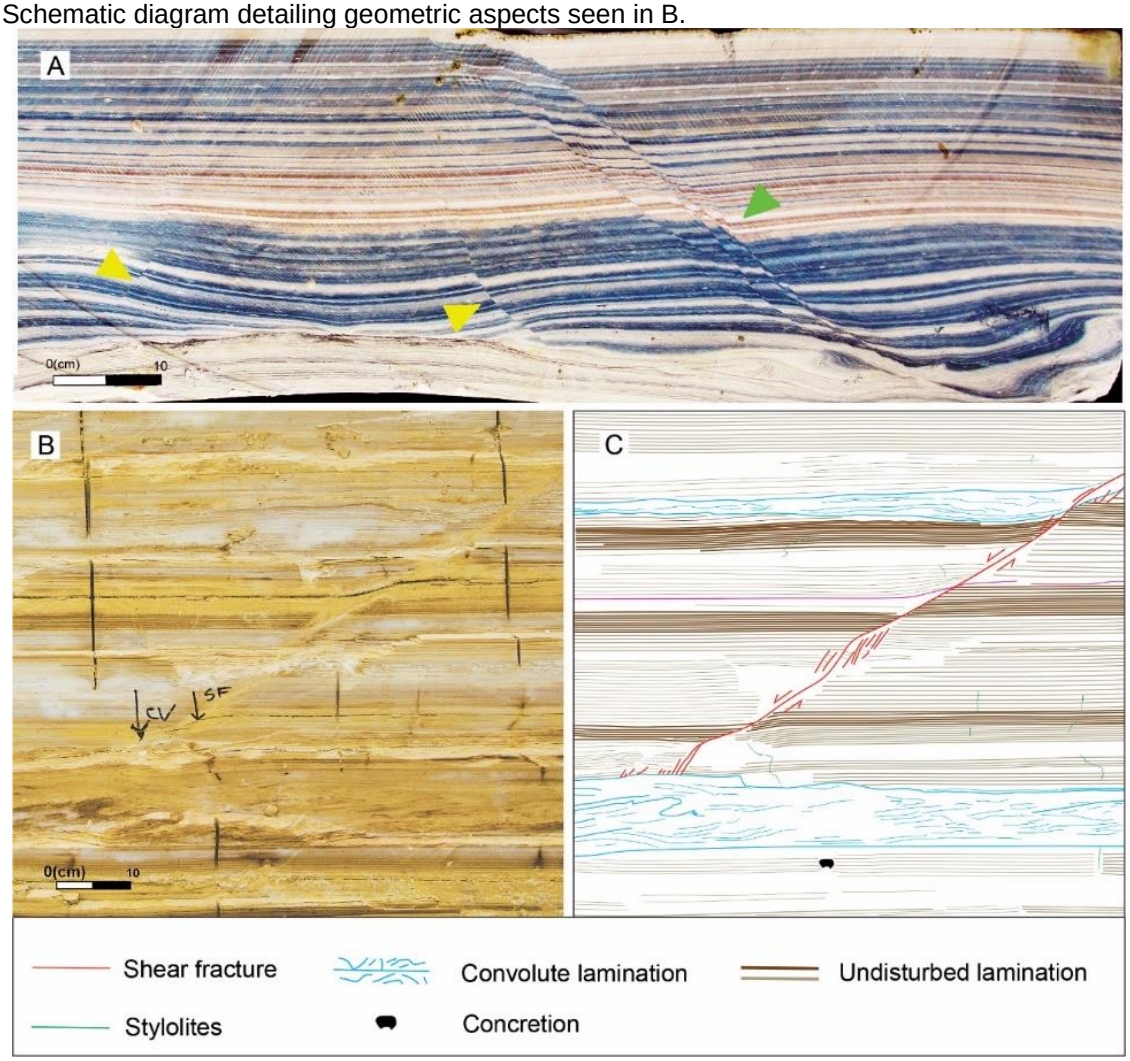

Source: The author

Based on the sedimentological evidence and similarities with other seismites described in fine-grained sediments, we suggest that Paleo-earthquakes probably caused the increase in pore pressure that induced the deformation of unconsolidated deposits of C6 interval under shallow burial conditions (Törő and Pratt, 2016), and originated the formation of shear fractures.

5.1.7 Seismic breccia pipes

Martill et al. (2008) described the occurrence of three pipe-like structures that cut and deformed the laminites of the C6 interval. These authors explained that these structures were sub-cylindrical in plan view. Laminite clasts filled the pipes and the authors referred to these structures as "dolomite pipes" because they found it contained

calcite, dolomite, and goethite. They suggested that the presence of brecciated clasts and homogenized filling matrix indicated a hydro-fracturing mechanism, possibly linked with the injection of fluids from paleoaquifers of the underlying sandstones of Cariri Formation. They proposed that water injection occurred during the earliest burial stages of the laminites. Our results showed that these vertical circular structures, which involved local liquefaction and brecciation, were created by the abrupt injection of overpressured water through the unconsolidated laminites (Fig. 5). We reinforce the proposition that seismic shocks caused the increase in the hydraulic pressure of porous rocks from the Cariri Formation (Martill et al., 2008), and the consequent water injections through the laminites of C6 interval. This study also confirms that the formation of pipe-like structures with brecciated material occurred during shallow burial because the surrounding laminites showed plastic deformation at the time of the fluid intrusion (Fig. 5). Hydraulic-fracturing induced by earthquakes can cause liquefaction of unconsolidated deposits or the formation of breccias, which consists of angular fragments of the host rock (intraclasts) with original sedimentary structures (Shukla and Sharma, 2018). Whetlay et al. (2016) described clastic pipes that occur in aeolian Jurassic strata of Colorado Plateau, and that represents an example of liquefaction and fluidization caused by earthquakes. The lack of syn-formational volcanic-related minerals or high-temperature products, linked to hydrothermal/volcanism triggering mechanism, reinforces the earthquakes hypothesis (Shukla and Sharma, 2018). The occurrence of other SSDS, which are associated with earthquakes in the C6 interval, like syn-depositional shear fractures and loop beddings, also contributes to the interpretation of earthquakes as the causal mechanism for the breccia pipes.

5.2 Triggering mechanism of SSDS of the laminites of Crato Formation

Liquefaction of sediment is a primary process responsible for the mechanism formation of SSDS that occurs in both clastic and carbonate rocks (Shanmungan, 2016). The triggering is a natural agent that enables the formation of SSDS due to the change of the solid-like deposit to a liquid-like state (Owen et al., 2011). The external agent causes internal tension increase, which disturbs the deposits by changing its physical properties causing loss of shear strength, which initiates the sediment failure and movement (Shanmugan, 2015). According to Shanmugan (2012, 2015, 2016), there are at least 21 processes-triggering agents associated with the formation of SSDS. These mechanisms are related to tectonic events, glaciation, and overload. We can divide these agents into three groups according to the estimated duration of the event: 1) short-

duration events, from few minutes to days (earthquakes, volcanic eruptions, meteorite impacts, tsunamis, tropical cyclones), 2) intermediate-duration, hundreds to thousands of years (tectonic events and glaciations), 3) long-duration events, thousands to millions of years (regressive events controlled by the sea-level change) (Shanmugam, 2012, 2016). To define the mechanism involved in the formation of SSDS that occur in laminites of Crato Formation we highlight the following aspects: 1 - centimetric beds with convolute structures and loop beddings occur repeatedly and interbedded with undisturbed laminites through the succession. This evidence indicates a mechanism of high energy and short-time duration (Owen et al., 2011; Shanmungam, 2016); 2 - beds affected by the loss of cohesion present high lateral continuity with tens to hundreds of meters; 3 - shear fractures and loop beddings are commonly associated with the effect of earthquakes in unconsolidated deposits formed in low energy environments (e.g. lakes); 4 - Fluid intrusion from basal deposits through the laminites suggests the occurrence of short-time events with high increase in the pore-fluid pressure which caused the hydraulic-fracturing of unconsolidated deposits.

There is no evidence of overload processes as the triggering mechanism that is commonly associated with lithological contrasts between interbedded deposits, like coarse sandstones and claystone (Moretti and Sabato, 2007), which present different cohesion states after deposition. The laminite succession is dominantly composed of micrite-dominated mudstones. Small variations in water saturation allowed the local deformation of specific beds due to a fluid escape driven process, but the increase in fluid pressure was not triggered by vertical loading. The deposition of laminites occurred in the proximal domains of the basin during the post-rift phase within a regional sag tectonic-stratigraphic configuration in low energy environments with very low-gradient settings (Neumann, 1999; Assine et al., 2014; Fabin et al., 2018). There are no evidence of gravity flows, slides, or slumps (Assine et al., 2007) that could be traced as the origin of the mechanical instability and deformation of the laminites. There is no record of the coeval occurrence of processes like glaciations, meteorite impact and volcanism during the deposition of the laminites (Assine, 1992; Neumann, 1999; Assine et al., 2014) that can be pointed as the trigger of seismic shocks (Shanmungam, 2016).

SSDS formed in lacustrine laminated micrites from the Eocene Green River Formation, Wyoming, and show good similarities with structures described in this work (Törő and Pratt, 2015a, 2015b). The structures described were formed by liquefaction, brittle-ductile, and plastic deformation of unconsolidated deposits (convolute lamination, micro-faults, fault-related folds, loop beddings, load structures, and breccias). These authors attributed their origin to syndepositional tectonic seismic shocks based on the

recurrence of deformed beds in different stratigraphic levels, the lateral extent of deformation structures, and similarity with structures naturally and experimentally produced by seismic shocks (Törő and Pratt, 2015a, 2015b; 2016).

The studied SSDS of Crato Formation present criteria that point to paleo-earthquakes (seismic shocks) as the triggering agent: the areal extent of deformed deposits, high lateral continuity of disturbed zones, stratigraphic recurrence of disturbed deposits, and morphology comparable with structures formed by liquefaction linked to recent earthquakes (Montenat et al., 2007; Martin-Chivillet et al., 2011; Owen And Moretti, 2011).

5.3 Origin of seismic activity that formed the SSDS of Crato Formation

The identification of structures formed by seismic activities in unconsolidated deposits as seismites presents a conceptual question: seismic activity can be triggered by many types of geological processes (Shanmugan, 2017)? Thus, it is necessary to define the relationship between the structures with tectonic activities and paleo-earthquakes. In this case, the post-rift reactivation of large shear zones that controlled the formation of the basins within the Borborema Province is the possible tectonic process that acted as the triggering agent (Fig. 1). The South Atlantic rift in the eastern border of the Borborema Province lasted until Early Albian, the same age of the deposition of the laminites (Matos, 1992, 1999; Turner et al., 2008; Caixeta et al., 2014; Buarque et al., 2016). This process possibly induced brittle reactivation of large shear zones complexes in the Borborema Province, including the PASZ (Fig. 1), where the interior rift that formed the Araripe Basin has ceased at this time. Celestino et al. (2020) showed that the Triunfo Fault (Fig.1) in the study area presents evidence of several brittle reactivation events, ranging from the Paleozoic to the Cretaceous, and remained active during the post-rift phase under an extensional regime. This data suggests that these faults near the basin´s border were the source of the seismic shocks that impacted the unconsolidated laminites.

To understand the hole of shear zones in the tectonic reactivation of the basement in the Borborema Province, one can observe that after the South Atlantic break up since the Late Cretaceous, evidence shows that a new tectonic regime is installed in the Borborema Province characterized by N-S distension and E-W compression (Bezerra et al., 2014). This regime is controlled by the reduction of spreading velocity of the Atlantic oceanic plate and the frictional effect of the Pacific oceanic plates against the South American plate, which was responsible for the

formation of the Andes Mountains (Ramos and Folguera, 2009; Marques et al., 2013; Bezerra et al., 2020). The Cenozoic sedimentary record shows that this tectonic regime created syndepositional deformation in marginal and interior basins (Bezerra et al., 2008; Rossetti et al., 2011a, b; Gandini et al., 2014; Nogueira et al., 2015), mainly controlled by the large shear zones (Ferreira et al., 2008; Bezerra et al., 2011; 2020). We suggest that in similar terms, the rift in the border of the Borborema Province produced tectonic reactivation of the shear zones in the interior basins and paleo-earthquakes that affected the Early Albian laminites. The historical record of earthquakes in the Borborema Province with a magnitude up to 5M is shown in Figure 7, which encompasses events recorded from 1986 until the present (Bezerra et al., 2011). The earthquakes are concentrated along the main shear zones, including shear zones like the PASZ in the northern border of Araripe Basin (Bezerra et al., 2011; 2020). In the studied case, the causal agent is proposed based on the proximity of the deposits to the PASZ (Fig. 7) and the long-time evidence of tectonic reactivation of the Borborema shear zone system related to different regimes since the Early Cretaceous (Matos, 1999; Assine et al., 2007; Miranda et al., 2020).

The main implication of the formation of seismites in the post-rift laminites deposits of Araripe Basin is the contribution to the understanding of the occurrence of this type of structure in deposits formed in areas considered as quiescent in terms of tectonics. Furthermore, as seismites represents structures associated with the modification of primary petrophysical rock properties like permeability and porosity, they can form important heterogeneities (hydraulic barriers or conduits) (Shanmugam, 2017), with high lateral continuity. Thus, the correct interpretation of their nature and origins is relevant for economic purposes, and as demonstrated in the present study the formation of seismites in post-rift deposits needs to be considered.

Figure 7 – Map of Borborema Province with sedimentary basins and the main shear zones. The map also shows the record of earthquakes, their magnitude, and distribution in the recent period. The earthquakes are concentrated in the shear zones. Note the proximity between the Patos shear zone (pink line) and the Study Area. (Modified from Bezerra et al., 2011, 2020).

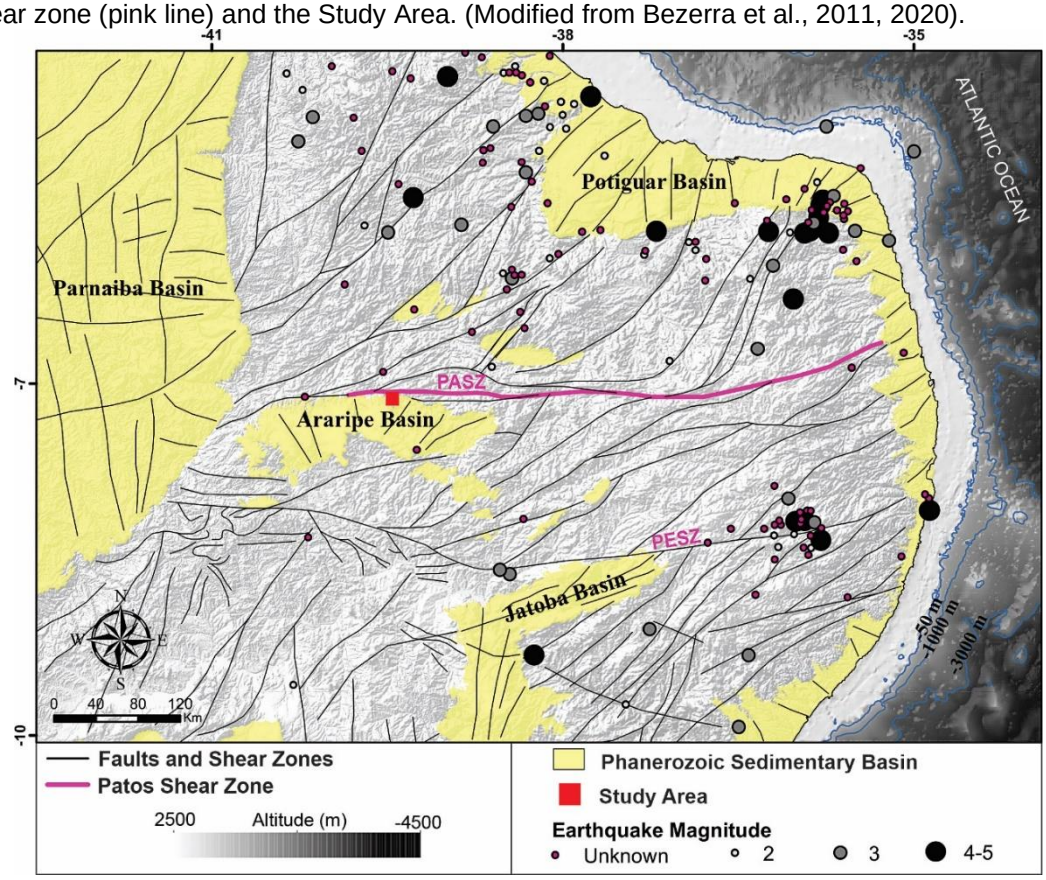

Source: The author.

5.4 Estimation of magnitude of seismic events based in the sedimentary record

Considering the tectonic origin of the SSDS and the excellent information provided by the outcrops we have tried to determine the intensity of the seismic shocks (paleo-earthquakes) that created the seismogenic structures. This interpretation was guided by studies that treated the correlation between the intensity of paleo-earthquakes and characteristics of SSDS (Sims, 1975; Allen, 1986; Calvin et al., 1998; Moretti, 2000; Rodriguez-Pascua et al., 2000). These studies have been developed in the last few decades, helped by the observation of present-day structures formed by seismic events since the term seismite was first used by Seilacher (1969). Figure 8 shows the relation between structures formed in unconsolidated deposits and the relative magnitude involved in its generation (Rodriguez-Pascua et al., 2000). The intensity of paleo-earthquakes is estimated according to the Richter scale (Richter, 1935). Several qualitative studies proposed that the minimum earthquake magnitude to trigger liquefaction was M > 5 (Rodriguez-Pascua et al., 2000; Wang et al., 2006; Green et al., 2019). Loop beddings represent SSDS not related to liquefaction and associated with

low-intensity events M < 5 (Calvo et al., 1998; Rodriguez-Pascua et al., 2000). Similarly, Neuwerth (2006) proposed that synsedimentary shear fractures could be generated by seismic energy events not associated with liquefaction, with magnitudes M < M5. Seismogenic convolute laminations are associated with liquefaction mechanism, and the estimation of the related trigger seismic energy is M > 5 (Rodriguez-Pascua et al., 2000; Neuwerth, 2006; Araújo-Gomes, 2013). Some SSDS observed in the C6 interval are linked to liquefaction mechanism (disruption of laminations, dike-like and fluid escape structures, breccia pipes, and load cast structures) (Allen, 1986; Unjoh et al., 2012; Shelley, 2015; Zhi-Xiong et al., 2015). The estimation of relative seismic energy necessary to generate these structures is M > 6 (Fig. 8). The estimative of the intensity of seismic events that formed SSDS of Green River Formation, similar to which occur in laminites of Crato Formation, pointed to minimum magnitudes between 6 and 7 (Törő and Pratt, 2016).

Other studies treated the relative distance between the location of the structures and the location of the source of the paleo-seismic events (epicenter) (Scott And Price, 1988; Obermeier et al., 2005; Gladkov, 2016). Based on these studies we suggest that the source of the paleo-seismic shocks, that generated the liquefaction/fluidization in deposits of the C6 interval, was located within a radius of 20 km of the study area. That is very compelling information, considering that the distance between the border of the basin formed by the PASZ shear zone and the studied outcrops is about 10 km (Figs. 1 and 7).

Figure 8 – Summary of Soft-sediment deformation structures types that occurs in the lacustrine laminites of the Crato Formation and the interpretation of the relative magnitude (Richter scale) of the paleo-earthquakes that generated the deformation in the unconsolidated deposits (modified from Rodriguez-Pascua et al., 2000).

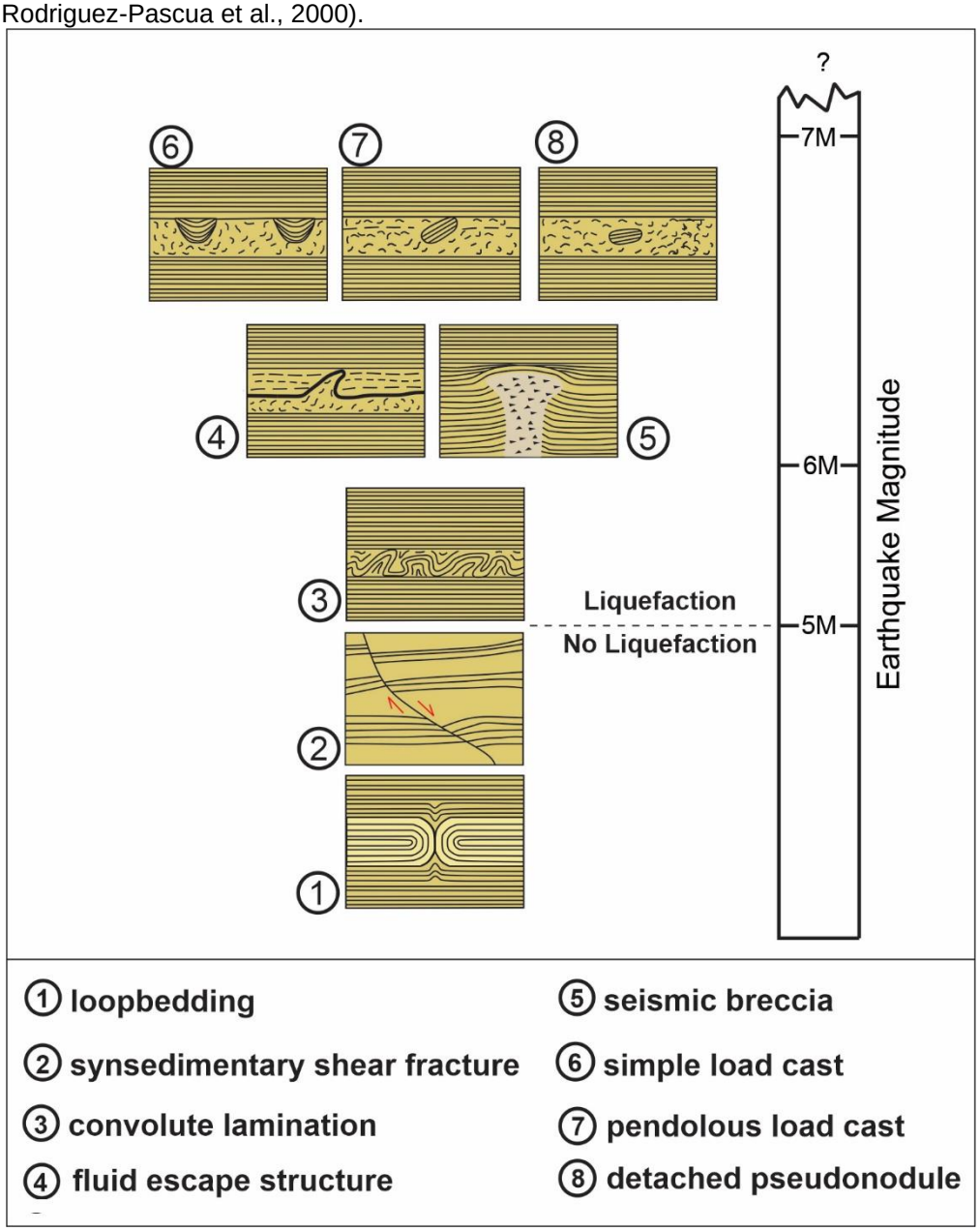

Source: The author.

6. Conclusions

Based on the integrated analyses of soft-sediment deformation structures that occur in laminites deposits of the C6 interval of the Crato Formation, we suggest the following conclusions:

1 - Abundant SSDS occur in the C6 interval of laminites of the Crato Formation. The record also shows a high diversity of structures, which encompasses loop beddings, shear fractures, convolute laminations, fluid escape structures, cast load structures

(simple and pendulous load cast, and detached pseudonodules), and seismic breccia pipes. The mechanisms involved in their formation were liquefaction and plastic (brittle-ductile) deformation; 2 - The evidence found (repetition of beds with deformed laminites between undisturbed laminations, lack of lithological contrast between the laminae that composes the laminites, high lateral continuity of disturbed stratigraphic intervals, the large areal extent of the SSDS) allowed to suggest that seismic shocks, paleo-earthquakes, were the triggering agent that impacted the unconsolidated deposits of the C6 interval and created the SSDS; 3 - The tectonic reactivation of shear zones of the basement near the studied area was the source of the seismic shocks that generated the SSDS. During the post-rift phase of Araripe Basin (Early Albian), the South Atlantic rift was still active in the eastern border of NE Brazil, and the propagation of tectonic stress along the shear zones possibly was the cause of seismic shocks. The brittle reactivation of the Borborema Province shear zone system in NE Brazil, under different tectonic regimes, continued during the Cenozoic and Recent times as proved by the historical seismic record and the sedimentary record; 4 - Considering the qualitative models used to estimate the magnitude of the seismic events necessary to generate SSDS, we estimate that the paleo-earthquakes that impacted the unconsolidated deposits of the C6 interval varied from $M < 5$ to $M > 6$. The estimation based on analog studies of the distance of seismic shocks capable of generating different types of SSDS indicated that the seismogenic source was in a radius within 20 km of the studied outcrops. Thus, we suggest that the PASZ, which is 10 km far from the studied area, was the source of tectonic earthquakes.

Acknowledgments

This study was supported by Petrobras that funded the projects "Crato" and "Pseudo-poços" through research agreements approved by the National Agency of Petroleum, Natural Gas and Biofuels (ANP). We thank Casa da Pedra – UFRJ, located in Satana do Cariri, CE, which provided crucial logistic support to fieldwork. Special thanks to Michangelo Martini and two other anonymous reviewers who helped to improve the manuscript.

References

Alencar, M.L., 2015. Caracterização dos Estilólitos Verticais do Nível Superior dos Calcários Laminados da Formação Crato, Borda Norte da Bacia do Araripe. Master's thesis. Federal University of Pernambuco. https://doi.org/10.1109/robot.1994.350900

Alfaro, P., Moretti, M., Soria, J.M., 1997. Soft-sediment deformation structures induced by earthquakes (seismites) in pliocene lacustrine deposits (Guadix-Baza Basin, Central Betic Cordillera). Eclogae Geol. Helv. 90, 531–540.

Allen, J.R.L., 1986. Earthquake magnitude-frequency, epicentral distance, and soft-sediment deformation in sedimentary basins. Sediment. Geol. 46, 67–75. https://doi.org/10.1016/0037-0738(86)90006-0

Allen, J.R.L., 1977. The possible mechanics of convolute lamination in graded sand beds. J. Geol. Soc. London. 134, 19–31. https://doi.org/10.1144/gsjgs.134.1.0019

Anketel, J.M., Cegla, J., Dzulynski, S. 1970. On the deformational structures in systems with reversed density gradients. N. Soc. Géol Pologne, 40(1): 3-30.

Araújo-Gomes, J., 2013. Deformações em sedimentos finos não consolidados interpretadas como sismitos. Finisterra 48, 125–138. https://doi.org/10.18055/finis3135

Assine, M.L., 1992. Análise Estratigráfica da Bacia Do Araripe, Nordeste Do Brasil. Rev. Bras. Geociências 22, 289–300. https://doi.org/10.25249/0375-7536.1992289300

Assine, M.L., 2007. Bacia do Araripe. Bol. de Geociencias da Petrobras 15, 371-389.

Assine, M. L., Perinotto, J. A. J., Custódio, M. A., Neumann, V. H., Varejão, F. G., Mescolotti, P. C., 2014. Sequências Deposicionais do Andar Alagoas da Bacia do Araripe, Nordeste do Brasil. Bol. de Geociências da Petrobras, Rio de Janeiro, 22:3-28.

Beck, C., 2011. Lake sediments as late Quaternary paleoseismic archives: Examples in the northwestern Alps and clues for earthquake-origin assessment of sedimentary disturbances. Spec. Pap. Geol. Soc. Am. 479, 159–179. https://doi.org/10.1130/2011.2479(07)

Bezerra, F.H.R., Rossetti, D.F., Oliveira, R.G., Medeiros, W.E., Neves, B.B.B., Balsamo, F., Nogueira, F.C.C., Dantas, E.L., Andrades Filho, C., Góes, A.M., 2014. Neotectonic reactivation of shear zones and implications for faulting style and geometry in the continental margin of NE Brazil. Tectonophysics 614, 78–90. https://doi.org/10.1016/j.tecto.2013.12.021

Bezerra, F.H., de Castro, D.L., Maia, R.P., Sousa, M.O.L., Moura-Lima, E.N., Rossetti, D.F., Bertotti, G., Souza, Z.S., Nogueira, F.C.C., 2020. Postrift stress field inversion in the Potiguar Basin, Brazil – Implications for petroleum systems and evolution of the equatorial margin of South America. Mar. Pet. Geol. 111, 88–104. https://doi.org/10.1016/j.marpetgeo.2019.08.001

Bezerra, F.H.R., Brito Neves, B.B., Corrêa, A.C.B., Barreto, A.M.F., Suguio, K., 2008. Late Pleistocene tectonic-geomorphological development within a passive margin - The Cariatá trough, northeastern Brazil. Geomorphology 97, 555–582. https://doi.org/10.1016/j.geomorph.2007.09.008

Bezerra, F.H.R., do Nascimento, A.F., Ferreira, J.M., Nogueira, F.C., Fuck, R.A., Neves, B.B.B., Sousa, M.O.L., 2011. Review of active faults in the Borborema Province, Intraplate South America - Integration of seismological and paleoseismological data. Tectonophysics 510, 269–290. https://doi.org/10.1016/j.tecto.2011.08.005

Bezerra, F.H.R., Takeya, M.K., Sousa, M.O.L., do Nascimento, A.F., 2007. Coseismic reactivation of the Samambaia fault, Brazil. Tectonophysics 430, 27–39. https://doi.org/10.1016/j.tecto.2006.10.007

Buarque, B. V., Barbosa, J.A., Oliveira, J.T.C., Magalhães, J.R.G., Filho, O.J.C., 2017. Carbonate buildups in the Pernambuco Basin, NE Brazil. An. Acad. Bras. Cienc. 89, 841–857. https://doi.org/10.1590/0001-3765201720160544

Cabral, F.A.A., Silveira, A.C., Silva Ramos, G.M., Miranda, T.S., Barbosa, J.A., De Miranda Lopes Neumann, V.H.M.L., 2019. Microfacies and diagenetic evolution of the limestones of the upper part of the Crato Formation, Araripe Basin, northeastern Brazil. Brazilian J. Geol. 49. https://doi.org/10.1590/2317-4889201920180097

Caixeta, J.M., Ferreira, T.S., Jr, D.L.M., Teixeira, J.L., Romeiro, M.A.T., 2014. Albian Rift Systems in the Northeastern Brazilian Margin: An Example of Rifting in Hyper-Extended Continental Crust. Int. Conf. Exhib. Istanbul, Turkey, Sept. 14-17, 2014, AAPG 2014 30378, 13. https://doi.org/10.1314/RG.02.1.3300.9769

Calvo, J.P., Rodriguez-Pascua, M., Martin-Velazquez, S., Jimenez, S., De Vicente, G., 1998. Microdeformation of lacustrine laminite sequences from Late Miocene formations of SE Spain: An interpretation of loop bedding.

Sedimentology 45, 279–292. https://doi.org/10.1046/j.1365-3091.1998.00145.x

Catto, B., Jahnert, R.J., Warren, L.V., Varejao, F.G., Assine, M.L., 2016. The microbial nature of laminated limestones: Lessons from the Upper Aptian, Araripe Basin, Brazil. Sediment. Geol. 341, 304–315. https://doi.org/10.1016/j.sedgeo.2016.05.007

Celestino, M.A.L., Miranda, T.S., Mariano, G., Alencar, M.L., Carvalho, B.R.B.M., Falcão, T.C., Topan, J.G., Barbosa, J.A., Gomes, I.F., 2020. Fault damage zones width: Implications for the tectonic evolution of the northern border of the Araripe basin, Brazil, NE Brazil. J. Struct. Geol. 138, 104-116. . https://doi.org/10.1016/j.jsg.2020.104116

Childs, C., Nicol, A., Walsh, J.J., Watterson, J., 2002. The growth and propagation of synsedimentary faults. J. Struct. Geol. 25, 633–648. https://doi.org/10.1016/S0191-8141(02)00054-8

Ettensohn, F.R., Zhang, C., Gao, L., Lierman, R.T., 2011. Soft-sediment deformation in epicontinental carbonates as evidence of paleoseismicity with evidence for a possible new seismogenic indicator: Accordion folds. Sediment. Geol. 235, 222–233. https://doi.org/10.1016/j.sedgeo.2010.09.022

Fabin, C.E., Correia Filho, O.J., Alencar, M.L., Barbosa, J.A., de Miranda, T.S., Neumann, V.H., Gomes, I.F., de Santana, F.R., 2018. Stratigraphic relations of the Ipubi formation: Siliciclastic-evaporitic succession of the Araripe basin. An. Acad. Bras. Cienc. 90, 2049–2071. https://doi.org/10.1590/0001-3765201820170526

Feng, Z.Z., 2017. A successful symposium of “Multi-origin of soft-sediment deformation structures and seismites.” J. Palaeogeogr. 6, 1–6. https://doi.org/10.1016/j.jop.2016.11.002

Feng, Z.Z., Bao, Z.D., Zheng, X.J., Wang, Y., 2016. Researches of soft-sediment deformation structures and seismites in China — A brief review. J. Palaeogeogr. 5, 311–317. https://doi.org/10.1016/j.jop.2016.06.001

Ferreira, J.M., Bezerra, F.H.R., Sousa, M.O.L., do Nascimento, A.F., Sá, J.M., França, G.S., 2008. The role of Precambrian mylonitic belts and present-day stress field in the coseismic reactivation of the Pernambuco lineament,

Brazil. Tectonophysics 456, 111–126. https://doi.org/10.1016/j.tecto.2008.01.009

Fossen, H.. 2012. Geologia Estrutural in: Fossen, H.. Translated by R. D. de Andrade. São Paulo: Oficina de Textos. 490-491.

Frey, S.E., Gingras, M.K., Dashtgard, S.E., 2009. Experimental Studies of Gas-Escape and Water-Escape Structures: Mechanisms and Morphologies. J. Sediment. Res. 79, 808–816. https://doi.org/10.2110/jsr.2009.087

Gandini, R., Rossetti, D. de F., Netto, R.G., Bezerra, F.H.R., Góes, A.M., 2014. Neotectonic evolution of the Brazilian northeastern continental margin based on sedimentary facies and ichnology. Quat. Res. (United States) 82, 462–472. https://doi.org/10.1016/j.yqres.2014.07.003

Gao, Y., Jiang, Z., Best, J.L., Liu, S., Zhang, J., 2019. Small- and large- scale soft-sediment deformations in a Triassic lacustrine delta caused by overloading and seismicity in the Ordos Basin, central China. Mar. Pet. Geol. 103, 126–149. https://doi.org/10.1016/j.marpetgeo.2019.02.009

Gladkov, A.S., Lobova, E.U., Deev, E. V., Korzhenkov, A.M., Mazeika, J. V., Abdieva, S. V., Rogozhin, E.A., Rodkin, M. V., Fortuna, A.B., Charimov, T.A., Yudakhin, A.S., 2016. Earthquake-induced soft-sediment deformation structures in Late Pleistocene lacustrine deposits of Issyk-Kul lake (Kyrgyzstan). Sediment. Geol. 344, 112–122. https://doi.org/10.1016/j.sedgeo.2016.06.019

Gomes, J.P., Bunevich, R.B., Tedeschi, L.R., Tucker, M.E., Whitaker, F.F., 2020. Facies classification and patterns of lacustrine carbonate deposition of the Barra Velha Formation, Santos Basin, Brazilian Pre-salt. Mar. Pet. Geol. 113, 104176. https://doi.org/10.1016/j.marpetgeo.2019.104176

Grasemann, B., Martel, S., Passchier, C., 2005. Reverse and normal drag along a fault. J. Struct. Geol. 27, 999–1010. https://doi.org/10.1016/j.jsg.2005.04.006

Green, R.A., Bommer, J.J., 2019. What is the smallest earthquake magnitude that needs to be considered in assessing liquefaction hazard? Earthq. Spectra 1–33. https://doi.org/10.1016/j.ssresearch.2016.09.015.This

Katz, O., Reches, Z., 2006. Reverse drag: Host rock deformation during slip along existing faults. Isr. J. Earth Sci. 55, 43–53. https://doi.org/10.1560/IJES_55_1_43

Liang, Q., Tian, J., Wang, F., Zhang, X., 2019. Soft-sediment Deformation Structures and Sand Body Architecture in the Chang 6 Oil Member of the Upper Triassic Yanchang Formation, Southwestern Ordos Basin, China. Earth Sci. Res. J. 23(2): 119-126. 10.15446/esrj.v23n1.69760

Lowe, D.R., 1975. Water escape structures in coarse-grained sediments. Sedimentology 22, 157–204. https://doi.org/10.1111/j.1365-3091.1975.tb00290.x

Marques, F.O., Nikolaeva, K., Assumpção, M., Gerya, T. V., Bezerra, F.H.R., do Nascimento, A.F., Ferreira, J.M., 2013. Testing the influence of far-field topographic forcing on subduction initiation at a passive margin. Tectonophysics 608, 517–524. https://doi.org/10.1016/j.tecto.2013.08.035

Marques, F.O., Nogueira, F.C.C., Bezerra, F.H.R., de Castro, D.L., 2014. The Araripe Basin in NE Brazil: An intracontinental graben inverted to a high-standing horst. Tectonophysics 630, 251–264. https://doi.org/10.1016/j.tecto.2014.05.029

Martill, D.M., Loveridge, R.F., Heimhofer, U., 2008. Dolomite pipes in the Crato Formation fossil lagerstätte (Lower Cretaceous, Aptian), of northeastern Brazil. Cretac. Res. 29, 78–86. https://doi.org/10.1016/j.cretres.2007.04.007

Martín-Chivelet, J., Palma, R.M., López-Gómez, J., Kietzmann, D.A., 2011. Earthquake-induced soft-sediment deformation structures in Upper Jurassic open-marine microbialites (Neuquén Basin, Argentina). Sediment. Geol. 235, 210–221. https://doi.org/10.1016/j.sedgeo.2010.09.017

Matos, R.M.D, 1999. History of the northeast Brazilian rift system: kinematic implications for the break-up between Brazil and West Africa. Geol. Soc. Spec. Publ. 153, 55–73. https://doi.org/10.1144/GSL.SP.1999.153.01.04

Matos, R.M.D., 1992. The Northeast Brazilian Rift System. Tectonics 11, 766–791. https://doi.org/10.4324/9781351219983-5

Menezes De Jesus, C., Luiz, A., Compan, M., Surmas, R., 2016. Permeability estimation using ultrasonic borehole image logs in dual-porosity carbonate reservoirs. Petrophysics 57, 620–637.

Mills, P.C., 1983. Genesis and diagnostic value of soft-sediment deformation structures-A review. Sediment. Geol. 35, 83–104. https://doi.org/10.1016/0037-0738(83)90046-5

Miranda, T.S., Santos, R.F., Barbosa, J.A., Gomes, I.F., Alencar, M.L., Correia, O.J., Falcão, T.C., Gale, J.F.W., Neumann, V.H., 2018. Quantifying aperture, spacing and fracture intensity in a carbonate reservoir analogue: Crato Formation, NE Brazil. Mar. Pet. Geol. 97, 556–567. https://doi.org/10.1016/j.marpetgeo.2018.07.019

Miranda, T.S., Neve, S.P., Celestino, M.A.L., Roberts, N. 2020. Structural evolution of the Cruzeiro do Nordeste shear zone: Brasiliano-Pan-African-ductile-to-brittle transition and Cretaceous brittle reactivation. J. Struct. Geol. 141, https://doi.org/10.1016/j.jsg.2020.104203

Montenat, C., Barrier, P., Ott dEstevou, P., Hibsch, C., 2007. Seismites: An attempt at critical analysis and classification. Sediment. Geol. 196, 5–30. https://doi.org/10.1016/j.sedgeo.2006.08.004

Moretti, M., 2000. Soft-sediment deformation structures interpreted as seismites in middle-late Pleistocene aeolian deposits (Apulian foreland, southern Italy). Sediment. Geol. 135, 167–179. https://doi.org/10.1016/S0037-0738(00)00070-1

Moretti, M., Sabato, L., 2007. Recognition of trigger mechanisms for soft-sediment deformation in the Pleistocene lacustrine deposits of the Sant'Arcangelo Basin (Southern Italy): Seismic shock vs. overloading. Sediment. Geol. 196, 31–45. https://doi.org/10.1016/j.sedgeo.2006.05.012

Neumann, V.H.L.M., 1999. Estratigrafia, sedimentologia, Geoquimica y Diagésesis Sistemas Lacustres K(AP-AB) Bacia do Araripe.

Neumann, V. H. & Cabrera, L. 1999. Una nueva propuesta estratigráfica para la tectonosecuencia post-rifte de la Cuenca de Araripe, Noroeste de Brasil. In: Bol. 5º Simpósio Sobre o Cretáceo do Brasil e 1º Simpósio Sobre el Cretácico de América del Sul. Serra Negra-SP. UNESP, Rio Claro. 279-285.

Neumann, V. H., Borrego, A. G., Cabrera, L., Dino, R., 2003. Organic matter composition and distribution through the Aptian-Albian lacustrine sequences of the Araripe Basin, northeastern Brazil. Internatio. J. Coal Geol., 54, 21-40.

Neuwerth, R., Suter, F., Guzman, C.A., Gorin, G.E., 2006. Soft-sediment deformation in a tectonically active area: The Plio-Pleistocene Zarzal Formation in the Cauca Valley (Western Colombia). Sediment. Geol. 186, 67–88. https://doi.org/10.1016/j.sedgeo.2005.10.009

Nóbrega, M.A., Sá, J.M., Bezerra, F.H.R., Hadler Neto, J.C., Iunes, P.J., Guedes, S., Tello Saenz, C.A., Hackspacher, P.C., Lima-Filho, F.P., 2005. The use of apatite fission track thermochronology to constrain fault movements and sedimentary basin evolution in northeastern Brazil. Radiat. Meas. 39, 627–633. https://doi.org/10.1016/j.radmeas.2004.12.006

Nogueira, F.C.C., Marques, F.O., Bezerra, F.H.R., de Castro, D.L., Fuck, R.A., 2015. Cretaceous intracontinental rifting and post-rift inversion in NE Brazil: Insights from the Rio do Peixe Basin. Tectonophysics 644, 92–107. https://doi.org/10.1016/j.tecto.2014.12.016

Novak, A., Egenhoff, S., 2019. Soft-sediment deformation structures as a tool to recognize synsedimentary tectonic activity in the middle member of the Bakken Formation, Williston Basin, North Dakota. Mar. Pet. Geol. 105, 124–140. https://doi.org/10.1016/j.marpetgeo.2019.04.012

Obermeier, S.F., Olson, S.M., Green, R.A., 2005. Field occurrences of liquefaction-induced features: A primer for engineering geologic analysis of paleoseismic shaking. Eng. Geol. 76, 209–234. https://doi.org/10.1016/j.enggeo.2004.07.009

Osés, G.L., Petri, S., Voltani, C.G., Prado, G.M.E.M., Galante, D., Rizzutto, M.A., Rudnitzki, I.D., Da Silva, E.P., Rodrigues, F., Rangel, E.C., Sucerquia, P.A., Pacheco, M.L.A.F., 2017. Deciphering pyritization-kerogenization gradient for fish soft-tissue preservation. Sci. Rep. 7, 1–15. https://doi.org/10.1038/s41598-017-01563-0

Owen, G., 1996. Anatomy of a water-escape cusp in Upper Proterozoic Torridon Group sandstones, Scotland. Sediment. Geol. 103, 117–128. https://doi.org/10.1016/0037-0738(95)00089-5

Owen, G., 1996. Experimental soft-sediment deformation: Structures formed by the liquefaction of unconsolidated sands and some ancient examples. Sedimentology 43, 279–293. https://doi.org/10.1046/j.1365-3091.1996.d01-5.x

Owen, G., 2003. Load structures: Gravity-driven sediment mobilization in the shallow subsurface. Geol. Soc. Spec. Publ. 216, 21–34. https://doi.org/10.1144/GSL.SP.2003.216.01.03

Owen, G., Moretti, M., 2011. Identifying triggers for liquefaction-induced soft-sediment deformation in sands. Sediment. Geol. 235, 141–147. https://doi.org/10.1016/j.sedgeo.2010.10.003

Owen, G., Moretti, M., Alfaro, P., 2011. Recognising triggers for soft-sediment deformation: Current understanding and future directions. Sediment. Geol. 235, 133–140. https://doi.org/10.1016/j.sedgeo.2010.12.010

Puy-alquiza, M.J., Miranda-avilés, R., Zanor, G.A., Salazar-hernández, M.M., Salazar-hernández, M.C., 2015. Cenozoic seismites and soft-sediment deformation structures in the Losero Formation, southern Sierra de Guanajuato, Mexico. Rev. Mex. Ciencias Geológicas 32, 203–218.

Ramos, V.A., Folguera, A., 2009. Andean flat-slab subduction through time. Geol. Soc. Spec. Publ. 327, 31–54. https://doi.org/10.1144/SP327.3

Richter, C.F., 1935. An instrumental earthquake magnitude scale. Bull. Seismol. Soc. Am. 25, 1–32.

Rodríguez-Pascua, M.A., Calvo, J.P., De Vicente, G., Gómez-Gras, D., 2000. Soft-sediment deformation structures interpreted as seismites in lacustrine sediments of the Prebetic Zone, SE Spain, and their potential use as indicators of earthquake magnitudes during the Late Miocene. Sediment. Geol. 135, 117–135. https://doi.org/10.1016/S0037-0738(00)00067-1

Rossetti, D.F., Bezerra, F.H.R., Góes, A.M., Neves, B.B.B., 2011. Sediment deformation in Miocene and post-Miocene strata, Northeastern Brazil: Evidence for paleoseismicity in a passive margin. Sediment. Geol. 235, 172–187. https://doi.org/10.1016/j.sedgeo.2010.02.005

Rossetti, D.F., Bezerra, F.H.R., Góes, A.M., Valeriano, M.M., Andrades-Filho, C.O., Mittani, J.C.R., Tatumi, S.H., Brito-Neves, B.B., 2011. Late Quaternary sedimentation in the Paraíba Basin, Northeastern Brazil: Landform, sea level and tectonics in Eastern South America passive margin. Palaeogeogr. Palaeoclimatol. Palaeoecol. 300, 191–204. https://doi.org/10.1016/j.palaeo.2010.12.026

Santos, M.G.M., Almeida, R.P., Mountney, N.P., Fragoso-Cesar, A.R.S., 2012. Seismites as a tool in the palaeoenvironmental reconstruction of fluvial deposits: The Cambrian Guarda Velha Formation, southern Brazil. Sediment. Geol. 277–278, 52–60. https://doi.org/10.1016/j.sedgeo.2012.07.006

Santos, R.F.V.C., Miranda, T.S., Barbosa, J.A., Gomes, I.F., Matos, G.C., Gale, J.F.W., Neumann, V.H.L.M., Guimaraes, L.J.N., 2015. Characterization of natural fracture systems: Analysis of uncertainty effects in linear scanline results. Am. Assoc. Pet. Geol. Bull. 99, 2203–2219. https://doi.org/10.1306/05211514104

Scott, B., Price, S., 1988. Earthquake-induced structures in young sediments. Tectonophysics 147, 165–170. https://doi.org/10.1016/0040-1951(88)90154-0

Seilacher, A., 1969. Fault-Graded Beds Interpreted as Seismites. Sedimentology 13, 155–159. https://doi.org/10.1093/oxfordjournals.humrep.a137463

Shanmugam, G., 2017. Global case studies of soft-sediment deformation structures (SSDS): Definitions, classifications, advances, origins, and problems. J. Palaeogeogr. 6, 251–320. https://doi.org/10.1016/j.jop.2017.06.004

Shanmugam, G., 2012. Process-sedimentological challenges in distinguishing paleo-tsunami deposits. Nat. Hazards 63, 5–30. https://doi.org/10.1007/s11069-011-9766-z

Shanmugam, G., 2016. The seismite problem. J. Palaeogeogr. 5, 318–362. https://doi.org/10.1016/j.jop.2016.06.002

Shanmugam, G., Wang, Y., 2015. The landslide problem. J. Palaeogeogr. 4, 109–166. https://doi.org/10.3724/SP.J.1261.2015.00071

Shelley, E.O., Mussio, V., Rodríguez, M., Chang, J.G.A., 2015. Evaluation of soil liquefaction from surface analysis. Geofis. Int. 54, 95–109. https://doi.org/10.1016/j.gi.2015.04.005

Shukla, M.K., Sharma, A., 2018. A brief review on breccia: it's contrasting origin and diagnostic signatures. Solid Earth Sci. 3, 50–59. https://doi.org/10.1016/j.sesci.2018.03.001

Sims, J.D., 1975. Determining earthquake recurrence intervals from deformational structures in young lacustrine sediments. Dev. Geotecton. 9, 141–152. https://doi.org/10.1016/B978-0-444-41420-5.50020-4

Singh, S., Jain, A.K., 2007. Liquefaction and fluidization of lacustrine deposits from Lahaul-Spiti and Ladakh Himalaya: Geological evidences of paleoseismicity along active fault zone. Sediment. Geol. 196, 47–57. https://doi.org/10.1016/j.sedgeo.2006.06.005

Terra, J.G.S., Spadini, A.R., França, A.B., Leite, C., Zambonato, E.E., Costa, L., Arienti, L.M., Erthal, M.M., Blauth, M., Franco, M.P., Matsuda, N.S., Goulart, N., Augusto, P., Junior, M., Francisco, R.S., Avila, D., Souza, R.S. De, Tonietto, S.N., Maria, S., 2010. Classificações de rochas carbonáticas aplicável às bacias sedimentares brasileiras. B. Geoci. Petrobras, Rio Janeiro 18, 9–29.

Topal, S., Özkul, M., 2014. Soft-sediment deformation structures interpreted as seismites in the kolankaya formation, denizli basin (SW Turkey). Sci. World J. 2014. https://doi.org/10.1155/2014/352654

Toro, B., Pratt, B.R., 2015a. Characteristics and Implications of Sedimentary Deformation Features in the Green River Formation (Eocene) in Utah and Colorado. Geol. Utah's Uinta Basin Uinta Mt. Utah Geol. Assoc. Publ. 44 371–422.

Toro, B., Pratt, B.R., 2015b. Eocene paleoseismic record of the green river formation, fossil basin, Wyoming, U.S.A.: Implications of synsedimentary deformation structures in lacustrine carbonate mudstones. J. Sediment. Res. 85, 855–884. https://doi.org/10.2110/jsr.2015.56

Törő, B., Pratt, B.R., 2016. Sedimentary record of seismic events in the Eocene Green River Formation and its implications for regional tectonics on lake

evolution (Bridger Basin, Wyoming). Sediment. Geol. 344, 175–204. https://doi.org/10.1016/j.sedgeo.2016.02.003

Turner, J.P., Green, P.F., Holford, S.P., Lawrence, S.R., 2008. Thermal history of the Rio Muni (West Africa)-NE Brazil margins during continental breakup. Earth Planet. Sci. Lett. 270, 354–367. https://doi.org/10.1016/j.epsl.2008.04.002

Unjoh, S., Kaneko, M., Kataoka, S., Nagaya, K., Matsuoka, K., 2012. Effect of earthquake ground motions on soil liquefaction. Soils Found. 52, 830–841. https://doi.org/10.1016/j.sandf.2012.11.006

Wallace, K., Eyles, N., 2015. Seismites within Ordovician-Silurian carbonates and clastics of Southern Ontario, Canada and implications for intraplate seismicity. Sediment. Geol. 316, 80–95. https://doi.org/10.1016/j.sedgeo.2014.12.004

Wang, C.Y., Wong, A., Dreger, D.S., Manga, M., 2006. Liquefaction limit during earthquakes and underground explosions: Implications on ground-motion attenuation. Bull. Seismol. Soc. Am. 96, 355–363. https://doi.org/10.1785/0120050019

Warren, L.V., Varejão, F.G., Quaglio, F., Simões, M.G., Fürsich, F.T., Poiré, D.G., Catto, B., Assine, M.L., 2017. Stromatolites from the Aptian Crato Formation, a hypersaline lake system in the Araripe Basin, northeastern Brazil. Facies 63, 3. https://doi.org/10.1007/s10347-016-0484-6

Wheatley, D.F., Chan, M.A., Sprinkel, D.A., 2016. Clastic pipe characteristics and distributions throughout the Colorado Plateau: Implications for paleoenvironment and paleoseismic controls. Sediment. Geol. 344, 20–33. https://doi.org/10.1016/j.sedgeo.2016.03.027

Yang, R., Tom Van Loon, A.J., Yin, W., Fan, A., Han, Z., 2016. Soft-sediment deformation structures in cores from lacustrine slurry deposits of the Late Triassic Yanchang Fm. (central China). Geologos 22, 201–211. https://doi.org/10.1515/logos-2016-0021

Zihms, S. G. Miranda, T., Lewis, Helen, Barbosa, J. A., Neumann, V. H., Souza, J. A. B., Falcão, T. C, D., 2017. Crato Formation laminites - a representative

geomechanical pre-salt analogue? 5th Atl. Conjug. Margins Conf. Porto Galinhas, Pernambuco, Brazil, 22th – 25th August 2017.

4.2 ARTIGO 2 – THE EFFECT OF FRACTURE NETWORKS ON THE VERTICAL PERMEABILITY OF A TIGHT CARBONATE RESERVOIR ANALOGUE: A CASE STUDY FROM THE CRATO FORMATION, NE BRAZIL

The effect of fracture networks on the vertical permeability of a tight carbonate reservoir analogue: a case study from the Crato Formation, NE Brazil

Márcio Lima Alencar[a]*, Tiago Siqueira de Miranda[a], Osvaldo José Correia Filho[a], José Antonio Barbosa[b], Igor Fernandes Gomes[c], Germano Mário Silva Ramos[b], Araly Fabiana Lima de Araújo[b], João Gabriel de Oliveira Topan[a], Maria Alcione Lima Celestino[a], Virginio Henrique Neumann[a]

[a]MODLAB, Departamento de Geologia - UFPE. Av da Arquitetura, s/n, Cid. Universitária, Recife, PE, Brazil - 50740550. mlimaalencar@gmail.com, tiago.smiranda@ufpe.br, osv.correia@gmail.com, gabrieltopan@gmail.com, alcionelimma22@gmail.com, neumann@ufpe.br;

[b]GEOQUANTT, Pesquisa em Geociências, Departamento de Geologia - UFPE. Av da Arquitetura, s/n, Cid. Universitária, Recife, PE, Brazil - 50740550. jose.antoniob@ufpe.br, nonogermano@gmail.com, aralyfabiana23@gmail.com,

[c]Geosciences Graduate Program, Federal University of Pernambuco, Recife, PE, 50740-530, Brazil. gomes@ufpe.br

*Corresponding author: e-mail: mlimaalencar@gmail.com; telephone: +55 81 2126-8240; postal address: Av. da Arquitetura, 953-995 - Cidade Universitária, Recife - PE, 50740-540, Brazil.

Highlights

-Mechanical strength has been analysed for determining vertical fracture patterns in the Aptian lacustrine laminated limestones;

-Pseudo-wells acquired over outcrops are used to study relationship between fractures and geomechanical properties;

-Discrete Fracture Network (DFN) models were created to perform quantitative analysis and fracture pattern extrapolation;

- DFN models revealed that vertical fracture patterns influence fracture porosity and permeability at different scales.

Abstract

The structural characterization of fractures is crucial to understand the processes of fluid flow in tight reservoirs. This contribution focuses on the role played by vertical fractures on the permo-porosity properties of the Aptian tight carbonate sequence of the Crato Formation, Araripe Basin (NE Brazil). The study performed a structural analysis in two different scales (reservoir and outcrop) of the fracture networks in lacustrine laminates, which have been investigated as an analogue of carbonate facies observed within the pre-salt reservoir sequence of the marginal basins in Brazil. This study employed a combination of systematic outcrop-based fracture characterization involving digital outcrop models and mechanical stratigraphy analysis. To evaluate the influence of vertical fracture systems in the fracture porosity and the equivalent permeability we performed DFN (Discrete Fracture Network) models. We focused on vertical calcite veins, which strike in two principal directions, NNW-SSE, NE-SW that show different linkage patterns due to the influence of the mechanical intervals. Results of the outcrop scale model show similar values for both fracture porosity and equivalent permeability, indicating that storage capacity and fluid flow may not be affected by vertical linkage of fractures. The reservoir scale DFN models showed that the fracture porosity was greater in models which consider through-going continuous fractures than in models that consider the segmentation (discontinuity) of vertical fractures. Considering the vertical connectivity of fractures, the equivalent horizontal permeability (Kxx and Kyy) showed similar values in both scale models. This implies that vertical segmentation of fractures does not impact fluid flow in horizontal directions. The calculated values of equivalent vertical fracture permeability (Kzz) at reservoir scale are one order of magnitude higher in the DFNs that consider continuous fractures. Our results suggested that vertically continuous fractures enhance preferential flow pathways allowing greater vertical fluid flow than segmented fracture networks in tight carbonate reservoirs.
Keywords: Vertical fractures. Fracture porosity. Pre-salt. Apitan. DFN. Fracture permeability.

1. Introduction

Due to the complex tectonic and diagenetic evolution of naturally fractured carbonate reservoirs, the fracture system has been widely investigated for

presenting considerable influence in both storage and fluid flow (Giuffrida et al., 2019; 2020; Smeraglia et al., 2021). The study of fracture networks is particularly important because they control the hydraulic behaviour in rock deposits where the primary porosity is not considered a significant contribution factor, as tight carbonate reservoirs (Rodriguez et al., 2004; Rosales and Luna., 2005; Rashid et al., 2021; Zhang et al., 2021; Li et al., 2022). Understanding the spatial distribution of the fracture network is essential to determine the structural control on fluid flow in this type of reservoir (Khelifa et al., 2014, Zhao et al., 2022). Therefore, the structural characterization of fracture arrangement provides the critical information for estimating the storage capacity of fracture systems and fluid flow aspects in geological reservoirs (Aydin, 2000; Graham-Wall et al., 2006; Agosta et al., 2010; Giuffrida et al., 2019; 2020). In addition, fractures can significantly affect oil, gas, water production and CO2 storage (Khelifa et al., 2014; Xu et al., 2023). This is due to the fact that fractures may be responsible for substantial impact to the natural flow of fluids, hence hindering or impeding their extraction or distribution (Rawnsley et al., 2007; Agosta et al., 2010).

Here, we present an integrated dataset of structural field observations and discrete fracture network (DFN) models of laminated limestones from the Aptian Crato Formation (NE Brazil). These laminated limestones have been investigated as an analogue to one of the carbonate facies encountered in the pre-salt reservoirs of the Southeastern Brazilian marginal basins (Santos et al., 2015; Catto et al 2016; Zihms, 2017; Miranda et al., 2018; Alencar et al., 2020; Celestino et al., 2021; Varejão et al., 2022). These rocks present primary porosity and permeability values of approximately 5% and 0,014 mD, respectively, being classified as a tight carbonate reservoir (Miranda et al., 2018). Although previous studies have provided detailed structural analyses of the structural context of the Crato Formation from the Araripe Basin (Miranda et al., 2018; Celestino et al., 2021), a reservoir modelling considering the discrete fracture network of this carbonate analogue reservoir is lacking.

The objective of this study is to analyse the effect of the vertical fracture connectivity on the permo-porosity of the fracture networks at different scales on naturally fractured carbonate rocks. In this work, the term "connectivity" refers to both the vertical continuity and discontinuity of fractures. Since, numerical

methods are powerful tools to investigate fracture spatial organisation in fractured reservoirs, we applied DFN models to calculate fracture porosity and equivalent permeabilities. A systematic data acquisition of fracture attributes was performed in outcrops using the scanline method (Ortega et al., 2006; Guerriero et al., 2015; Lepillier et al., 2020) and digital outcrop modelling techniques (Bisdom et al., 2014; Tavani et al., 2014; Savastano et al., 2016). We also performed data acquisition through pseudo-wells (virtual scanlines) executed in outcrops and digital outcrop models (Nilsen et al, 1999; Kraft, 2004; Pringle et al., 2001; Smeraglia et al., 2021). In addition, we collected mechanical strength data in order to analyse the vertical segmentation (discontinuity) of fractures due to the mechanical interfaces of the laminites (e.g., Underwood et al., 2003; Cooke et al., 2006; Laubach et al., 2009; Lyu et al., 2022). Then, the data were integrated into a geocellular volume (Gapillou et al., 2009; Corlett et al., 2021; Lutome et al., 2022) to integrate with DFN models (Bisdom et al., 2014; Giuffrida et al., 2019; 2020; Smeraglia et al., 2021).

Our study analyses at two different modelling scales regarding the outcrop data, to define the influence of storage capacity and the distribution of the equivalent horizontal and vertical permeabilities considering different configurations of the vertical fracture networks. Furthermore, these results offer significant insights applicable to the advancement of strategies and activities concerning oil extraction and the investigation of aquifers within carbonate rock formations (e.g., Lander et al., 2008; Olson et al., 2009; Corniello et al., 2018). Therefore, our study provides data that can be used to build better models used for numerical simulations of fractured carbonate reservoirs.

2. Geological Setting

The study area is located in the Araripe Basin (AB) the largest intraplate basin of northeastern Brazil, with an area of ~ 9000 km^2 (Fig. 1a). The AB is located in the Transversal Domain of the Borborema Province (BP), between the Patos and Pernambuco shear zones. During the BP formation, the Neoproterozoic Brasilian orogenic cycle had an important influence on the deformation of the rocks, being responsible for its current configuration (Almeida, 1977; Brito Neves, 2000; Oliveira, 2008; Santos et al., 2012; Araújo et al., 2013; Celestino et al., 2020; Alencar et al., 2021). The basin shows a shape elongated

in east-west direction, and its limits to the northern border are demarcated by the Triunfo Fault. This fault is indicative of the brittle reactivation of the Patos shear zone (Celestino et al., 2020).

The stratigraphy column of the Araripe Basin has been classified into five tectono-sequences: a) Paleozoic, which is characterized by the Silurian-Devonian continental deposits of the Cariri Formation; b) Pre-rift, represented by the Tithonian continental deposits from the Brejo Santo and Missão Velha formations; c) Rift sequence, composed of Hauterivian-Berriasian continental deposits found in the Abaiara Formation; d) Post-rift I, known as Santana Group, containing Aptian-Albian continental to transitional deposits of the Barbalha, Crato, and Ipubi formations, as well as shallow-marine deposits in the Romualdo Formation; e) Post-rift II, comprised by Upper Albian alluvial deposits in the Araripina Formation and Albian-Cenomanian fluvial deposits of the Exu Formation (Assine, 2007; Assine et al., 2014).

This study was performed in the northern border of the AB (Fig. 1b), precisely in Crato Formation, a Upper Aptian post-rift lacustrine deposits formed during a cyclic lake level expansion (Assine et al., 2014; Catto et al 2016; Fabin et al., 2018; Miranda et al., 2018; Alencar et al., 2020; Celestino et al., 2021). The Crato Formation is composed of intervals of fine laminated limestone interbedded with siliciclastics deposits (Neumann, 1999; Neumann and Cabrera, 1999). The origin of the laminites is a matter of debate, with some authors arguing for an inorganic authigenic origin while others point to a microbial origin as the main source (Heimhofer et al., 2010; Catto et al., 2016). The Crato Formation shows six intervals of laminated limestones, denoted as C1 to C6. These layers exhibit a progressive increase in both their thickness and areal extent (Neumann, 1999). Our study was performed at the C6 level, which comprises a thin reservoir analogue interval with good outcrop exposures in quarries located on the northern border of the basin (Fig. 1b). The study was performed in outcrops in the Williams Quarry, which present tridimensional exposures providing a good opportunity to collect data of fracture networks.. Previous works, which were carried out at the C6 level, studied the vertical calcite veins present in the C6 interval and the results pointed to two predominant sets: 1) primary set NNW-SSE and b) secondary set ENE-SSW (Miranda et al., 2012; 2014; 2018).

The laminites of the Crato Formation have been considered as analogous deposits of low-permeability of the pre-salt reservoirs of the Barra Velha Formation of the Santos Basin, situated along the southeastern margin of Brazil (Gomes et al., 2020). The laminated limestones features in C6 interval show comparable petrophysical and mechanical attributes to those observed in the reservoir lithofacies present in the pre-salt succession (Terra et al., 2010; Catto et al., 2016; Menezes et al., 2016; Zihms et al., 2017; Miranda et al., 2018).

Figure 1. Location of the study area in the Araripe Basin, NE Brazil. a) Digital elevation model highlighting the location of the main Brazilian Northeastern sedimentary basins. The red polygon points to the location of the study area. b) Detailed geological map of the study area showing the occurrence of Crato Formation deposits in the northern border of the Araripe Basin. c) General view of outcrop studied in Williams Quarry near the Nova Olinda city. d) Simplified stratigraphic chart showing chronostratigraphy of units near the study area.

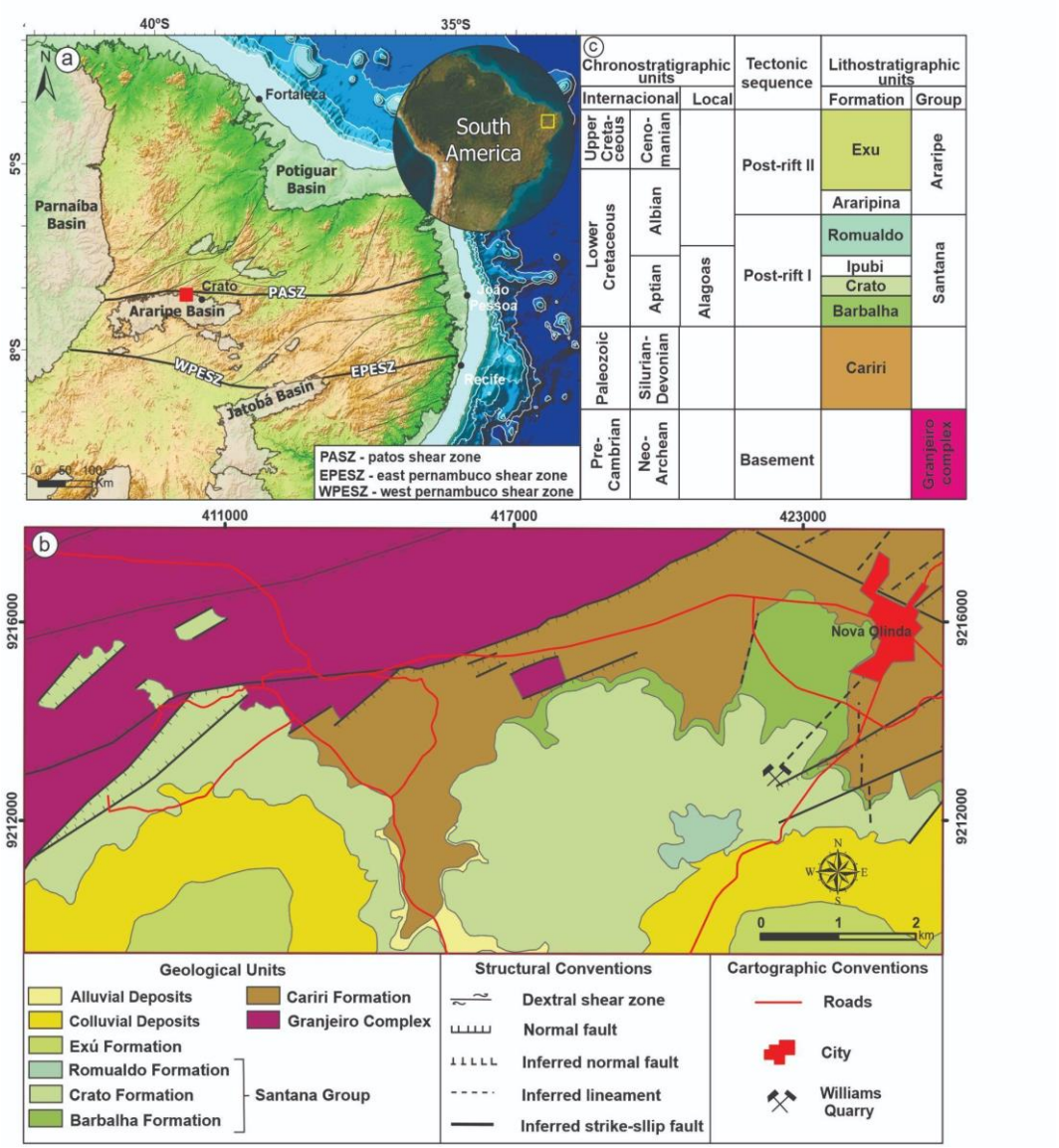

Source: The author.

3. Material and methods

Figure 2 shows the flowchart illustrating the main stages of this work. The workflow begins with outcrop data and concludes with porosity and permeability calculated through DFN modelling.

Figure 2. Schematic flowchart showing the main stages to construct the DFN models of the laminated limestone of the Crato Formation. (UAV = unmanned aerial vehicle; UCS = unconfined compressive strength; DOM = digital outcrop model; DFN = discrete fracture network).

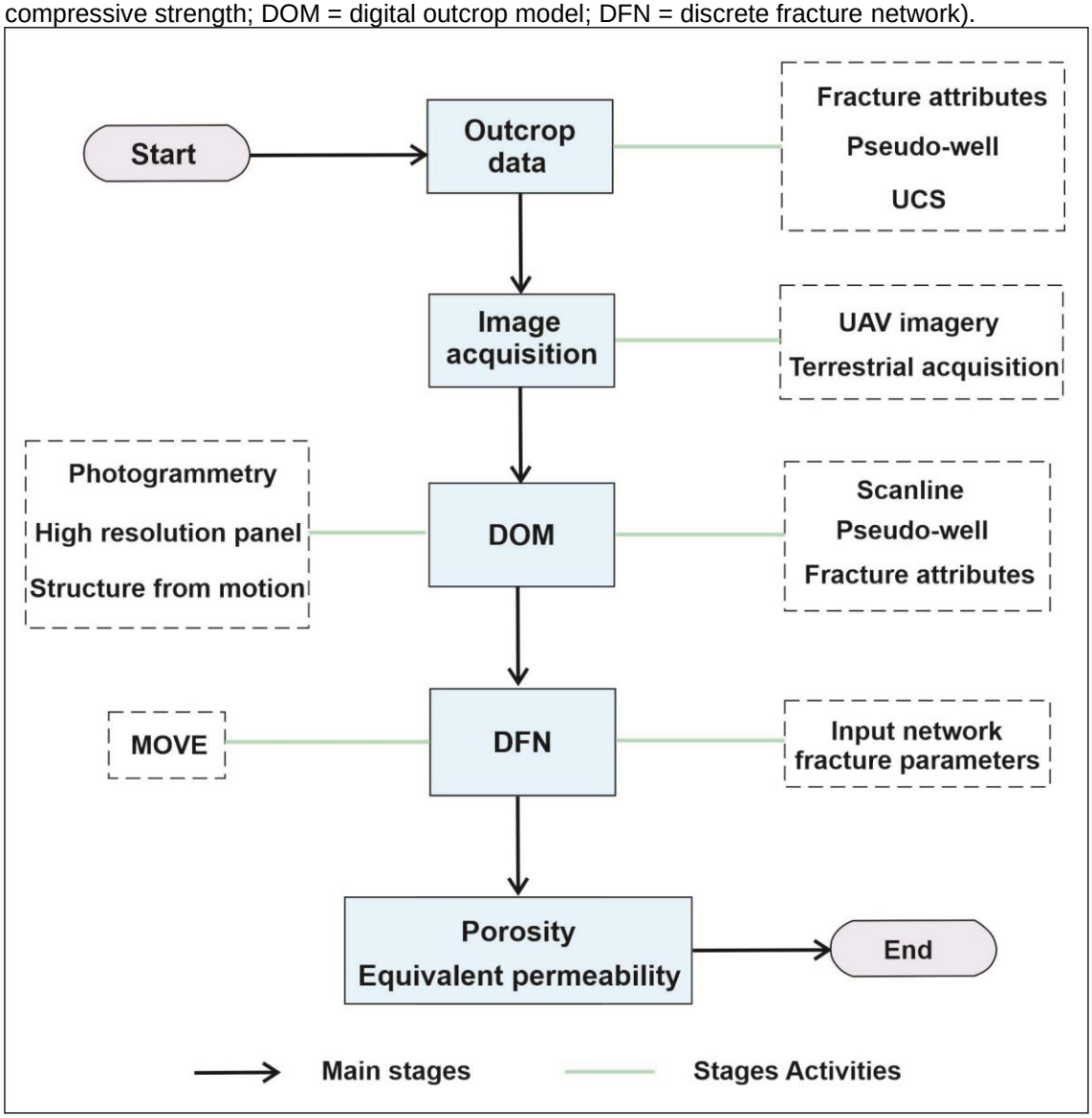

Source: The author.

3.1. Outcrop data

The field analyses were performed on outcrops aiming to collect data that allowed understanding of fracture networks present in laminated limestone of the Crato Formation. According to Lei et al. (2017), the properties and attributes associated with a fracture network consist of the elements identified in its structure, such as orientation, aperture, height, length, shape, and intersection with other fractures present in the network (Fig. 3). The aperture values were collected by employing the comparator (Ortega et al., 2006), while the length of the fractures was collected from the top and base outcrop. A total of 68 fractures were measured at the outcrop (Fig. 4d). These data allow us to build models that

enhance our understanding of geometry, rock porosity and permeability, as well as mechanical and hydraulic properties of the network fracture.

3.1.1. Rock strength measurement

We used the Schmidt Hammer (Proceq L-N type) in order to obtain the uniaxial compressive strength (UCS) of the laminites. These measurements play a crucial role in understanding the control of fractures, their formation, propagation and segmentation. This technique involves measuring the number of rebounds produced by impacts against the surface of the rock (Fig. 4b). The data acquisition was performed through vertical pseudo-well using a systematic acquisition at every regular single interval of 10 cm. To ensure accuracy, the Proceq standard procedure requires the number of rebounds to be measured 12 times per interval. Then, the rebound values (UCS) were calculated by discarding the highest and lowest values and taking the mean of the remaining 10 values. The UCS values obtained from the tests were converted into megapascals (MPa), which is the standard unit for measuring rock strength, by utilizing a conversion table which has been provided by Proceq. This data analysis provides reliable and precise estimates of the mechanical properties of the carbonates under investigation.

Figure 3. a) An example of the linear scanline technique used in the laminated limestone of Crato Formation to collect fracture attributes in outcrop surfaces: height, length, aperture, and attitude (b) Schematic drawing highlighting fracture attributes.

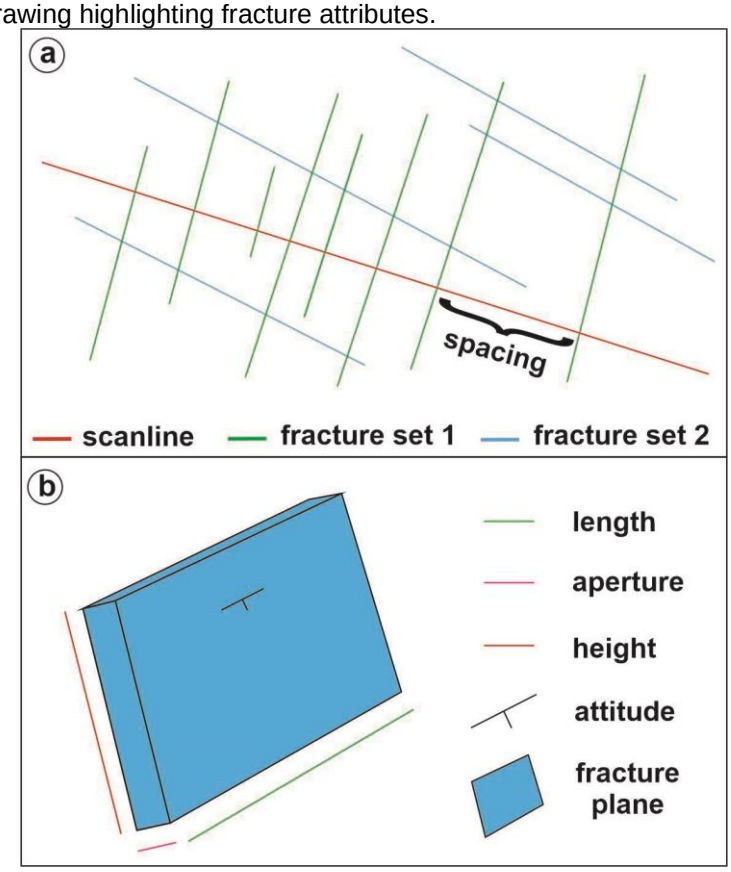

Source: The author.

Figure 4. General aspects of the data collected in the outcrop from the Willian Quarry, Crato Formation, Araripe Basin. a) Three-dimensional exposure overview of a laminated limestone outcrop where the study was carried out. b) Acquisition of UCS data using a Schmidt hammer. c) Photograph showing location and measurement of vertical calcite veins on the outcrop vertical surface. d) High resolution panel showing the outcrop vertical surface. Red and pink traces - vertical fractures.

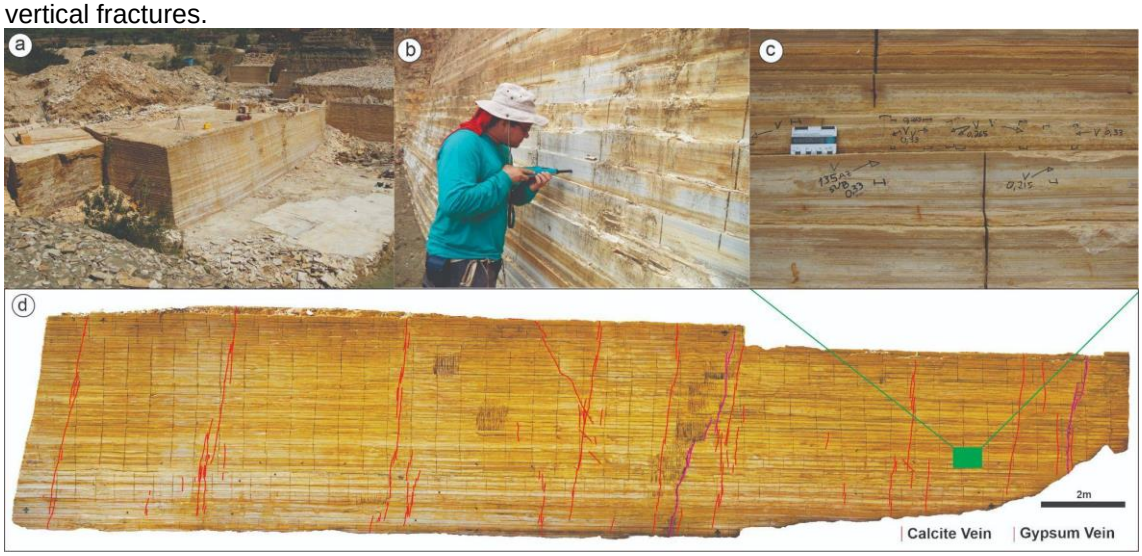

Source: the author.

3.1.2. Pseudo-wells

According to Nilsen et al (1999), pseudo-well is a point of compiled information within a given área. The pseudo-wells application allowed the insertion of data from different attributes in the same environment, creating a direct relationship between the data and enabling the delimitation of fracture geometry (Kraft, 2004).

Pseudo-wells are scanlines used to extract valuable information from digital outcrop models. We used both horizontal and vertical pseudo-wells. Zakirov and Zakirov (1996) discussed the significance of the sensitivity of vertical and horizontal wells to the heterogeneities existing in a reservoir that can vary based on spatial relationship between the wells and these features. This means that the orientation and positioning of wells in relation to geological structures, such as fractures, faults, layers, and other types of heterogeneities, can affect their ability to detect and measure reservoir properties, such as porosity, permeability, and fluid saturation. Therefore, the choice of well orientation and positioning is a critical factor to access representative data for the modelling of potential reservoir properties.

In this work, horizontal pseudo-wells were used in plan view and cross sections, and played a crucial role as virtual scanlines (intensity P10 scanline), which allow us efficient access to the fracture network attribute data needed for our analysis (Fig. 5). We used horizontal pseudo-wells on the cross-sections due to the fact that the studied fracture network is predominantly vertical (Zakirov and Zakirov, 1996). Consequently, an adequate representation of geological features was collected through the use of horizontal scanlines. On the other hand, it is important to highlight that the vertical pseudo-wells were employed in cross-sections for the specific purpose of representing the mechanical strength logs of the rocks under study.

Figure 5. Block diagram highlighting the relationship between pseudo-wells and some heterogeneities in the laminated limestones of the Crato Formation. Note that for horizontal features, vertical pseudo-wells are more representative, whereas for vertical structures, horizontal pseudo-wells are more representative.

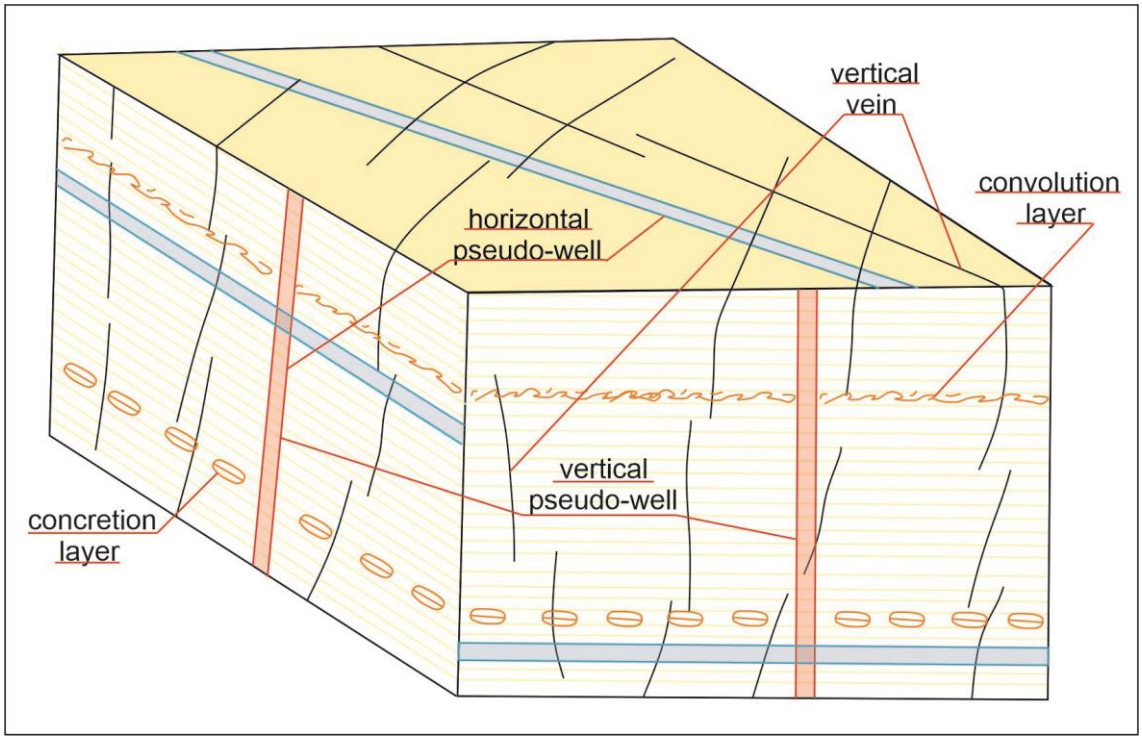

Source: The author.

3.2. Digital outcrop model

In this work, two different models were used to build the 3D digital outcrop models: 1) The first one was built from photograph acquisition using an unmanned aerial vehicle (UAV) model Phantom 4 Advanced (Fig. 6). The UAV used in the image acquisition has a SONY EXMOR 1" CMOS RGB sensor that allows the acquisition of images with a resolution of 20 megapixels, constructing images with 4864 x 3648 pixels. During the field work, flights were performed to cover the entire area of the outcrop under study, with the aim of acquiring aerial photographs that allowed a detailed analysis of the surface in question. A total number of 198 images were collected. Subsequently, a careful evaluation of these images was performed with the aim of selecting those that were in line with the research objectives. The careful selection of these images allowed the acquisition of precise and relevant data for the study developed. 2) The second model consisted of 56 photos taken by a camera model Sony Alpha 77, lens 28/75 SAM. All the photos were taken in front of the outcrop, in perpendicular.

The image processing used the algorithm called Structure from Motion (SfM) and the Metashape Photoscan software. For this procedure, the processing

consists in superposition of two images of the same object taken from different points (Fig. 6b) (Tavani et al., 2014). Firstly, the algorithm aligns the images according to their respective coordinates, in order to maintain the original overlap of the acquisition. The subsequent stage of the processing, the software creates a dense point cloud, which increases the number of points and a consequent reduction of void spaces. From the dense point cloud, a triangular surface (mesh) can be constructed. In order to complete the model, the algorithm generates a texturing surface, which was applied to the model to improve the visual aspect of the image. The texturing surface is then applied to the model and orthophoto mosaics of the constructed model can be obtained (Fig. 7a-e).

The application of orthomosaics in the DFN construction is highly advantageous due to facility to extract statistical information of the fracture network, from 1D and 2D samplings, and extrapolate these informations to generate 3D models of the fracture system (Wang, 2005; Giuffrida et al., 2019; Parrino et al., 2019; 2020; Martinelli et al., 2020). Volumetric fracture intensity (P32) are usually derived from P10 and p21 scanline acquisition and are associated through C_{13} and C_{23} constants (Wang, 2005), respectively. This author discussed that these constants are conversion factors that take into account the probability density function between the scanline and the fracture plane normal. In this work, we utilized P10 scanlines (pseudo-wells) to calculate P32, and we calculated this parameter through the following equation: $P32 = C_{13} * P10$ (Wang, 2005).

Figure 6. a) Photograph of Phantom 4 Advanced model drone. The image illustrates a model of the equipment used to acquire aerial images. b) Figure showing associated parameters in a stereoscopic view. P is considered as an object photographed by two cameras (C1 and C2), its position will be determined by the focal distance and camera orientation (modified from Tavani et al., 2014). c) Example of photomosaic alignment of the outcrop surface.

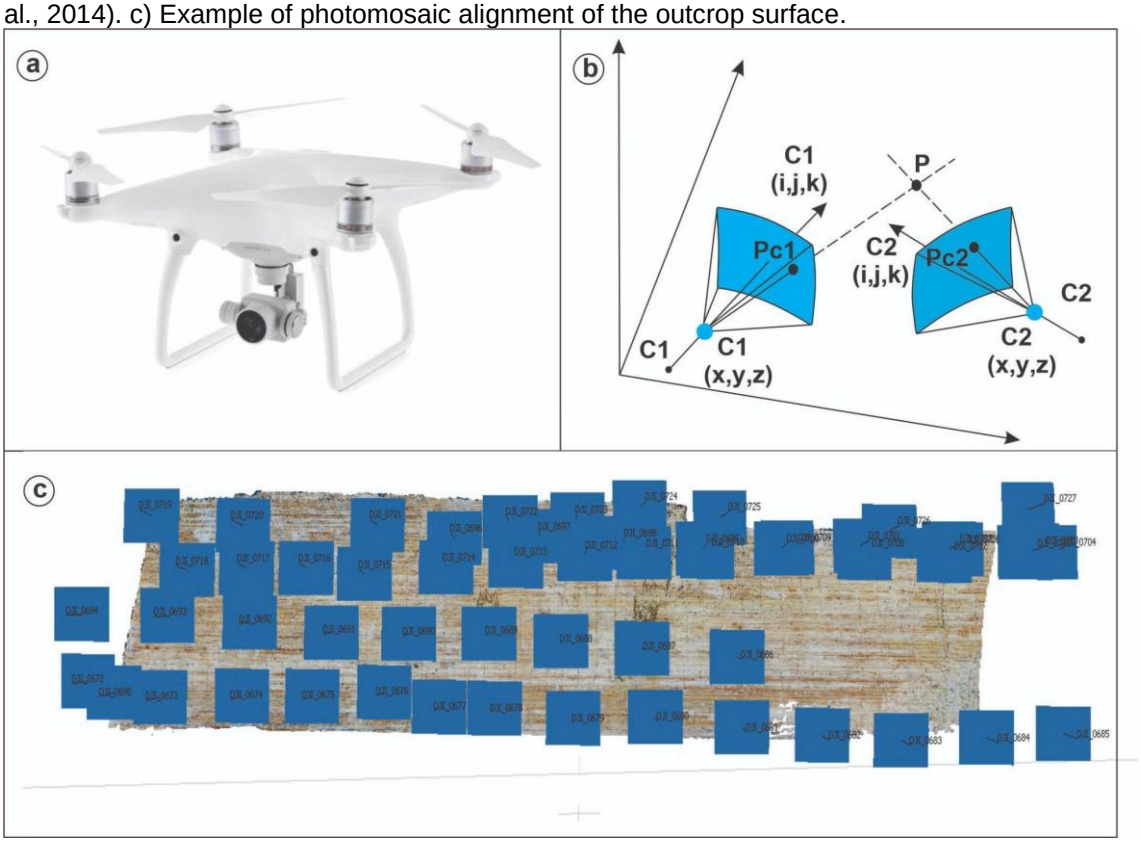

Source: The author.

Figure 7. Figure highlighting the outcrop virtual model processing. a) Aerial image of outcrop showing the face where the data was collected to build a high-resolution panel. b) Dense point cloud. c) Triangulation surface connecting the points of the dense cloud. d) Triangulation surface in detail. e) Texturing surface applied to the mosaic.

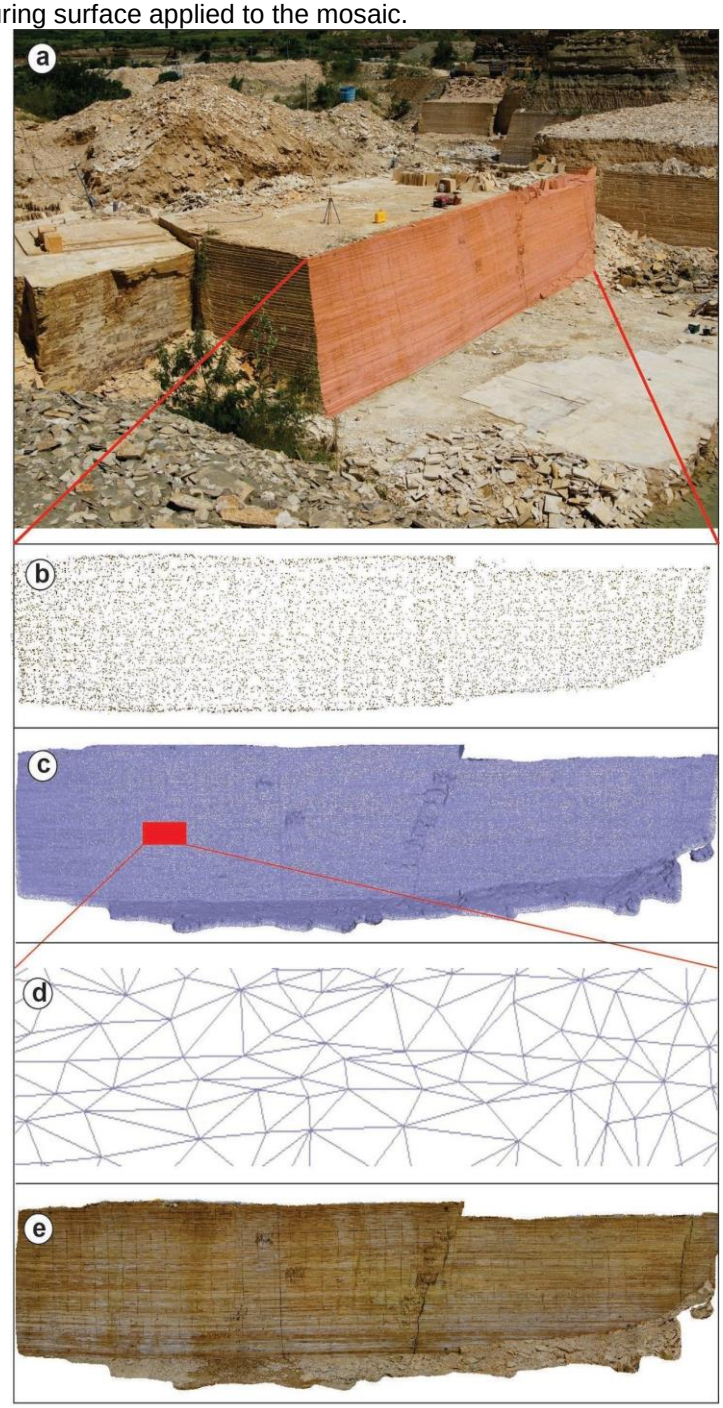

Source: The author.

3.3. DFN modelling

The DFN is a computational model that represents the geometric properties and attributes of each fracture within a fracture network (Lei et al., 2017). These authors suggest that building a DFN based on the stochastic approach makes use of statistical variations of fracture network attributes to build

scenarios where sampling is limited. The DFN objective is to numerically represent the fracture network of a given outcrop based on the statistics involved in the fracture attributes (Miyoshi et al., 2018; Nyberg et al., 2018; Racolte, 2021). The importance of the DFN method is to provide detailed information about the fracture network, including its density and connectivity. This information is essential for understanding the porosity and permeability of the fracture system and how fluids move through the geological reservoir (Long et al., 1985; Anderson and Dverstorp, 1987). Additionally, DFN modelling is a useful tool for predicting the behaviour of the fracture network under different scenarios, such as fluid injection or geological resource exploration.

In this study we aimed to compare the similarity of the fracture network. Stochastic DFN models were generated at both reservoir and outcrop scales, type 1 and type 2, respectively. Stochastic DFN are models built from field analysis that aim to populate geocellular volume representative of the study rock volumes (Giuffrida et al., 2019).

Firstly, a reservoir scale model (type 1) was built utilizing imagery data acquired by UAV. During the operation, neighbouring quarries of limestone of the Crato Formation were flown over by the drone, which captured a series of images that were subsequently processed for further analysis. We also used the Fracpaq software (Healy et al., 2017) to collect fracture intensity data P10 through scanline and calculate volumetric fracture intensity (P32), following the methodology developed by Wang (2005). We create a 150 x 150 x 15m geocellular volume to represent the reservoir scale model. The specific value of 15m represents the thickness of the geocellular volume. This information was collected from wellbore profiles available from the SIAGAS (Groundwater Data System - CPRM - Brazil Geologic Service).

We also built a stochastic DFN model representing the outcrop scale (Type 2). To build this model we used data collected directly from outcrops. We also used data collected from orthomosaics, which provide highly detailed visual representations of the outcrop under investigation. Furthermore, to complete the fracture network data for the outcrop model, we used data collected from classic scanlines performed in the same area (Miranda et al, 2018). Finally, to represent the outcrop scale model, we built a 25 x 5 x 5m geocellular volume. Every cell of

the geocellular volume presents dimensions up to 0,2 m^3. The table 1 presents the input data used to build the stochastic DFN.

Additionally, parameters such as attitude and aperture were acquired directly in outcrops during the fieldwork. Fracture length and height values were obtained from digital outcrops models. Fracture intensity (P10) was taken by pseudo-wells applied on digital models. The aspect ratio value is due to vertical discontinuities caused by mechanical stratigraphy variation. We used the MOVE software to obtain the Fisher value (k) from the stereograms of each fracture set.

After the integration of all field data, digital models, pseudo-wells and the creation of DFN models at different scales, quantitative models were computed for both fracture porosity and equivalent fracture permeability. Equivalent fracture permeability refers to the constant permeability tensor that serves as a representative value of the fluid flow resulting from the combination between the rock's matrix and fracture system (Renard and Marsily, 1997). The permeability models were built according to methodology developed by Oda (1985), which is an analytical method to obtain the equivalent fracture permeability and has been widely accepted and widely applied when examining fracture networks (Cotterau et al, 2010; Lei et al, 2016; Alvarez et al, 2021). Additionally, this method uses only geometric characteristics of the fractures such as aperture, orientation and length.

The DFN models present in this work were built using the academic license of Move software, which have been widely used in the scientific community as a tool for modelling and analyzing reservoirs allowing a better understanding of the features that comprises a reservoir (Giuffrida et al., 2019, 2020; Smeraglia et al., 2021).

Table 1. Input values for various parameters associated with the fractures were used for the DFN Modelling. We used different colours to distinguish the source of data acquisition. The green colour represents data acquired from field data and pseudo-well, orange colour represents data from Miranda et al (2018), light blue colour represents data from Fracpaq analysis and dark blue colour represents data obtained from Field data and FracPaq Analysis.

Input Parameters	Outcrop DFN Model				Reservoir DFN Model			
	Vertically Discontinuous Fracture		Vertically Continuous Fracture		Vertically Discontinuous Fracture		Vertically Continuous Fracture	
	NNW-SSE	NE-SW	NNW-SSE	NE-SW	NNW-SSE	NE-SW	NNW-SSE	NE-SW
p32	1.71	2.98	1.71	2.98	0.45	0.85	0.45	0.85
Fracture length mean (m)	4.8	4.8	4.8	4.8	49.6	59.4	49.6	59.4
Fracture length std dev (m)	1.8	1.8	1.8	1.8	30.5	40.7	30.5	40.7
Dip (deg)	85	89	85	89	90	89.52	90	89.52
Dip direction (Az)	263	168	263	168	252	147.64	252	147.64
Fisher vector	52.02	58.3	52.02	58.3	91.15	58.3	91.15	58.3
Aspect ratio	1 : 1.2	1 : 1.2	1 : 4.8	1 : 4.8	1 : 8	1 : 8	1 : 50	1 : 50
Aperture (mm)	1	1	1	1	1	1	1	1

Field data + pseudo-well | Miranda et al., 2018 | FracPaq analysis | Field data + FracPaq analysis

Source: The author

4. Results

4.1. Fracture and mechanical stratigraphy

Fractures identified in the laminites of Crato Formation were principally veins and joints (Fig. 8a). The veins are filled by calcite and can be easily highlighted by the presence of two distinct sets of vertical fractures that present an orthogonal pattern with NNW-SSE and NE-SW directions (Fig. 8e). The joints commonly show apertures with different sizes and partial fillings, indicating possible evidence of dissolution. Therefore, this fact probably suggests that the joints made use of pre-existing veins' weak planes during their own formation (**Fig. 8**).

Fig. 8. Field aspects of the joints and veins of the laminites of the Crato Formation. a-b). Photographs showing joints and vein planes. c) Schematic drawing of Figure A revealing the relation between joint planes (black traces and polygon) and a cluster of veins (blue traces). d) Schematic drawing of Figure b showing the relation between a joint and an isolated calcite vein. The observed relation between the structures suggests that some joints formed of pre-existing veins due to the pre-existing weakness planes. e) Lower hemisphere stereogram showing the contours of the pole of the fracture planes.

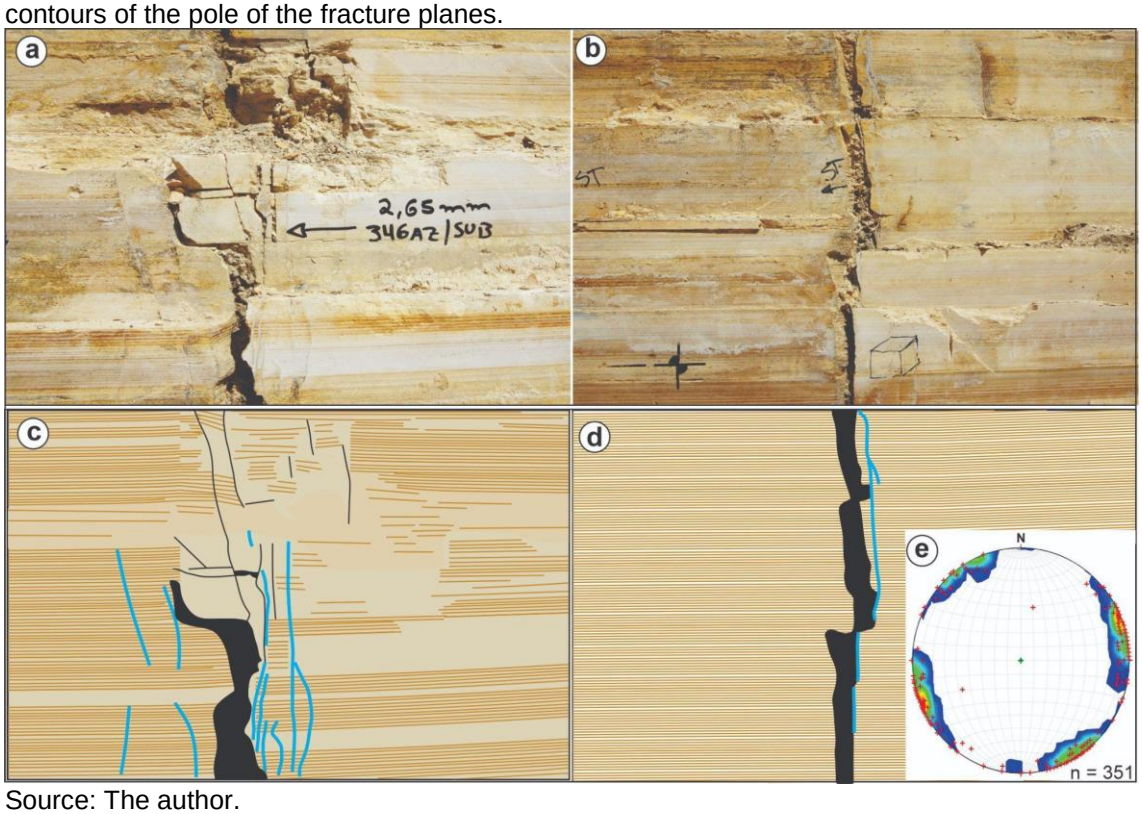

Source: The author.

We observed that some geometries of the vein intersections observed in plan view (Fig. 9-1d), demonstrate the occurrence of isolated tips (i-node) and splay patterns (y-node) (Sanderson and Nixon, 2015). Miranda et al (2018)

conducted a study where, apart from these highlighted intersections, the pattern of crossing fracture (X-node) (Sanderson and Nixon, 2015) was also observed. On the other hand, we examined vein trace patterns through a cross-section view, resulting in the identification of preference for vein traces with isolated tips (Figure 9e-h). In the observed veins, the isolated tips pattern creates discontinuities along the vein due to overlapping regions created by fracture propagation across mechanical interfaces, such as pyritized (Fig. 9f) and convolute-laminations beds (Fig. 9h).

Figure 9. Image showing the intersection of vein trace patterns in both plan and cross section views. a) Plan view with veins exhibiting isolated tips. b) Schematic drawing highlighting the veins (blue lines). It is observed that the pattern forms an overlapping region creating a discontinuity. c) Plan view with veins exhibiting isolated tips splay intersection. d) Schematic drawing highlighting the veins (blue lines). It is observed that the pattern does not create a discontinuity. e) Cross section view with veins exhibiting isolated tips. f) Schematic drawing highlighting the veins (blue lines). It is observed that the pattern results in an overlapping region around the pyritized layer (black features), leading to the creation of discontinuity. g) Cross section view showing veins with isolated tips. h) Schematic drawing highlighting the veins (blue lines). The pattern generates an area of overlap around the convolute layer, resulting in the formation of a discontinuity.

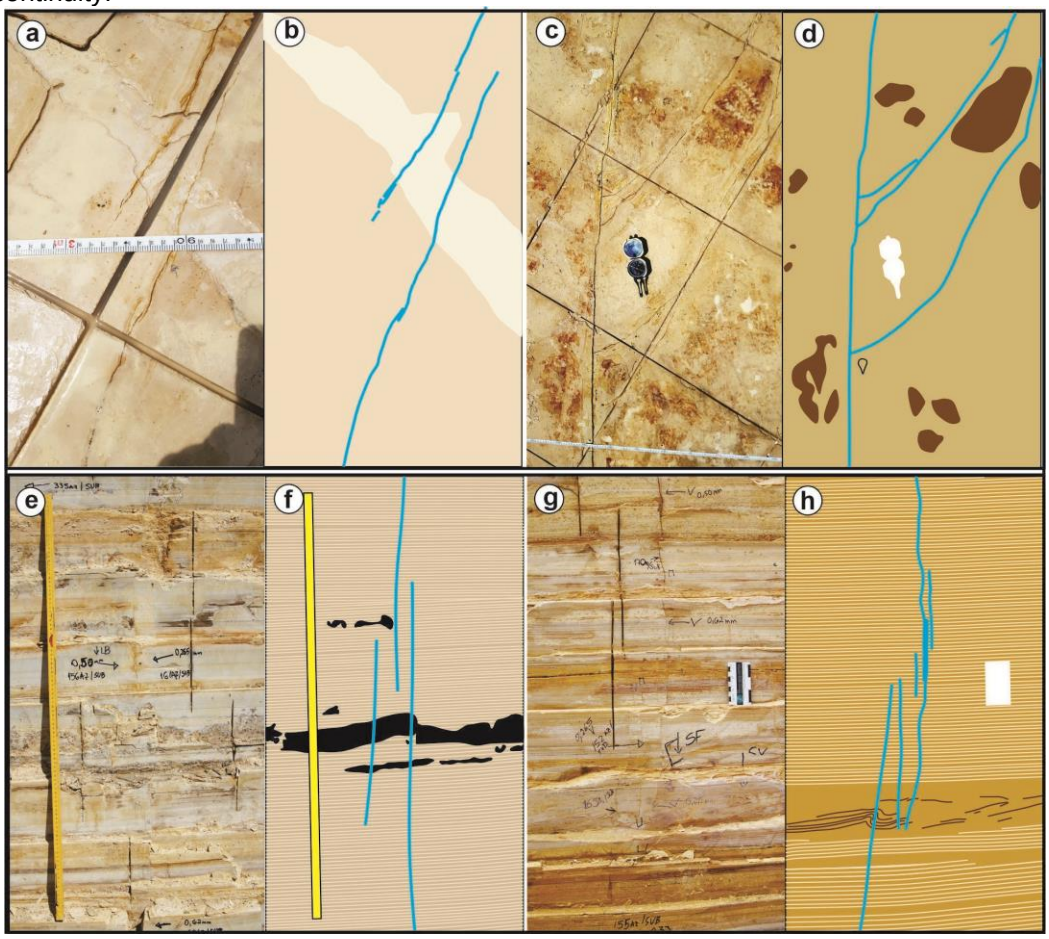

Source: The author.

We carried out UCS measurements on two pseudo-wells (logs 1 and 2) (Fig. 10a). The mechanical strength values recorded in Log 1 showed a mean of 152 MPa and maximum and minimum values of 422 and 66 MPa, respectively. Additionally, the log 1 displayed variations in curve behaviour, with specific focus on the intervals of 0 to 1.40 m and 2.00 to 3.00 m, where the mechanical strength values are notable for their high values. Similarly, mechanical strength values recorded in Log 2 showed a mean of 109 MPa and maximum and minimum values of 245 and 29.6 MPa, respectively. Additionally, the log 2 displayed variations in the curve behaviour, with particular emphasis on the intervals of 0 to 1.40 m, which showed high values of strength. Above this interval, the curve experienced a decline in mechanical strength, reaching values below the mean and approaching 50 MPa. Then, the curve presented an increase above mean values near the 3.00 m interval before experiencing another decrease towards the top of the log 2. After analysis of mechanical strength in logs 1 and 2, we were able to observe occurrence of high resistance values in specific intervals within these records (Fig. 10b).

These values were considered and applied to divide the outcrop into mechanical units and, later, analyse the behaviour of the fractures (Fig. 10b). Through the mechanical strength logs, we observed that fractures present vertical discontinuity at points where the UCS values show considerable variations. The vertical discontinuities are highlighted by overlapping regions that display steps-like features (see black circles in Fig. 10b). These steps show regular spacing between individual planes. However, despite the regularity in spacing, there is notable variability in the strike orientation of these steps. As a result, we can divide the outcrop into three mechanically distinct interfaces. Due to vertical discontinuity, we build DFN models considering both vertically continuous and discontinuous fractures.

Figure 10. Image showing the UCS results of the laminated limestone of the Crato Formation. a) Photograph indicating the locations of the pseudo-wells where we conducted mechanical strength data acquisition. b) Schematic drawing showing traces of vertical veins (red and pink traces), two profiles of mechanical resistance (dark blue lines) and the division of mechanical stratigraphy (coloured scale on the left side). Black circles point discontinuity on vertical fractures.

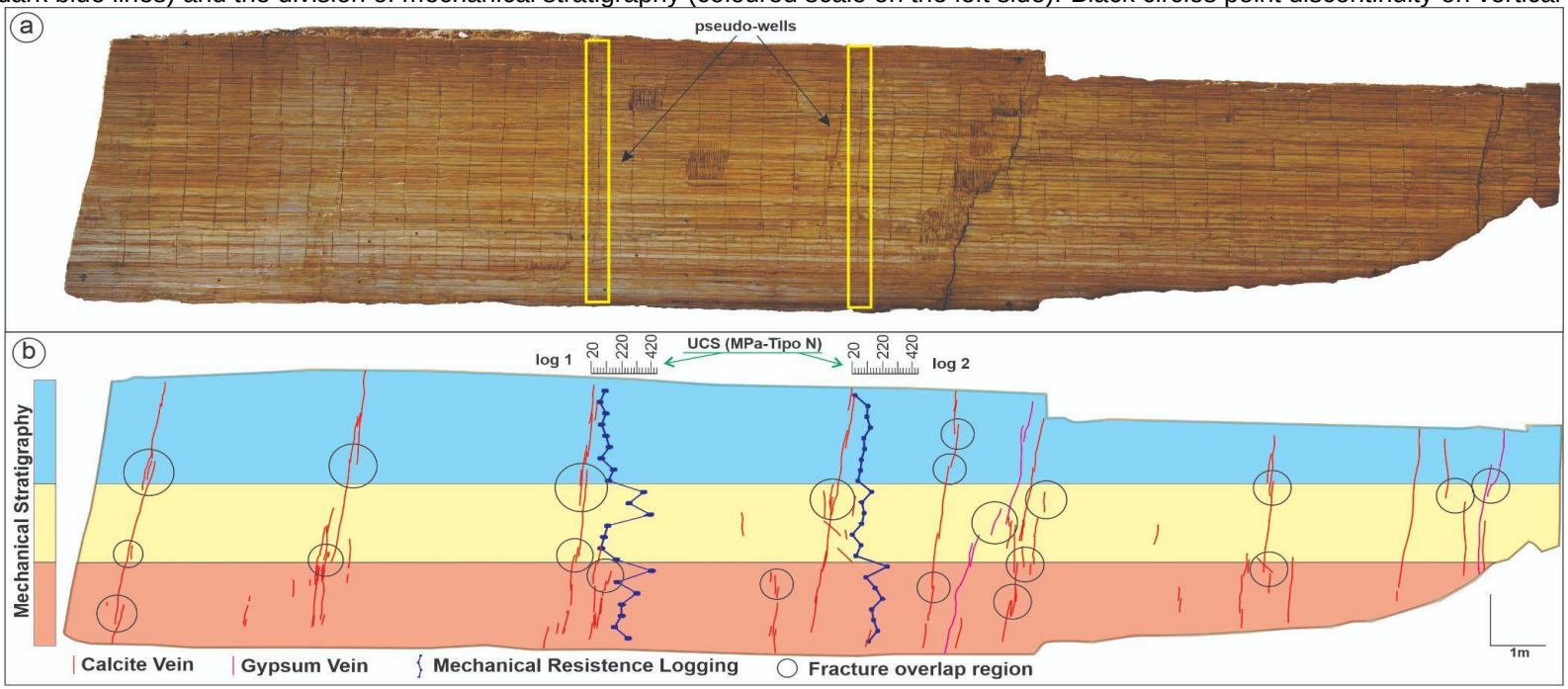

Source: The author

4.2. Digital image analysis

The capability of identifying and quantifying reservoir fracture networks by digital image analysis is demonstrated by the present result. This was made possible by the extraction of attributes from fracture networks that were present in reservoir and outcrop scale models, based on their corresponding digital images. In the reservoir-scale model, 63 fracture traces were recognized in the 100 x 140 m-wide digital model. These individual traces of fractures (Fig. 11b) are inputted into FracPaQ software with the purpose of calculating the intensity values using virtual scanlines (P10) (Fig. 11b). In order to perform a more detailed analysis, we isolated the fracture traces belonging to the individual sets, Set 1 strikes NNW-SSE and Set 2 strikes NE-SW. After performing the calculations, we observed that the intensity values for the fracture traces in Set 1 were 0.45, while the intensity values for the fracture traces in Set 2 were 0.85.

The calculated intensity values are then further utilized for the subsequent computation of the 3D intensity (P32), which is important to assess the properties of the fracture network. The values of P32 were about 0.45, for set 1, and 0.85, for set 2. These values were obtained from Wang (2005), which relates the Fisher number (k) to the angle between the scanline strike (ρ) and fracture plane. The P32 results of this intensive analysis are presented in Table 1.

Figure 11. Fracture system of the Crato Formation. a) Regional scale orthomosaic from the laminate limestone. b) Fracture trace map derived from a. The fracture traces were inserted into FracPaQ software with the aim of calculating the intensity values using virtual scanlines, P10 NE-SW (red line), and P10 NW-SE (blue line). c) Rose diagram showing the strike of fracture traces, NNW-SSE and NE-SW, extracted from b.

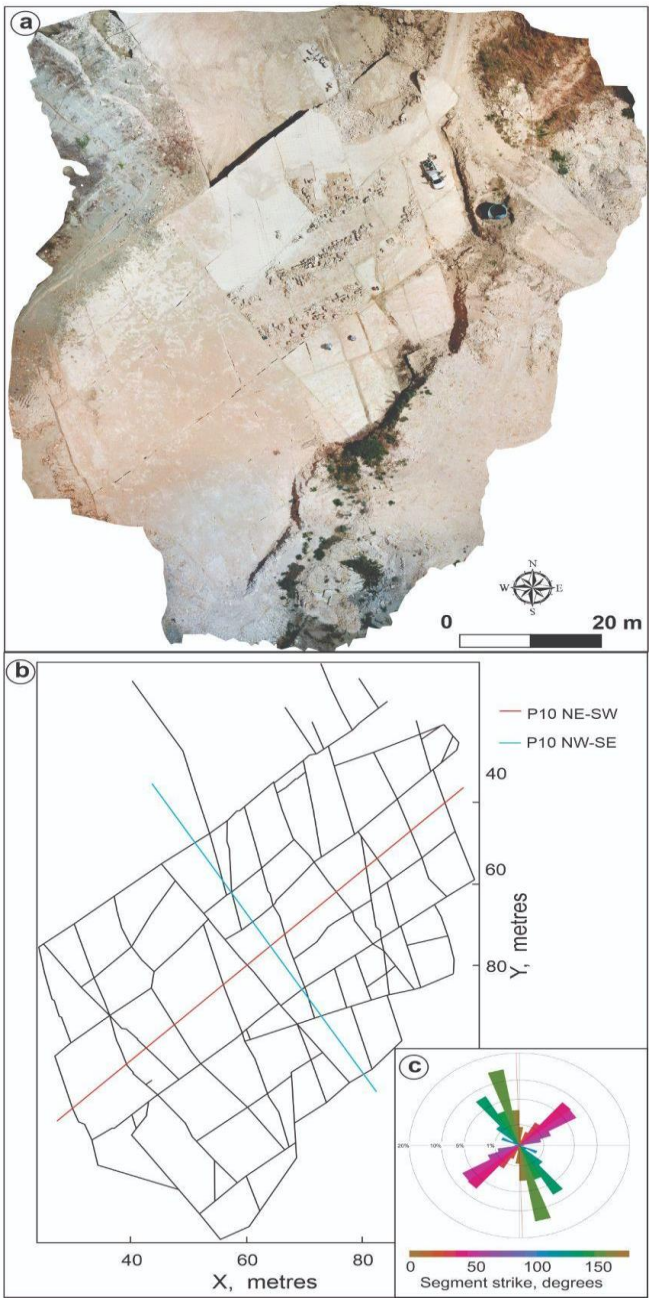

Source: The author.

Similarly, in the outcrop-scale model, 68 fracture planes were recognized in the 5x25 m-wide high-resolution panel, representing the outcrop digital model. In order to represent the better fit of the fracture network, structural data of the veins were collected directly from the studied outcrop and later integrated into the outcrop digital model. These individual traces of veins (Fig. 12c) also were inputted into FracPaQ software to calculate the intensity values using virtual

scanlines (P10) (Fig. 12d). In the studied outcrop, we observed that the ENE-SSW (set 2) fracture set was undersampled due to the angle relation between the sampling line and the orientation of the fracture strike. In order to fill this gap of information we considered the processing of data collected from previous published works in the same area (Miranda et al., 2018) (Fig. 12f). As a result, the intensity values for the fracture traces in the fractures Set 1 is 1.71, whereas the intensity values for fractures in Set 2 is 2.98. The calculated volumetric intensity values of P32 for the two sets is ~1.71, and ~2.98, respectively. The P32 results of this analysis are shown in Table 1.

Height and length attributes of the fracture network were also acquired. The attribute height that represents a small section of a fracture was measured from the outcrop-scale model, and its mean height value was 1 mm. On the other hand, the attribute length that represents a larger area of the fracture was measured from both regional and outcrop scale models (Fig. 11b and 12b). The mean value was 4.8 m for the outcrop-scale model. Additionally, the reservoir scale model shows a mean for the fracture length of 49.6 m for Set 1 and 59.4 m for Set 2. However, it is important to note that the maximum length of the fractures is about 140 m.

Using digital image analysis, we were able to collect both the length and height values of the fractures to determine the aspect ratio used to build the DFN models. For the regional-scale model, we considered aspect ratio values of 1:8 and 1:50 for DFN models with vertically continuous and vertically discontinuous fractures, respectively. Similarly, for outcrop-scale models, we considered aspect ratio values of 1:1.2 and 1:4.8 for DFN models with vertically continuous and vertically discontinuous fractures, respectively. The aspect ratio values are displayed in Table 1.

Figure 12. Fracture characterization of the laminated limestone of the Crato Formation. a) 3D outcrop image. b) Schematic drawing highlighting the analysed veins. c) Digital image showing frontal face of the studied outcrop. d) Vertical veins analysed from Fracpaq, highlighting scanlines P10 (blue lines). e) Lower hemisphere stereogram showing the behaviour of the fracture network in the analysed outcrop. f) Lower hemisphere stereogram representing the attitudes of the fracture network in the region (Miranda et al., 2018).

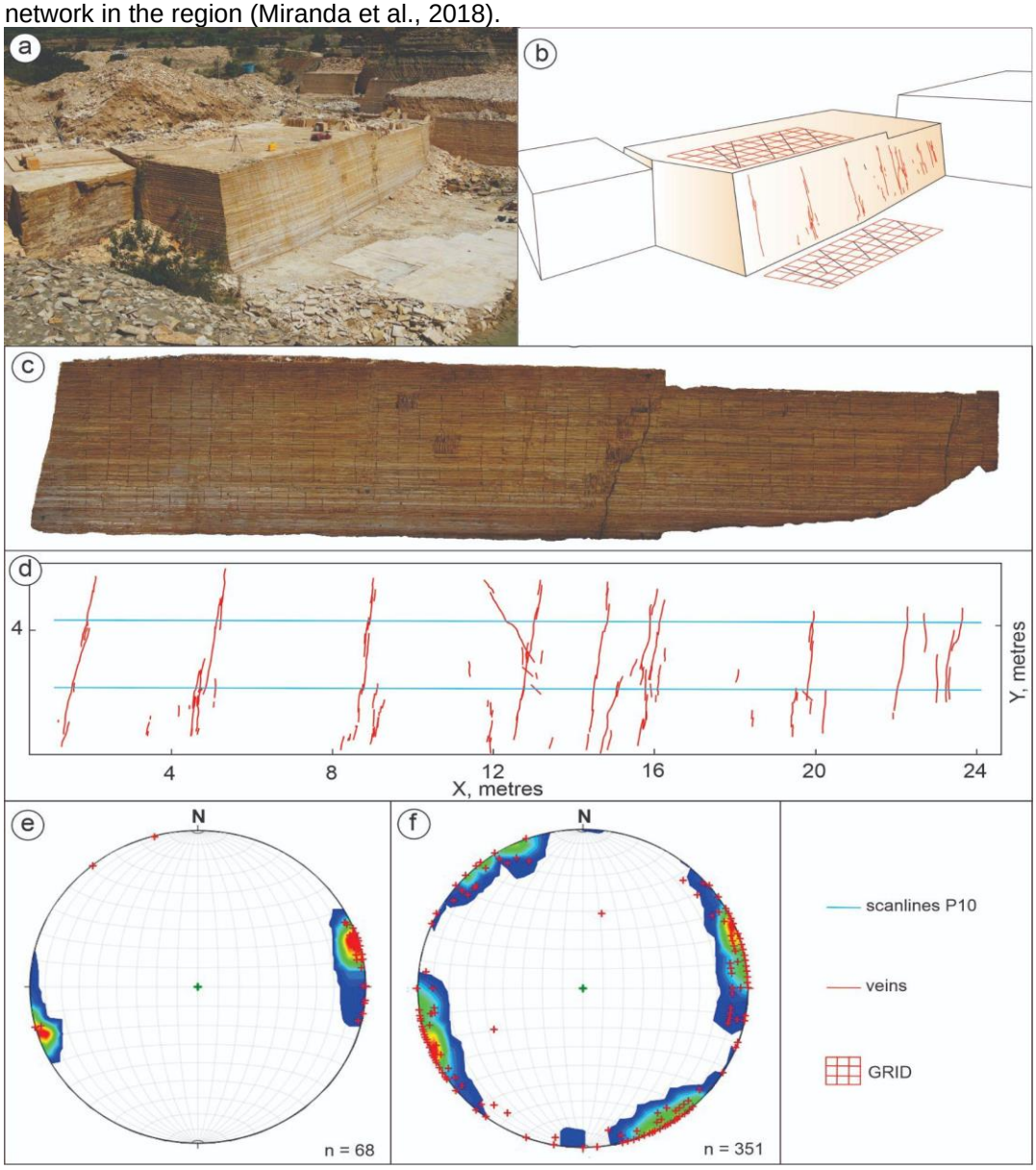

Source: The author.

4.3. DFN Modelling

The DFN models were built using the data collected in situ from two primary sources: 1) at the outcrops and 2) from pseud-wells. Firstly, measurements taken at the outcrop were collected and analysed in detail, providing better insights into the geological properties of the surrounding area. Secondly, data obtained from pseudo-wells were utilized to further refine the models. Two distinct types of models were developed as part of this study: the

Type 1 model, which represents the reservoir scale, and the Type 2 model, which was elaborated to represent the specific properties at the outcrop scale.

4.3.1 Type 1 Model - Reservoir scale

We created two DFN models for type 1 (representing the reservoir scale), each one was built using the vertical discontinuity and continuity of fractures, respectively, as a key criterion.

The first DFN model was built based on vertical discontinuous fractures (Fig. 13). This model features an extensive fracture network, totaling a number of 44802 of individual fractures modelled within the 150 m x 150 m x 15 m geocellular volume. The results obtained from this model represent both the porosity and the equivalent permeability of the fracture network, which are essential parameters for estimating both storage and fluid flow in hydrocarbon reservoirs. Results obtained from this study indicates that the storage level of fracture porosity has a maximum value up to 2.27 x 10^{-2} percent (Fig. 13c). Additionally, the results demonstrate that the equivalent horizontal permeability is estimated up to 1.26 x 10^{3} D for Kxx (Fig. 13d), and 1.21 x 10^{3} D for Kyy (Fig. 13e). Furthermore, the study showed that the calculated value of equivalent vertical permeability, Kzz, is estimated to be 2.22 x 10^{3} D (Fig. 13f).

The second DFN model was built based on vertical continuous fractures (Fig 14). This model represents an extensive fracture network that comprises a significant number of 22897 fractures stochastically modelled within the 140m x 140m x 15 m geocellular volume. The results obtained from this model represent both porosity and equivalent permeability of the fracture network, which are essential parameters for estimating both storage and fluid flow in hydrocarbon reservoirs. As result, fracture porosity shows maximum value up to 0.13 x10^{1} percent (Fig. 14c). Additionally, the calculated equivalent horizontal permeability Kxx shows a maximum value up to 5.46 x10^{3} D (Fig. 14d), while the equivalent horizontal permeability Kyy shows a maximum value up to 2.07 x10^{3} D (Fig. 14e). Furthermore, the study shows that the calculated value of equivalent vertical permeability, Kzz, is estimated to be 1.12 x10^{4} D (Fig. 14f).

Figure 13. Reservoir scale DFN models considering the vertical discontinuity of fractures. a) Vertically discontinuous fracture network built by regional scale DFN modelling. b) 150 x 150 x 15 m geocellular volume built by DFN model showing the overall view of the porosity and equivalent permeability. C) Fracture porosity values calculated for the outcrop geocellular volume. d and e) Equivalent horizontal fracture permeability calculated for the outcrop geocellular volume, kxx and kyy respectively. f) Equivalent vertical fracture permeability calculated for the outcrop geocellular volume (Kzz). The model lowest values were hidden to have a better view of the highest values.

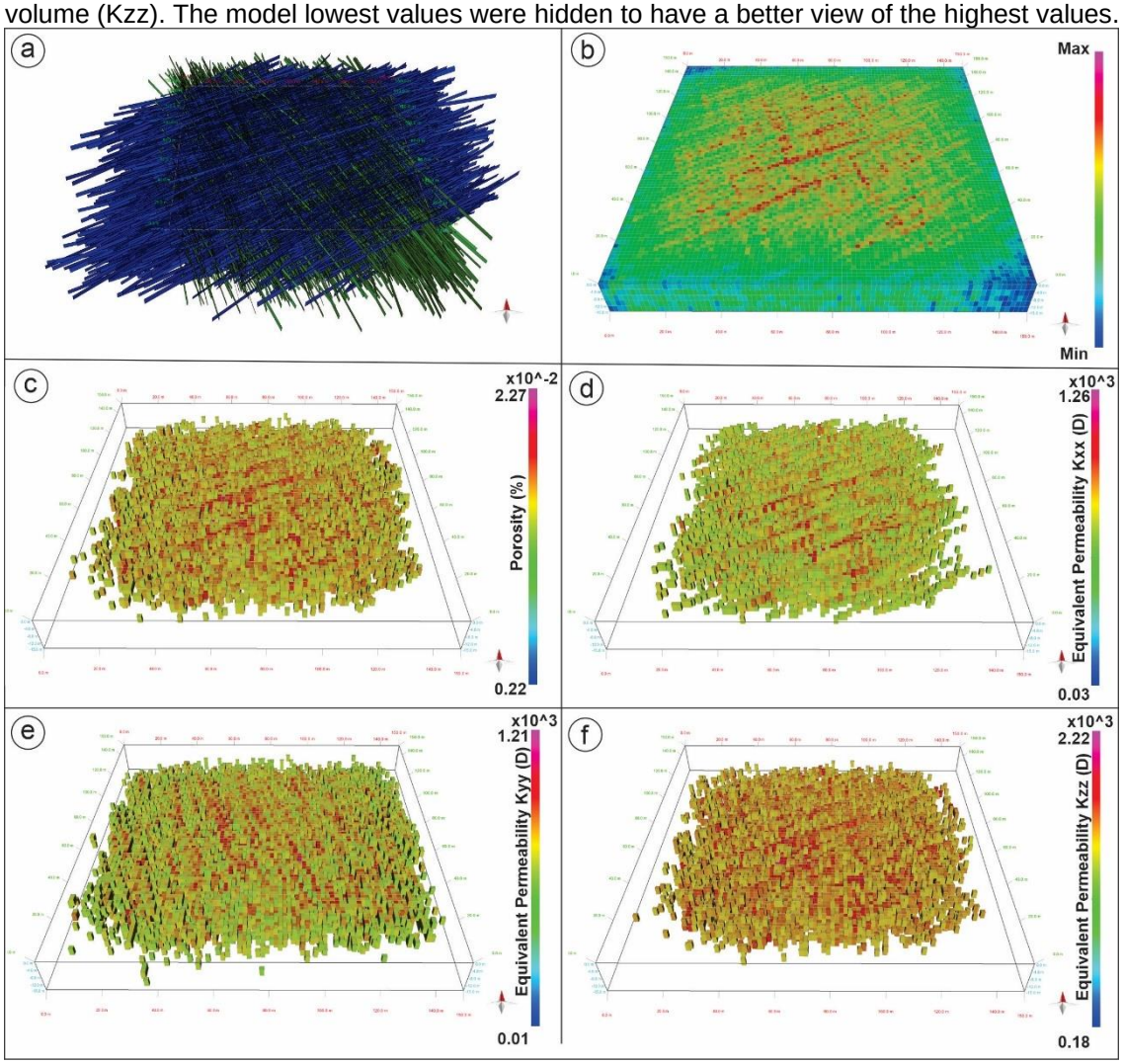

Source: The author.

Figure 14. DFN models in reservoir scale considering the vertical continuity of fractures. a) Vertically continuous fracture network built by regional scale DFN modelling. b) 140 x 140 x 15 m geocellular volume built by DFN model showing the overall view of the porosity and equivalent permeability. C) Fracture porosity values calculated for the outcrop geocellular volume. d and e) equivalent horizontal fracture permeability calculated for the outcrop geocellular volume, kxx and kyy respectively. f) equivalent vertical fracture permeability calculated for the outcrop geocellular volume (Kzz). The model lowest values were hidden to have a better view of the highest values.

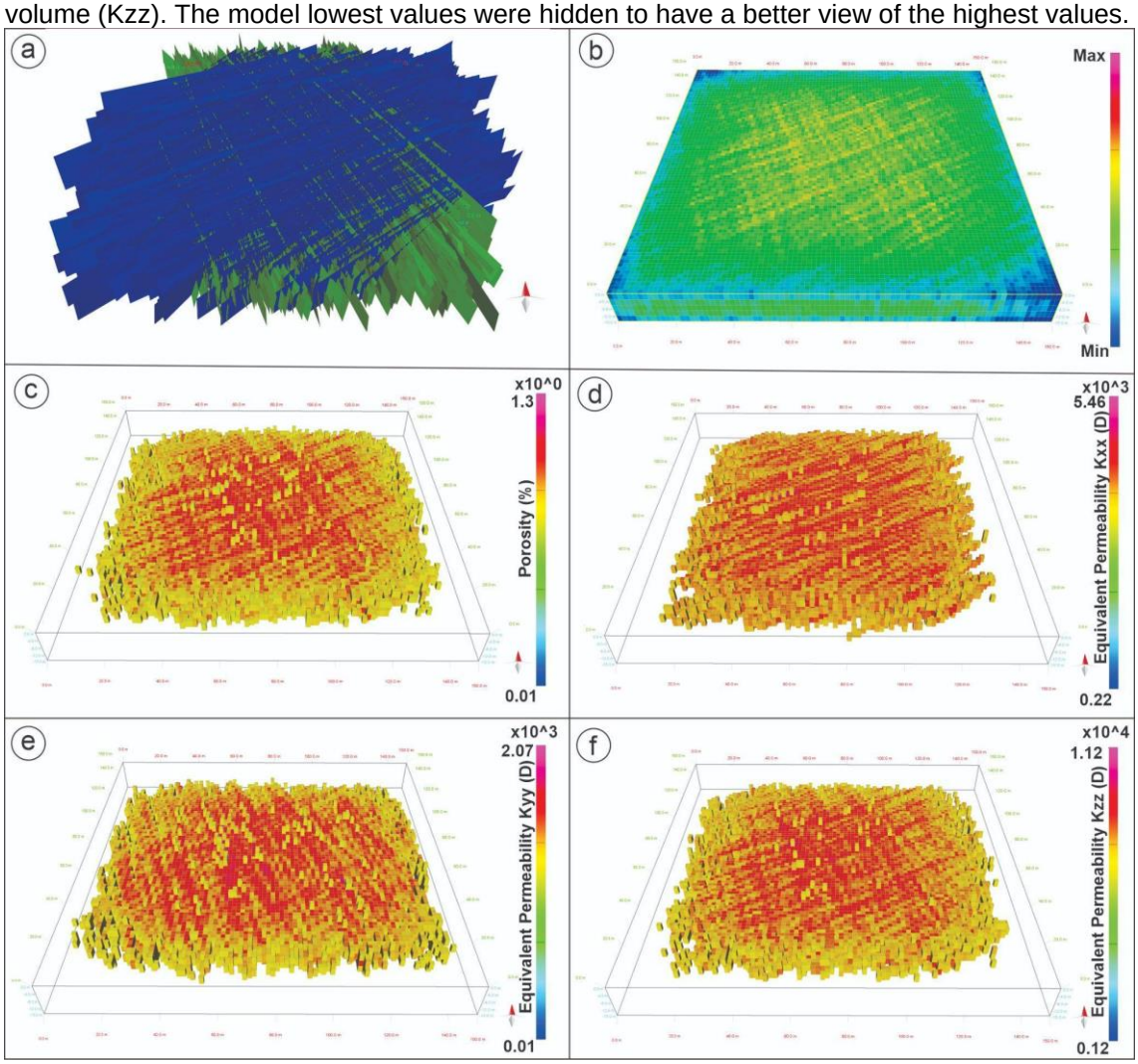

Source: The author.

4.3.2. Type 2 Model - Outcrop Scale

We also created two DFN models for type 2 (representing the outcrop scale). Each model was built considering the vertical discontinuity and continuity of fractures, respectively.

The first DFN model was built based on vertical discontinuous fractures (Fig. 15). This model highlights a dense fracture network that shows a number of 1404 of individual fracture elements modelled within the 5 m x 25 m x 5 m geocellular volume. The results obtained from this model represent both the porosity and the equivalent permeability of the fracture network, which are

considered as hydrodynamics parameters for calculating both storage and fluid flow in hydrocarbon reservoirs. The results show that the fracture porosity has a maximum value up to 3.94 $x10^{-2}$ percent (Fig. 15c). The results also demonstrated that the equivalent horizontal permeability values are 2.45 $x10^{3}$ D for Kxx (Fig. 16d), and 2.25 $x10^{3}$ D for Kyy (Fig. 15e). Additionally, this study reports that the calculated value of equivalent vertical permeability, Kzz, is estimated to be 3.25 $x10^{3}$ D (Fig. 15f).

The second DFN model was built based on vertical continuous fractures (Fig. 16). This model shows an extensive fracture network with a number of 353 individual fractures within the 5m x 25m x 5 m geocellular volume. As result, fracture porosity shows maximum values up to 3.72 $x10^{-2}$ % (Fig. 16c). Additionally, the calculated equivalent horizontal permeability Kxx shows a maximum value up to 2.17 $x10^{3}$ D (Fig. 16d), while the equivalent horizontal permeability Kyy shows a maximum value up to 1.89 $x10^{3}$ D (Fig. 16e). Furthermore, the result shows that the calculated value of equivalent vertical permeability, Kzz, is estimated to be 3.09 $x10^{3}$ D (Fig. 16f).

Table 2 provides a comprehensive and concise summary of the results obtained from DFN modelling.

Figure 15. Image showing outcrop scale models considering the vertical discontinuity of fractures. a) Vertically discontinuous fracture network built by DFN modelling. b) 5 x 25 x 5 m geocellular volume built by DFN model showing the overall view of the porosity and equivalent permeability. C) Fracture porosity values calculated for the outcrop geocellular volume. d and e) Equivalent horizontal fracture permeability calculated for the outcrop geocellular volume, kxx and kyy respectively. f) Equivalent vertical fracture permeability calculated for the outcrop geocellular volume (Kzz). The model lowest values were hidden to have a better view of the highest values.

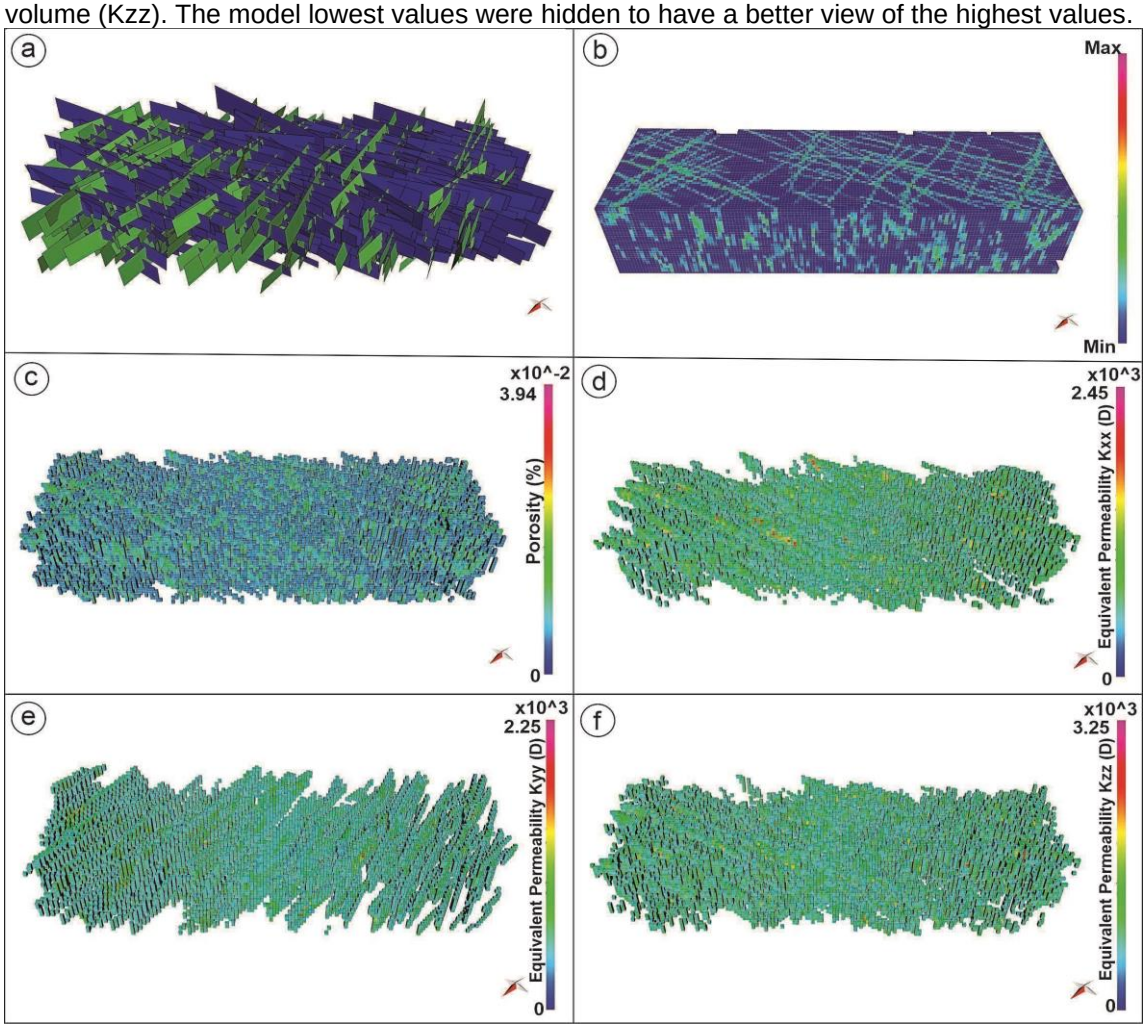

Source: The author

Figure 16. Outcrop scale DFN models considering the vertical continuity of fractures. a) Vertically continuous fracture network built by DFN modelling. b) 5 x 25 x 5 m geocellular volume built by DFN model showing the overall view of the porosity and equivalent permeability. C) Fracture porosity values calculated for the outcrop geocellular volume. d and e) Equivalent horizontal fracture permeability calculated for the outcrop geocellular volume, kxx and kyy respectively. f) Equivalent vertical fracture permeability calculated for the outcrop geocellular volume (Kzz). The lowest values were hidden to have a better view of the highest values.

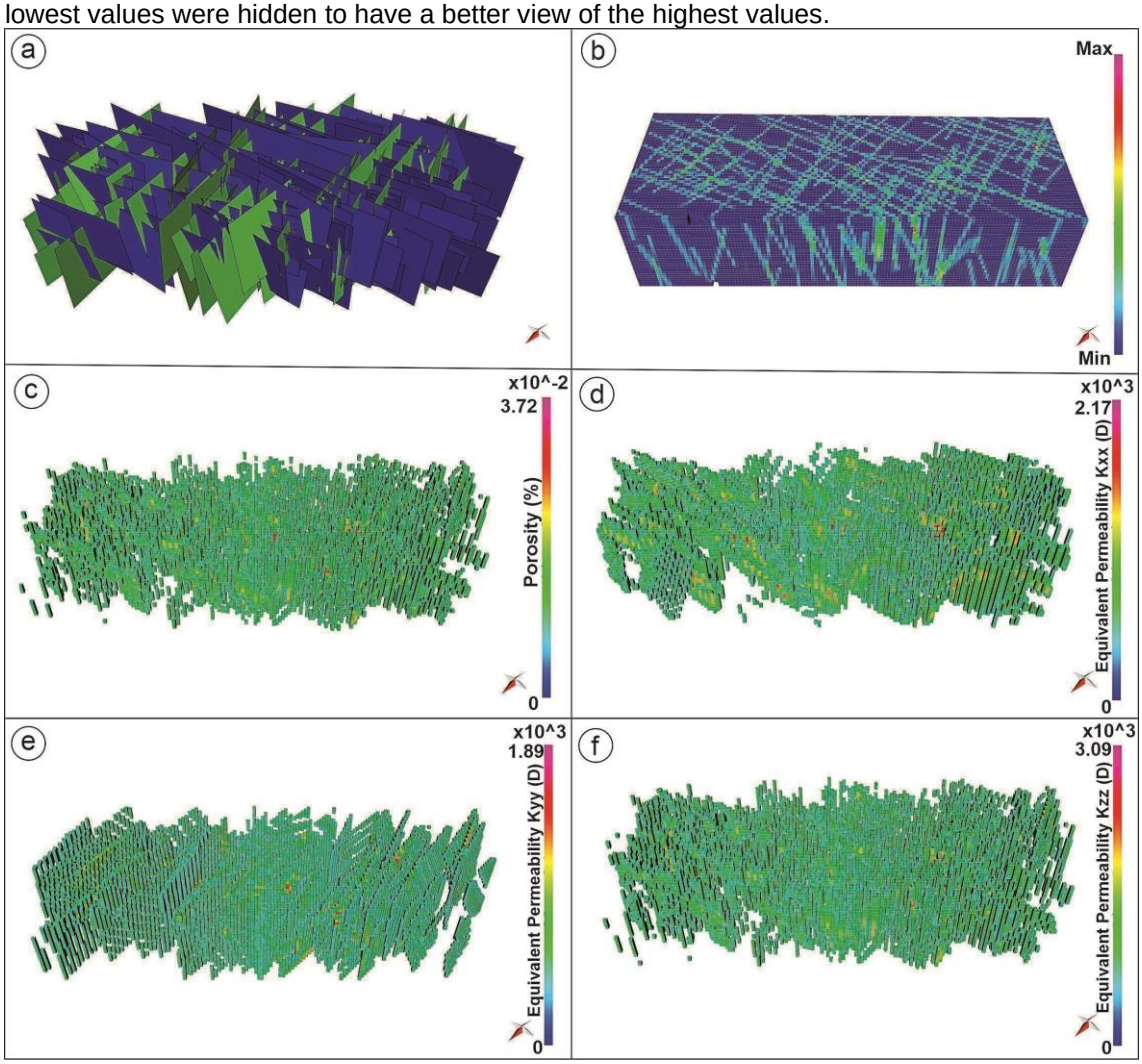

Source: The author

Table 2. Table summarising the results of the DFN modelling.

DFN Model	Outcrop DFN Model				Reservoir DFN Model			
	Vertically Discontinuous Fracture		Vertically Continuous Fracture		Vertically Discontinuous Fracture		Vertically Continuous Fracture	
	min	max	min	Max	min	max	min	max
Fracture Porosity (%)	0	3.94×10^{-2}	0	3.72×10^{-2}	0.02	2.27×10^{-2}	0.01	1.3×10^{0}
Equivalent Horizontal Fracture Permeability Kxx (D)	0	2.45×10^{3}	0	2.17×10^{3}	0.03	1.26×10^{3}	0.22	5.46×10^{3}
Equivalent Horizontal Fracture Permeability Kyy (D)	0	2.25×10^{3}	0	1.89×10^{3}	0.01	1.21×10^{3}	0.01	2.07×10^{3}
Equivalent Vertical Fracture Permeability Kzz (D)	0	3.25×10^{3}	0	3.09×10^{3}	0.18	2.22×10^{3}	0.12	1.12×10^{4}

Source: The author

5. Discussions

5.1. Fracture and mechanical stratigraphy

Fracture stratigraphy aims to divide rocks into intervals based on vertical extent, considering the attributes that characterise the fracture network (Laubach et al., 2009; Ferrill et al., 2017). In this study a set of subvertical fractures cuts the carbonates of the Crato Formation, composing the background deformation according to mechanical interfaces and other heterogeneities (pyritized and convolute layers) (Araújo et al., 2020). The results of the fracture analysis are consistent with a brittle deformation of the host rock, mainly composed of joints and veins. Joints are highlighted due to the presence of aperture of different sizes and partial fillings, suggesting a dissolution process in this region, leading to creation of voids that may have been subsequently filled by other minerals or sediments. Alternatively, preexisting structures may have provided planes of weakness for joints development, suggesting that they may have formed utilizing preexisting planes as guides. On the other hand, veins in the Crato Formation are highlighted for their pattern in response to mechanical intervals. We observed vertical discontinuities in fractures at points where significant variations in UCS values were evident. These vertical discontinuities in the fracture network may lead to a lack of connectivity within the system, which can limit the fluid flow between compartmentalised fractured units (e.g., Underwood et al., 2003; Cooke et al., 2006). In other words, the presence of vertical discontinuities in fracture planes can create barriers that hinder the movement of fluids between different parts of the fracture system. This effect may have significant implications for the reservoir's permeable network, even isolated flow zones (Cooke et al., 2006). Subdividing the outcrop into mechanically distinct intervals may be of great importance for understanding vertical behaviour of fractures and their influence on the distribution of the permeable network.

5.2. Pseudo-wells as a tool for reservoir analogue modelling

Pseudo-wells used as P10 intensity scanlines demonstrated useful applications in this study. Valuable information was extracted from digital outcrop models by the technique employed. Both horizontal and vertical pseudo-wells were employed, playing essential roles in different aspects of the analysis.

In plan view and cross-sections, horizontal pseudo-wells were utilized as virtual P10 intensity scanlines. Access to data related to the fracture network, necessary for the analysis, was efficiently provided by these virtual scanlines. The decision to use horizontal pseudo-wells in the cross-sections was motivated by the predominantly vertical nature of the studied fracture network (Zakirov and Zakirov, 1996).

Vertical pseudo-wells played a critical role in investigating the mechanical strength layering patterns of the examined rocks. Within the cross-sectional views, they were specifically utilized to serve this objective. This approach allowed a detailed analysis of the mechanical strength along the cross-sections, complementing the information provided by the horizontal pseudo-wells.

P10 pseudo-wells employed for obtaining statistical data and representing geometric aspects of the fracture network, offer detailed information on a small scale. Subsequently, this data can be extrapolated to a larger scale using the DFN (Lepillier et al., 2020).

Therefore, the effectiveness of this approach in extracting valuable information from digital outcrop models was reinforced by the combination of pseudo-wells as P10 intensity scanlines and consideration of the reservoir fracture network. The utilization of horizontal and vertical pseudo-wells facilitated the analysis of reservoir properties, such as fracture porosity and permeability, providing a better understanding of geological and mechanical characteristics of the rocks under study.

5.3. Fracture porosity

The calculated values for fracture porosity at Upper Cretaceous carbonates of the Crato Formation are shown in Figure 17a. DFN modelled at outcrop scale showed interesting results regarding fracture porosity. Fracture porosity values in vertically discontinuous models were slightly higher than vertically continuous models. This observation suggests a consistent behaviour of fracture porosity at outcrop-scale, indicating a degree of uniformity and possibly underlying geological controls. On the other hand, different results for fracture porosity were obtained from DFNs modelled at the reservoir-scale. The analysis also considered the presence of vertical discontinuities and continuity of fractures, leading to observation of distinct values with magnitude up to 10^2.

Notably, magnitudes values of 10^{-2} and 10^{0} are exhibited by fracture porosity when influenced by vertical discontinuity and continuity fractures, respectively. These observations highlight the critical role played by fracture characteristics in the distribution and magnitude of fracture porosity within reservoirs. The discontinuous behaviour of fractures is due to the mechanical control exerted by the heterogeneities present in carbonates as convolute layers.

A slight reduction in fracture porosity with increasing scale was observed when analyzing the vertical discontinuity of fractures and its scale effect. The reduction in fracture porosity with increasing scale has already been reported by Giuffrida et al (2019). These authors reported that the reduction in porosity was much more significant, reaching magnitudes greater than 10^{-2}. The reduction in fracture porosity shown in our results may be related to the absence of stratabound fractures within the analysed fracture network. On the other hand, a significant increase in fracture porosity with increasing scale was observed when analyzing the vertical continuity of fractures and its scale effect. Panza et al (2016) studied carbonate rocks in Italy and reported an increase in fracture porosity with increasing scale. These authors attributed the increase in fracture porosity to the existence of fracture zones up to 10 meters in height. The significant increase in fracture porosity observed in our model may also be associated with fracture cluster zones (as observed by Miranda et al., 2018) reaching heights of tens meters, exhibiting good connectivity. Furthermore, the discrepancy in storage capacity between the different modelling scales suggests that the influence of vertical fracture continuity may play an important role in storage characteristics. These results highlight the importance of considering scale-dependent effects and specific reservoir conditions, such as vertical continuity of fractures, when assessing storage capacity in fractured reservoir systems.

Figure 17. Graphs showing the relationship between the fracture network permo-porosity and scale effect. a) Fracture porosity shows a significant increase in values in the vertically continuous fracture model with increasing scale. b) Equivalentes horizontal fracture permeability (Kxx and Kyy) around 10^3 D. These values exhibit a low degree of anisotropy, almost isotropic behaviour. c) Equivalent Vertical fracture permeability (Kzz) shows a significant increase in the vertically continuous fracture model with increasing scale. All models computed from vertical discontinuity fracture show a low reduction in their properties with increasing scale.

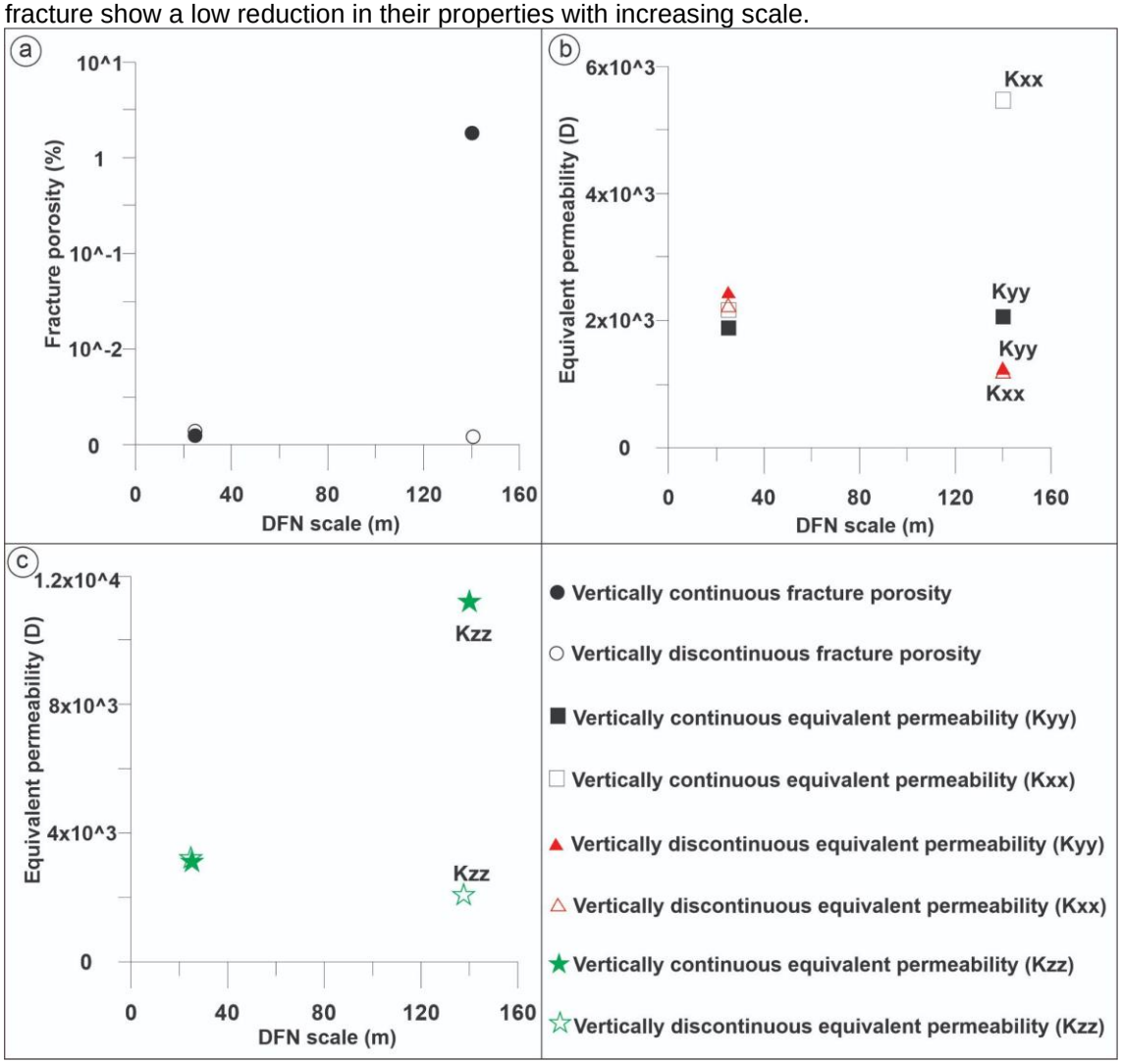

Source: The author

5.4. Equivalent fracture permeability

DFNs modelled at the outcrop-scale demonstrated notable similarities in the magnitudes of the equivalent fracture permeability, which ranged around 10^3. Remarkably, this consistency persisted in both different fracture directions (Kxx, Kyy, and Kzz) and different vertical continuity of fractures (Fig. 17). These observations imply that fracture permeability at the outcrop-scale is primarily influenced by factors other than fracture orientation or vertical connectivity, such as fracture aperture and network characteristics (Oda, 1982; Klimezak et al.,

2010; Giuffrida et al., 2019). According to Oda (1982), the impact of fracture aperture on permeability is a critical factor in determining fracture permeability. Furthermore, the computed model demonstrated values with low degree of anisotropy, almost isotropic conditions for the horizontal permeability of fractures. Previous studies with similar results related isotropic phenomenon to fracture saturation (Bai and Pollard, 2000) and cross-orthogonal jointing (Bai et al., 2002), conditions that exert strong control over horizontal fluid flow in a fracture network. Despite the low anisotropy in horizontal equivalent permeability, we noted that the Kxx values in the vertically continuous and reservoir scale models were higher than in the discontinuous model (Fig. 17b). We believe that this behaviour is associated with the greater volume and length of fractures in the NE-SW fracture set.

Similarly, consistent magnitudes values, ranging around 10^3, were also observed in horizontal equivalent fracture permeability in DFNs modelled at reservoir scale. These values consistency was maintained regardless of the fracture direction (Kxx and Kyy) but different from vertical continuity of fractures (Kzz). The low anisotropy showed by Kxx and Kyy magnitude values is analogous to that computed at outcrop scale, suggesting that the controlling conditions (Bai and Pollard, 2000; Bai et al., 2002) and distribution of horizontal fluid flow may be similar and repeatable along different scales. Despite the differences in vertical fracture continuity, the magnitude of horizontal permeability showed similarities in both scale models. This observation suggests that vertical fracture continuity does not have a significant impact on horizontal permeability.

On the other hand, for the vertical equivalent fracture permeability Kzz (Fig. 17c), the magnitudes show distinct values considering vertical discontinuity and continuity. For this property, magnitudes of 10^3 and 10^4 were observed when influenced by vertical discontinuity and continuity, respectively. Permeability values in Kzz direction greater than permeability values in Kxx and Kyy directions have been documented in studies conducted on carbonate rocks of the Altamura Formation in the Murge Plateau of southern Italy (Panza et al., 2015; 2016). This difference can be attributed to the presence of preferential flow paths along vertically continuous fractures, which allow greater connectivity and facilitate vertical fluid flow (Cooke et al., 2006).

6. Conclusions

The analysis of the fracture networks in the Crato Formation revealed that deformation in the carbonates is predominantly brittle, characterised by joints and veins.

A relevant aspect observed in the behaviour of the fracture networks was its response regarding mechanical intervals. The presence of vertical discontinuities was observed in fractures coinciding with points where considerable variations in UCS values occur. This indicates that the fracture networks exhibited a differentiated mechanical response. This characteristic was considered in the DFN models.

We employed pseudo-wells as P10 intensity scanlines and obtained significant results for this study. They enabled efficient extraction of crucial information from digital outcrop models, providing relevant statistical data and geometric aspects regarding the fracture network and rock's mechanical strength. Thus, we found that pseudo-wells are effective in acquiring detailed information at a smaller scale, enabling extrapolation to a larger scale by the use of DFN models.

The results obtained from field analyses and digital outcrop models were used to build DFN models at different scales (outcrop and reservoir scale). The DFNs were built to represent aspects of the fracture network such as volume, vertical continuity, impact on porosity and permeability properties, and scale effects. The outcrop-scale DFN models showed similar porosity values, suggesting that storage capacity may not be affected by the vertical continuity of fractures. Similarly, the equivalent permeability of fractures at the same scale exhibited similar values in all three directions: Kxx, Kyy, and Kzz. This suggests that, maybe at this scale analysis, the vertical connectivity of fractures does not have influence on fluid flow.

The reservoir-scale DFNs show distinct values in fracture porosity. The models built with vertical continuity fractures showed higher values compared to those built with vertical discontinuity. This indicates that increase in fracture porosity may be associated with fracture zones that reach heights of tens of meters and exhibit good connectivity.

At the same reservoir scale, the equivalent horizontal fracture permeability showed similar values in both models for the Kxx and Kyy directions. Based on this research, the vertical continuity of fractures does not have a significant impact on fluid flow in horizontal directions. On the other hand, the results for the equivalent vertical fractures permeability (Kzz) showed higher values in the DFNs that considered vertically continuous fractures. This indicates that, perhaps at this study scale, the fluid flow is positively influenced by the vertical continuity of fractures.. Additionally, the higher flow in the vertical direction (Kzz) compared to the horizontal direction may be attributed to the existence of preferential flow paths along vertically continuous fractures, which contribute for greater connectivity and facilitate vertical fluid flow.

Considering the scale effect, we can observe some particularities about equivalent permeability of the fracture systems. Horizontal permeability appears to be less affected by vertical continuity of fractures; this may indicate that these characteristics of horizontal fluid flow and transport in a fractured reservoir can be well represented by downscaled models, such as outcrop models. On the other hand, equivalent vertical fracture permeability showed a strong dependence on the presence of continuous fractures. This may indicate that vertically continuous fractures enhance preferential flow pathways, allowing for greater vertical fluid movement.

These results highlight the importance of considering scale-dependent effects and specific reservoir conditions, such as vertical continuity of fractures, when assessing storage capacity and permeability in fractured reservoir systems.

Authors Contributions

Márcio Lima Alencar: Conceptualization, Investigation, Methodology, Writing - Original Draft, Writing - Review & Editing **Tiago Siqueira de Miranda**: Conceptualization, Investigation, Methodology, Resources, Writing - Original Draft, Writing - Review & Editing, Supervision **Osvaldo José Correia Filho**: Investigation, Writing - Review & Editing **José Antonio Barbosa**: Conceptualization, Investigation, Methodology, Resources, Writing - Review & Editing, Supervision **Igor Fernandes Gomes**: Conceptualization, Methodology, Writing - Review & Editing, **Germano Mário Silva Ramos**: Investigation **Araly Fabiana Lima de Araújo**: Investigation **Virginio Lopes Neumann:**

Investigation **Maria Alcione Lima Celestino**: Investigation **João Gabriel de Oliveira Topan**: Investigation

Acknowledgments

We are grateful to Petrobras who funded the projects "Pseudo-poços" and “Zona de Falhas” through research agreements approved by the National Agency of Petroleum, Natural Gas and Biofuels (ANP) and executed by the Department of Geology - UFPE. These projects provided the financial and logistic support for this research. We are also grateful to Petroleum Experts for academic license of MOVE software

References

Agosta, F., Alessandroni, M., Antonellini, M., Tondi, E., Giorgioni, M., 2010. From fractures to flow: A field-based quantitative analysis of an outcropping carbonate reservoir. Tectonophysics 490, 197–213. https://doi.org/10.1016/j.tecto.2010.05.005

Alencar, M.L., Correia Filho, O.J., Miranda, T.S. de, Barbosa, J.A., Celestino, M.A.L., Ramos, G.M.S., Araújo, A.F.L. de, Neumann, V.H., Topan, J.G. de O., Roemers-Oliveira, E., 2021. Soft-sediment deformation structures in Aptian lacustrine laminites: Evidence of post-rift paleoseismicity in the Araripe basin, NE Brazil. J South Am Earth Sci 105. https://doi.org/10.1016/j.jsames.2020.102955

Alvarez, L.L., Guimarães, L.J.N., Gomes, I.F., Beserra, L., Pereira, L.C., Miranda, T. S.; Maciel, B., Barbosa, J. A., 2021. Impact of Fracture Topology on the Fluid Flow Behavior of Naturally Fractured Reservoirs. Energies. https://doi.org/10.3390/en14175488

Andersson, J., Dverstorp, B., 1987. Conditional Simulations of Fluid Flow in Three-Dimensional Networks of Discrete Fractures, Water Resources Research.

Araujo, A.F.L., Ramos, G.M.S., Barbosa, J.A., Correia Filho, O.J., Alencar, M.L., De Miranda, T.S., Neumann, V.H., Celestino, A.M., Topan, J.G., 2020. Depositional and diagenetics controls on the mechanical stratigraphy of

aptian laminated limestones of crato formation. Rio Oil and Gas Expo and Conference 20, 35–36. https://doi.org/10.48072/2525-7579.rog.2020.035

Assine, M.L., 2007. Bacia do Araripe. Bol. Geociencias Petrobras 15, 371–389.Barling, N., Martill, D.M., Heads, S.W., Gallien, F., 2015. High fidelity preservation of fossil insects from the Crato Formation (lower cretaceous) of Brazil. Cretac. Res. 52, 605–622. https://doi.org/10.1016/j.cretres.2014.05.007.

Assine, M.L., 1994. Paleocorrentes e paleogeografia na Bacia do Araripe, Nordeste do Brasil. Revista Brasileira de Geociências 24, 223–232.

Assine, M.L., 1992. Análise estratigráfica da Bacia do Araripe, Nordeste do Brasil. Revista Brasileira de Geociências 22, 289–300.

Aydin, A., 2000. Fractures, faults, and hydrocarbon entrapment, migration and flow. Mar Pet Geol 17, 797–814.

Bai, T., Maerten, L., Gross, M.R., Aydin, A., 2002. Orthogonal cross joints: do they imply a regional stress rotation? J Struct Geol 24, 77–88.

Bai, T., Pollard, D.D., 2000. Fracture spacing in layered rocks: a new explanation based on the stress transition. J Struct Geol 22, 43–57.

Bense, V.F., Gleeson, T., Loveless, S.E., Bour, O., Scibek, J., 2013. Fault zone hydrogeology. Earth Sci Rev. https://doi.org/10.1016/j.earscirev.2013.09.008

Bilmes, A., D'Elia, L., Lopez, L., Richiano, S., Varela, A., Alvarez, M. del P., Bucher, J., Eymard, I., Muravchik, M., Franzese, J., Ariztegui, D., 2019. Digital outcrop modelling using "structure-from- motion" photogrammetry: Acquisition strategies, validation and interpretations to different sedimentary environments. J South Am Earth Sci 96. https://doi.org/10.1016/j.jsames.2019.102325

Bisdom, K., Bertotti, G., Nick, H.M., 2016. The impact of different aperture distribution models and critical stress criteria on equivalent permeability in fractured rocks. J Geophys Res Solid Earth 121, 4045–4063. https://doi.org/10.1002/2015JB012657

Bisdom, K., Gauthier, B.D.M., Bertotti, G., Hardebol, N.J., 2014. Calibrating discrete fracture-network models with a carbonate three-dimensional outcrop fracture network: Implications for naturally fractured reservoir

modelling. Am Assoc Pet Geol Bull 98, 1351–1376. https://doi.org/10.1306/02031413060

Bisdom, K., Nick, H.M., Bertotti, G., 2017. An integrated workflow for stress and flow modelling using outcrop-derived discrete fracture networks. Comput Geosci 103, 21–35. https://doi.org/10.1016/j.cageo.2017.02.019

Catto, B., Jahnert, R.J., Warren, L.V., Varejao, F.G., Assine, M.L., 2016. The microbial nature of laminated limestones: Lessons from the Upper Aptian, Araripe Basin, Brazil. Sediment Geol 341, 304–315. https://doi.org/10.1016/j.sedgeo.2016.05.007

Celestino, M.A.L., Miranda, T.S. de, Mariano, G., Alencar, M. de L., Carvalho, B.R.B.M. de, Falcão, T. da C., Topan, J.G., Barbosa, J.A., Gomes, I.F., 2020. Fault damage zones width: Implications for the tectonic evolution of the northern border of the Araripe Basin, Brazil, NE Brazil. J Struct Geol 138. https://doi.org/10.1016/j.jsg.2020.104116

Celestino, M.A.L., Miranda, T.S., Mariano, G., Alencar, M.L., Buckman, J., Roberts, N.M.W., Barbosa, J.A., Neumann, V.H.M.L., Braz Souza, J.A., Roemers-Oliveira, E., 2021. Structural control and geochronology of Cretaceous carbonate breccia pipes, Crato Formation, Araripe Basin, NE Brazil. Mar Pet Geol 132. https://doi.org/10.1016/j.marpetgeo.2021.105190

Cooke, M.L., Simo, J.A., Underwood, C.A., Rijken, P., 2006. Mechanical stratigraphic controls on fracture patterns within carbonates and implications for groundwater flow. Sediment Geol 184, 225–239. https://doi.org/10.1016/j.sedgeo.2005.11.004

Corlett, H., Hodgetts, D., Hirani, J., Rotevatn, A., Taylor, R., Hollis, C., 2021. A geocellular modelling workflow for partially dolomitized remobilized carbonates: An example from the Hammam Faraun Fault block, Gulf of Suez, Egypt. Mar Pet Geol 126. https://doi.org/10.1016/j.marpetgeo.2020.104831

Corniello, A., Ducci, D., Ruggieri, G., Iorio, M., 2018. Complex groundwater flow circulation in a carbonate aquifer: Mount Massico (Campania Region, Southern Italy). Synergistic hydrogeological understanding. J Geochem Explor 190, 253–264. https://doi.org/10.1016/j.gexplo.2018.03.017

Cottereau, N.; Garcia, M.H.; Gosselin, O.R.; Vigier, L., 2010. Effective Fracture Network Permeability: Comparative Study of Calculation Methods. Presented at the SPE EUROPEC/EAGE Annual Conference and Exhibition, Barcelona, Spain, 14–17 June; pp. 1–31.

Fabin, C.E., Correia Filho, O.J., Alencar, M.L., Barbosa, J.A., de Miranda, T.S., Neumann, V.H., Gomes, I.F., de Santana, F.R., 2018. Stratigraphic relations of the Ipubi formation: Siliciclastic-evaporitic succession of the Araripe basin. An Acad Bras Cienc 90, 2049–2071. https://doi.org/10.1590/0001-3765201820170526

Ferrill, D.A., Morris, A.P., McGinnis, R.N., Smart, K.J., Wigginton, S.S., Hill, N.J., 2017. Mechanical stratigraphy and normal faulting. J Struct Geol 94, 275–302. https://doi.org/10.1016/j.jsg.2016.11.010

Fisher, R., 1953. Dispersion on a sphere. Royal Society of London 217, 295–305.

Ganade de Araujo, C.E., Weinberg, R.F., Cordani, U.G., 2014a. Extruding the Borborema Province (NE-Brazil): A two-stage Neoproterozoic collision process. Terra Nova 26, 157–168. https://doi.org/10.1111/ter.12084

Gapillou, C., Thibeau, S., Mouronval, G., Lescanne, M., 2009. Building a geocellular model of the sedimentary column at Rousse CO2 geological storage site (Aquitaine, France) as a tool to evaluate a theorical maximum injection pressure, in: Energy Procedia. pp. 2937–2944. https://doi.org/10.1016/j.egypro.2009.02.069

Giuffrida, A., Agosta, F., Rustichelli, A., Panza, E., La Bruna, V., Eriksson, M., Torrieri, S., Giorgioni, M., 2020. Fracture stratigraphy and DFN modelling of tight carbonates, the case study of the Lower Cretaceous carbonates exposed at the Monte Alpi (Basilicata, Italy). Mar Pet Geol 112. https://doi.org/10.1016/j.marpetgeo.2019.104045

Giuffrida, A., La Bruna, V., Castelluccio, P., Panza, E., Rustichelli, A., Tondi, E., Giorgioni, M., Agosta, F., 2019. Fracture simulation parameters of fractured reservoirs: Analogy with outcropping carbonates of the Inner Apulian Platform, southern Italy. J Struct Geol 123, 18–41. https://doi.org/10.1016/j.jsg.2019.02.007

Graham Wall, B.R., Girbacea, R., Mesonjesi, A., Aydin, A., 2006. Evolution of fracture and fault-controlled fluid pathways in carbonates of the Albanides

fold-thrust belt. American Association of Petroleum Geologists Bulletin 90, 1227–1249. https://doi.org/10.1306/03280604014

Guerriero, V., Vitale, S., Ciarcia, S., Mazzoli, S., 2011. Improved statistical multi-scale analysis of fractured reservoir analogues. Tectonophysics 504, 14–24. https://doi.org/10.1016/j.tecto.2011.01.003

Healy, D., Rizzo, R.E., Cornwell, D.G., Farrell, N.J.C., Watkins, H., Timms, N.E., Gomez-Rivas, E., Smith, M., 2017. FracPaQ: A MATLAB™ toolbox for the quantification of fracture patterns. J Struct Geol 95, 1–16. https://doi.org/10.1016/j.jsg.2016.12.003

Heimhofer, U., Ariztegui, D., Lenniger, M., Hesselbo, S.P., Martill, D.M., Rios-Netto, A.M., 2010. Deciphering the depositional environment of the laminated Crato fossil beds (Early Cretaceous, Araripe Basin, North-eastern Brazil). Sedimentology 57, 677–694. https://doi.org/10.1111/j.1365-3091.2009.01114.x

Khelifa, C., Zeddouri, A., Djabes, F., 2014. Influence of natural fractures on oil production of unconventional reservoirs, in: Energy Procedia. Elsevier Ltd, pp. 360–367. https://doi.org/10.1016/j.egypro.2014.06.043

Klimczak, C., Schultz, R.A., Parashar, R., Reeves, D.M., 2010. Loi cubique et corrélation ouverture-longueur: Application à l'écoulement d'un fluide à l'échelle du réseau. Hydrogeol J 18, 851–862. https://doi.org/10.1007/s10040-009-0572-6

Korneva, I., Cilona, A., Tondi, E., Agosta, F., Giorgioni, M., 2015. Characterisation of the permeability anisotropy of cretaceous platform carbonates by using 3D Fracture modelling: The case study of Agri Valley fault zones (Southern Italy). Italian Journal of Geosciences 134, 396–408. https://doi.org/10.3301/IJG.2014.26

Kraft Ronaldo Paulo, 2004. Integração de dados de poços e afloramentos para a caracterização de arenitos fraturados-estudo de caso nos arenitos Vila Velha. Universidade Federal do Paraná. Dissertação de Mestrado, 179p

Lander, R.H., Larese, R.E., Bonnell, L.M., 2008. Toward more accurate quartz cement models: The importance of euhedral versus noneuhedral growth rates. American Association of Petroleum Geologists Bulletin 92, 1537–1563. https://doi.org/10.1306/07160808037

Laubach, S.E., Olson, J.E., Cross, M.R., 2009. Mechanical and fracture stratigraphy. Am Assoc Pet Geol Bull 93, 1413–1426. https://doi.org/10.1306/07270909094

Lei, Q., Latham, J.P., Tsang, C.F., 2017. The use of discrete fracture networks for modelling coupled geomechanical and hydrological behaviour of fractured rocks. Comput Geotech. https://doi.org/10.1016/j.compgeo.2016.12.024

Lepillier, B., Bruna, P.O., Bruhn, D., Bastesen, E., Daniilidis, A., Garcia, Ó., Torabi, A., Wheeler, W., 2020. From outcrop scanlines to discrete fracture networks, an integrative workflow. J Struct Geol 133. https://doi.org/10.1016/j.jsg.2020.103992

Li, Y., Hu, W., Wei, S., Li, L., Zhang, Z., Song, S., 2022. Influence of preexisting discontinuities on hydraulic fracture complexity in a naturally fractured reservoir. Eng Geol 311, 106919. https://doi.org/10.1016/j.enggeo.2022.106919

Long, J.C.S., Remer, J.S., Wilson, C.R., Witherspoon, P.A., 1982. Porous Media Equivalents for Networks of Discontinuous Fractures, Water Resources Research.

Lutome, M.S., Lin, C., Chunmei, D., Zhang, X., Bishanga, J.M., 2022. 3D geocellular modelling for reservoir characterization of lacustrine turbidite reservoirs: Submember 3 of the third member of the Eocene Shahejie Formation, Dongying depression, Eastern China. Petroleum Research 7, 47–61. https://doi.org/10.1016/j.ptlrs.2021.08.005

Lyu, W., Zeng, L., Lyu, P., Yi, T., Dong, S., Wang, S., Xu, X., Chen, H., 2022. Insights into the mechanical stratigraphy and vertical fracture patterns in tight oil sandstones: The Upper Triassic Yanchang Formation in the eastern Ordos Basin, China. J Pet Sci Eng 212, 110247. https://doi.org/10.1016/j.petrol.2022.110247

Martinelli, M., Bistacchi, A., Mittempergher, S., Bonneau, F., Balsamo, F., Caumon, G., Meda, M., 2020. Damage zone characterization combining scan-line and scan-area analysis on a km-scale Digital Outcrop Model: The Qala Fault (Gozo). J Struct Geol 140. https://doi.org/10.1016/j.jsg.2020.104144

Miranda, T.S. de, Barbosa, J.A., Gomes, I.F., Neumann, V.H. de M.L., Santos, R.F.V.C., Matos, G.C. de, Guimarães, L.J. do N., Florêncio, R.Q., Alencar, M.L., 2012. Applying scanline technique to geologicalgeomechanical modelling of fracturing systems in carbonate and evaporite. Boletim Geociências da Petrobras 20, 305–326.

Miranda, T.,S., 2015. Caracterização Geológica e Geomecânica dos Depósitos Carbonáticos e Evaporíticos da bacia do Araripe. Tese de Doutorado, NE Brasil 259p.

Miranda, T., Barbosa, A., Gale, J., Marrett (jsg-Utexas, R., Gomes, I., Neumann, V., Matos, G., Correia, O., Alencar, M., 2014. Natural fracture characterization in Aptian carbonates, Araripe Basin, NE Brazil, Amsterdam RAI.

Miranda, T.S., Santos, R.F., Barbosa, J.A., Gomes, I.F., Alencar, M.L., Correia, O.J., Falcão, T.C., Gale, J.F.W., Neumann, V.H., 2018. Quantifying aperture, spacing and fracture intensity in a carbonate reservoir analogue: Crato Formation, NE Brazil. Mar Pet Geol 97, 556–567. https://doi.org/10.1016/j.marpetgeo.2018.07.019

Miyoshi, T., Elmo, D., Rogers, S., 2018. Influence of data analysis when exploiting DFN model representation in the application of rock mass classification systems. Journal of Rock Mechanics and Geotechnical Engineering 10, 1046–1062. https://doi.org/10.1016/j.jrmge.2018.08.003

Narr, W., Schechter, D.S., Thompson, L.B., 2006. Naturally Fractured Reservoir Characterization.

Nelson, R.A., 2001. Geologic Analysis of Naturally Fractured Reservoirs.

Neumann, V.H., 1999. Estratigrafía, Sedimentología, Geoquímica y Diagénesis de los sistemas lacustres Aptiense – Albienses de la Cuenca de Araripe (NE Brasil). PhD Thesis. Barcelona University 233 p.

Neumann, V.H., Cabrera, L., 1999. Una nueva propuesta estratigrafica para la tectonosecuencia post-rifte de la Cuenca de Araripe, Noroeste de Brasil. In: Bol. 5◦ Simpósio Sobre o Cretáceo do Brasil e 1◦ Simpósio Sobre el Cretácico de América del Sul. Serra Negra-SP. UNESP, Rio Claro, pp. 279–285.

Neves, S.P., Bruguier, O., da Silva, J.M.R., Mariano, G., da Silva Filho, A.F., Teixeira, C.M.L., 2015. From extension to shortening: Dating the onset of the Brasiliano Orogeny in eastern Borborema Province (NE Brazil). J South Am Earth Sci 58, 238–256. https://doi.org/10.1016/j.jsames.2014.06.004

Nielsen, L.H., Mathiesen, A., Bidstrup, T., Vejbñk, O. V, Dien, P.T., Tiem, P. V, 1999. Modelling of hydrocarbon generation in the Cenozoic Song Hong Basin, Vietnam: a highly prospective basin. J Asian Earth Sci 17, 269–294.

Nyberg, B., Nixon, C.W., Sanderson, D.J., 2018. NetworkGT: A GIS tool for geometric and topological analysis of two-dimensional fracture networks. Geosphere 14, 1618–1634. https://doi.org/10.1130/GES01595.1

Ortega, O.J., Marrett, R.A., Laubach, S.E., 2006. A scale-independent approach to fracture intensity and average spacing measurement. American Association of Petroleum Geologists Bulletin 90, 193–208. https://doi.org/10.1306/08250505059

Panza, E., Agosta, F., Rustichelli, A., Zambrano, M., Tondi, E., Prosser, G., Giorgioni, M., Janiseck, J.M., 2016. Fracture stratigraphy and fluid flow properties of shallow-water, tight carbonates: The case study of the Murge Plateau (southern Italy). Mar Pet Geol 73, 350–370. https://doi.org/10.1016/j.marpetgeo.2016.03.022

Panza, E., Agosta, F., Zambrano, M., Tondi, E., Prosser, G., Giorgioni, M., Janiseck, J.M., 2015. Structural architecture and discrete fracture network modelling of layered fractured carbonates (Altamura Fm., Italy). Italian Journal of Geosciences 134, 409–422. https://doi.org/10.3301/IJG.2014.28

Panza, E., Sessa, E., Agosta, F., Giorgioni, M., 2018. Discrete Fracture Network modelling of a hydrocarbon-bearing, oblique-slip fault zone: Inferences on fault-controlled fluid storage and migration properties of carbonate fault damage zones. Mar Pet Geol 89, 263–279. https://doi.org/10.1016/j.marpetgeo.2017.09.009

Parrino, N., Agosta, F., Di Stefano, P., Napoli, G., Pepe, F., Renda, P., 2019. Fluid storage and migration properties of sheared Neptunian dykes. Mar Pet Geol 102, 521–534. https://doi.org/10.1016/j.marpetgeo.2019.01.008

Pérez-Rosales, C., Luna, E., Mexicano, I., Petróleo, D., 2005. Naturally Fractured Reservoirs: How to Estimate Secondary Porosity. SPE International.

Pringle, J.K., Clark, J.D., Westerman, A.R., Stanbrook, D.A., Gardiner, A.R., Morgan, B.E.F., 2001. Virtual Outcrops: 3-D reservoir analogues, Journal of the Virtual Explorer.

Pringle, J.K., Howell, J.A., Hodgetts, D., Westerman, A.R., Hodgson, D.M., 2006. Virtual outcrop models of petroleum reservoir analogues: A review of the current state-of-the-art. First Break. https://doi.org/10.3997/1365-2397.2006005

Racolte, G., 2021. Redes de fraturas discretas baseadas em modelos digitais e virtuais de afloramentos carbonáticos. Universidade do Vale do Rio dos Sinos. Dissertação de Mestrado. 147p.

Rashid, F., Hussein, D., Lawrence, J.A., Ahmed, Z., 2021. Fluid flow and permeability analysis of tight gas carbonate reservoir rocks using fractures and dynamic data. J Nat Gas Sci Eng 90. https://doi.org/10.1016/j.jngse.2021.103894

Rawnsley, K., De Keijzer, ~ M, Wei, L., Bettembourg, S., Asyee, W., Massaferro, J.-L., Swaby, P., Drysdale, D., Boettcher, & D., 2007. Characterizing fracture and matrix heterogeneities in folded Devonian carbonate thrust sheets, Waterton tight gas fields, Western Canada. Geological Society of London 270, 265–279.

Rodríguez, F., Arana-Ortiz, V., Cinco-Ley, H., 2004. Well Test Characterization of Small- and Large-Scale Secondary Porosity in Naturally Fractured Reservoirs. SPE 90287.

Santos, M.G.M., Almeida, R.P., Mountney, N.P., Fragoso-Cesar, A.R.S., 2012. Seismites as a tool in the palaeoenvironmental reconstruction of fluvial deposits: The Cambrian Guarda Velha Formation, southern Brazil. Sediment Geol 277–278, 52–60. https://doi.org/10.1016/j.sedgeo.2012.07.006

Santos, R.F.V.C., Miranda, T.S., Barbosa, J.A., Gomes, I.F., Matos, G.C., Gale, J.F.W., Neumann, V.H.L.M., Guimaraes, L.J.N., 2015. Characterization of natural fracture systems: Analysis of uncertainty effects in linear scanline results. Am Assoc Pet Geol Bull 99, 2203–2219. https://doi.org/10.1306/05211514104

Smeraglia, L., Mercuri, M., Tavani, S., Pignalosa, A., Kettermann, M., Billi, A., Carminati, E., 2021. 3D Discrete Fracture Network (DFN) models of damage

zone fluid corridors within a reservoir-scale normal fault in carbonates: Multiscale approach using field data and UAV imagery. Mar Pet Geol 126. https://doi.org/10.1016/j.marpetgeo.2021.104902

Tavani, S., Granado, P., Corradetti, A., Girundo, M., Iannace, A., Arbués, P., Muñoz, J.A., Mazzoli, S., 2014. Building a virtual outcrop, extracting geological information from it, and sharing the results in Google Earth via OpenPlot and Photoscan: An example from the Khaviz Anticline (Iran). Comput Geosci 63, 44–53. https://doi.org/10.1016/j.cageo.2013.10.013

Terra, J.G.S., Spadini, A.R., França, A.B., Leite, C., Zambonato, E.E., Costa, L., Arienti, L.M., Erthal, M.M., Blauth, M., Franco, M.P., Matsuda, N.S., Goulart, N., Augusto, P., Junior, M., Francisco, R.S., Avila, D., Souza, R.S., De, Tonietto, S.N., Maria, S., 2010. Classificações Clássicas De Rochas Carbonáticas, vol 18. B. Geoci. Petrobras, Rio Janeiro, pp. 9–29.

Wang, X., 2005. Stereological Interpretation of Rock Fracture Traces on Borehole Walls and Other Cylindrical Surfaces. Virginia Polytechnic, Blacksburg.

Underwood, C.A., Cooke, M.L., Simo, J.A., Muldoon, M.A., 2003. Stratigraphic controls on vertical fracture patterns in Silurian dolomite, northeastern Wisconsin. AAPG (Am. Assoc. Pet. Geol.) Bull. 87 (1), 121–142.

Xu, J.C., Zhou, W.X., Li, H.Y., 2023. Efficient production optimization for naturally fractured reservoir using EDFM. Pet Sci. https://doi.org/10.1016/j.petsci.2023.02.007

Zakirov, S.N., Zakirov, E.S., n.d. Pseudo-Horizontal Well: Alternative to Horizontal and Vertical Wells, Canada.

Zhang, Y., Zeng, L., Lyu, W., Sun, D., Chen, S., Guan, C., Tang, L., Shi, J., Zhang, J., 2021. Natural fractures in tight gas sandstones: A case study of the Upper Triassic Xujiahe Formation in Xinchang gas field, Western Sichuan Basin, China. Geol Mag 158, 1543–1560. https://doi.org/10.1017/S001675682100008X

Zhao, J., Fu, Y., Wang, Z., Song, Y., Ren, L., Lin, R., Hu, D., Zhou, X., 2022. Diagnosis model of shale gas fracture network fracturing operation pressure curves. Natural Gas Industry B 9, 448–456. https://doi.org/10.1016/j.ngib.2022.10.003

Zihms, S.G., Miranda, T., Lewis, H., Barbosa, J.A., Neumann, V.H., Souza, J.A.B., Falcão, T.C., 2017. Crato Formation laminites-a representative geomechanical pre-salt analogue?

5 CONSIDERAÇÕES FINAIS

As estruturas sin-sedimentares (SSDS) que ocorrem no intervalo C6 dos laminitos da Formação Crato apresentam grande diversidade e estão associadas a processos de liquefação e fluidização, são elas: *loopbeddings*, falhas sin-sedimentares, laminações convolutas, escape de fluidos, brechas sísmicas e estruturas de sobrecarga. A ocorrência das SSDS destaca-se pela repetição de lâminas deformadas intercaladas com laminações não deformadas, pela falta de contraste litológico entre as laminações, pela alta continuidade lateral das estruturas e pela ocorrência em áreas de grande extensão. Essas evidências sugerem que abalos sísmicos são o gatilho responsável pela deformação das laminações e, consequentemente, pela formação das SSDS. Este trabalho sugere que a ZCPA, que dista em torno de 10km da área de estudo, seja a fonte dos terremotos responsáveis pela criação das SSDS. Durante o início do Albiano, o rif te atlântico sul ainda estava ativo na borda leste da PB e a propagação do stress tectônico ao longo da ZCPA possivelmente causou os terremotos.

Segundo modelos qualitativos usados para estimar a magnitude dos eventos sísmicos necessários para gerar as SSDS, foi estimado que os terremotos que afetaram os depósitos do intervalo C6 dos laminitos da Formação Crato alcançaram valores de magnitude maiores que 6.

Os DFNs em escala de afloramento (1:1) apresentaram valores de porosidade com magnitudes semelhantes, indicando que a capacidade de armazenamento pode não ser afetada pela continuidade vertical das fraturas. Da mesma forma, a permeabilidade equivalente das fraturas, nesta mesma escala, exibiu magnitudes similares em todas as três direções: Kxx, Kyy e Kzz. Isso sugere que, nessa escala de estudo, a continuidade vertical das fraturas não impacta significativamente o fluxo de fluidos.

Os modelos DFNs em escala de reservatório (1:15.000) apresentam comportamentos distintos na porosidade das fraturas. Os modelos construídos

com fraturas de continuidade vertical mostraram magnitudes maiores em comparação com aqueles construídos com fraturas de descontinuidade vertical. Isso indica que o aumento na porosidade das fraturas pode estar associado a zonas de fratura que atingem alturas de dezenas de metros e apresentam boa conectividade. Na mesma escala, a permeabilidade horizontal equivalente de fraturas apresentou valores semelhantes em ambos os modelos nas direções Kxx e Kyy. Isso implica que, nessa escala de estudo, a continuidade vertical das fraturas não impacta significativamente o fluxo de fluidos nas direções horizontais. Por outro lado, os resultados para a permeabilidade vertical equivalente de fraturas (Kzz) mostraram valores maiores nos DFNs que consideraram fraturas verticalmente contínuas. Isso implica que, nessa escala de estudo, a continuidade vertical das fraturas afeta o fluxo de fluidos. Além disso, o maior fluxo na direção vertical (Kzz) em comparação com a direção horizontal pode ser atribuído à existência de caminhos de fluxo preferenciais ao longo de fraturas verticalmente contínuas, o que contribui para uma maior conectividade.

Em relação ao efeito de escala, é possível observar algumas particularidades sobre a permeabilidade equivalente das fraturas. A permeabilidade horizontal mostrou-se ser menos afetada pela continuidade vertical das fraturas; isso pode indicar que as características do fluxo e transporte de fluidos horizontais em um reservatório fraturado podem ser bem representadas por modelos em escala de afloramento. Por outro lado, a permeabilidade vertical equivalente das fraturas mostrou dependência da presença de fraturas contínuas. Isso pode indicar que fraturas verticalmente contínuas intensificam os caminhos preferenciais de fluxo, permitindo um maior movimento vertical dos fluidos.

Pseudopoços, ao desempenharem o papel de *scanlines* de intensidade P10, demonstraram sua eficácia na obtenção de dados tanto em afloramentos quanto de modelos digitais de afloramento. Eles oferecem informações estatísticas e geométricas de grande importância referentes a redes de fraturas e à resistência mecânica das formações rochosas.

De forma geral, os resultados deste trabalho sugerem que a segmentação da rede de fraturas dos laminitos da Formação Crato está relacionada diretamente com a resistência mecânica dos seus estratos.

Para trabalhos futuros sugerimos o estudo da rede de fraturas dos laminitos da Formação Crato como uma oportunidade estratégica para o armazenamento de CO2, visando o comportamento do reservatório e em relação ao CO2 injetado e a rede de fraturas.

REFERÊNCIAS

ALLEN, J.R.L., 1977. The possible mechanics of convolute lamination in graded sand beds. **Journal Geology Society London** 134, 19–31. https://doi.org/10.1144/gsjgs.134.1.0019.

ALMEIDA, F.F.M., HASUI, Y., BRITO NEVES, B.B., FUCK, R.A. 1977. Províncias Estruturais Brasileiras. In: **8° Simpósio de Geologia do Nordeste, Campina Grande**, 6: 363-392.

AKARA, M. E. M.; REEVES, D. M.; PARASHAR, R. 2020. Enhancing fracture-network characterization and discrete-fracture-network simulation with high-resolution surveys using unmanned aerial vehicles. **Hydrogeology Journal**., [S.l.], n. Odling 1997, 2020.

ANDREWS, B. J. 2019. 2019. How do we see fractures? quantifying subjective bias in fracture data collection. **Solid Earth**, [S.l.], v. 10, n. 2, p. 487–516.

ANDERSSON, J. & DVERSTORP, B.. 1987. Conditional simulations of fluid flow in three-dimensional networks of discrete fractures. **Water Resource**, 23 (1987), p. 1876, 10.1029/WR023i010p01876

ANKETEL, J.M., CEGLA, J., DZULYNSKI, S., 1970. On the deformational structures in systems with reversed density gradients. **N. Soc. G´ eol Pologne** 40 (1), 3–30.

ARAÚJO, A. F. L de.. 2020. **Estratigrafia mecânica de laminitos aptianos da bacia do araripe: aplicação à caracterização de reservatórios naturalmente fraturados**. Dissertação de Mestrado. 170p.

ARAÚJO, C.E.G., WEINBERG, R.F., CORDANI, U.G., 2014. Extruding the Borborema Province (NE-Brazil): a two-stage Neoproterozoic collision process. Terra Nova 26, 157-168. Barbarin, B., 1999. A review of the relationships between granitoid types, their origins and their geodynamic environments. **Lithos** 46, 605-626.

AYDIN, A. & BASU, A.. 2005. The Schmidt Hammer in rock Material Characterization. **Engineering Geology**, n. 81, p. 1-14.

ASSINE, M. L. 1992. Análise Estratigráfica da Bacia do Araripe, Nordeste do Brasil. **Revista Brasileira de Geociências**, 22(3): 289-300.

ASSINE, M.L.. 1994. Paleocorrentes e Paleogeografia na Bacia do Araripe, Nordeste do Brasil. **Brazilian Journal of Geology**, 24 (4): 223-232.

ASSINE, M. L. 2007. Bacia do Araripe. **Boletim de Geociências da Petrobras**, 19:371-389.

ASSINE, M. L., PERINOTTO, J. A. J., CUSTÓDIO, M. A., NEUMANN, V. H., VAREJÃO, F. G., MESCOLOTTI, P. C.. 2014. Sequências Deposicionais do Andar Alagoas da Bacia do Araripe, Nordeste do Brasil. **Boletim de Geociências da Petrobras**, Rio de Janeiro, 22:3-28.

BAECHER, G.B.. 1983. Statistical analysis of rock mass fracturing. **Math Geolology**, 15 (1983), pp. 329-348, 10.1007/BF01036074

BALLY, A. W. & SNELSON, S.. 1980. Realms of Subsidence. In: MIAL., A. D. (Ed.) Facts and Principles of World Petroleum occurrence. **Canadian Society of Petroleum Geologist**. Memoir., v.6, n.1, p. 9 – 94

BEURLEN, K., 1962. A Geologia da Chapada do Araripe. **Anais da Academia Brasileira de Ciências**, 34(3): 365-370.

BEURLEN, K., 1963. Geologia e Estratigrafia da Chapada do Araripe. **Congresso Brasileiro de Geologia**, 17:47.

BEURLEN, K. 1971. As Condições Ecológicas e Faciológicas da Formação Santana na Chapada do Araripe (Nordeste do Brasil). **Anais da Academia Brasileira de Ciências**, Rio de Janeiro, 43, 411-415.

BELAYNEH, M., & COSGROVE, J. W.. 2004. **Fracture-pattern variations around a major fold and their implications regarding fracture prediction using limited data: an example from the Bristol Channel Basin**

J.W. COSGROVE, T. ENGELDER (Eds.), Initiation, propagation, and arrest of joints and other fractures, Geological Society, London, **Special Publications**, London (2004), pp. 89-102

BISDOM, K., GAUTHIER, B. D. M., BERTOTTI, G., HARDEBOL, N. J.. 2014. Calibrating discrete fracture-network models with a carbonate three-dimensional outcrop fracture network: Implications for naturally fractured reservoir modeling. **American Association of Petroleum Geologists Bulletin**, v. 98, n. 7, p. 1351-1376.

BRITO NEVES B.B., SANTOS E.J., VAN SCHMUS W.R. 2000. Tectonic History of the Borborema Province. In: Cordani G, Milani E.J., Thomaz Filho A.T., Campos D.A. (Eds.). Tectonic Evolution of South America. **31st International Geological Congress**, Rio de Janeiro, 151–182.

BOUR, O., DAVY, P., DARCEL, C., ODLING, N. 2002. A statistical scaling model for fracture network geometry, with validation on a multiscale mapping of a joint network (Hornelen Basin, Norway) **Journal Geophysic**, 107 (2002), 10.1029/2001JB00017

BURCHETTE, T. P.. 2012. Carbonate Rocks and Petroleum Reservoirs: a Geological Perspective from the Industry. **Geological Society**, London, Special Publications, first published October 16, 2012; doi 10.1144/SP370.14.

CASTRO D.L. & CASTELO BRANCO R.M.G. 1999. Caracterização da Arquitetura Interna das Bacias Rifte do Vale do Cariri (NE do Brasil), com Base em Modelagem Gravimétrica 3-D. **Revista Brasileira de Geofísica**, 17: 129-144.

CATTO, B.. 2015. **Laminitos Microbiais no Membro Crato (Neoaptiano), Bacia do Araripe, Nordeste do Brasil**. Dissertação de Mestrado. 111p.

CATTO, B., JAHNERT, R. J., WARREN, L. V., VAREJÃO, F. G., ASSINE, M. L.. 2016. The Microbial Nature of Laminated Limestones: Lessons from the Upper Aptian, Araripe Basin, Brazil. **Sedimentary Geology** 341: 304-315. Doi: 10.1016/j.sedgeo.2016.05.007.

CUSTÓDIO, M.A., QUAGLIO F., WARREN, L.V., SIMÕES, M.G., FÜRSICH F.T., PERINOTTO, J.A.J., ASSINE M. L., 2017. The transgressive-regressive cycle of the Romualdo Formation (Araripe Basin): Sedimentary archive of the Early Cretaceous marine ingression in the interior of Northeast Brazil, **Sedimentary Geology**, v. 359, p. 1-15. ISSN: 0037-0738. https://doi.org/10.1016/j.sedgeo.2017.07.010.

COIMBRA, J. C., ARAI, M., CARREÑO, A. L., 2006. Biostratigraphy of Lower Cretaceous Microfossils from the Araripe Basin, Northeastern Brazil. **Geobios**, Paris, 35: 687-698.

POLLARD, D. D. & SEGALL, P.. 1987. Theoretical displacements and stresses near fractures in rock: with applications to faults, joints, veins, dikes, and solution surfaces B.K. Atkinson (Ed.), Fracture mechanism of rock, **Academic Press**, San Diego (1987), pp. 277-349

EINSTEIN, H.H. & BAECHER, G.B.. 1983. Probabilistic and statistical methods in engineering geology **Rock Mechanic Rock Engenering**, 16 (1983), pp. 39-72, 10.1007/BF01030217

ELSHERIF, A., GZARA, K., IBRAHIM, H AND KRAFFT, J. 2016. Facies Analysis and Permeability Estimation in Late Cretaceous Giant Carbonate Reservoir using LWD Technology: A Case Study in Sabriyah Field, North Kuwait. Adapted from extended abstract based on oral presentation given at AAPG GEO 2016, **The 12th Middle East Geosciences Conference and Exhibition** March 7-10, 2016, Manama, Bahrain.

ENGELDER, T. & GEISER, P.. 1980. On the use of regional joint sets as trajectories of paleostress fields during the development of the Appalachian Plateau New York. **Journal Geophysic**, 85 (1980), p. 6319, 10.1029/JB085iB11p06319

FABIN, C. E. G. S. O., CORREIA FILHO, O. J., ALENCAR, M. L., BARBOSA, J. A., MIRANDA, T. S., NEUMANN, V. H., GOMES, I. F., RIBEIRO, F. S.. 2017. Stratigraphic Relations of the Ipubi Formation: Siliciclastic-Evaporitic Succession of the Araripe Basin. Anais da Academia Brasileira de Ciencias.

FISHER, R., 1953. Dispersion on a sphere. **Royal Society London** A217 (1130), 295–305.

JARDIM DE SÁ, E. F., VASCONCELOS, P. M., SAADI, A., GALINDO, A. C., LIMA, M. G., & OLIVEIRA, M. J.. 2005. Marcos Temporais para a Evolução Cenozoica do Planalto da Borborema. In: **SBG/Núcleo Paraná, Simpósio Nacional de Estudos Tectônicos**, 10°, Curitiba, Boletim de Resumos Expandidos, 160-162.

GARCIA, X., JULIÀ, J., NEMOCÓN, A.M., NEUKIRCH, M., 2019. Lithospheric thinning under the Araripe Basin (NE Brazil) from a long-period magnetotelluric survey: Constraints for tectonic inversion. **Gondwana Research** 68, 174–184. https://doi.org/10.1016/j.gr.2018.11.013

GIUFFRIDA, A., AGOSTA, F., RUSTICHELLI, A., PANZA, E., LA BRUNA, V., ERIKSSON, M.J., TORRIERI, S., & GIORGIONI, M., 2020. Fracture stratigraphy and DFN modelling of tight carbonates, the case study of the Lower Cretaceous carbonates exposed at the Monte Alpi (Basilicata, Italy). **Marine and Petroleum Geology***, 112*, 104045.

GIUFFRIDA, A., LA BRUNA, V., CASTELLUCCIO, P., PANZA, E., RUSTICHELLI, A., TONDI, E., GIORGIONI, M., AGOSTA, F., 2019. Fracture simulation parameters of fractured reservoirs: Analogy with outcropping carbonates of the Inner Apulian Platform, southern Italy. **Journal of Structural Geology**.

GUERRIERO, V., S. VITALE, S. CIARCIA, S. MAZZOLI, S.. 2011. Improved statistical multi-scale analysis of fractured reservoir analogues: **Tectonophysics**, v. 504, n. 1–4, p. 14–24. Doi: 10.1016/j.tecto.2011.01.003.

HEIMHOFER, U., ARIZTEGUI, D., LENNINGER, M., HESSELBOL, S.P., MARTILL, D., RIOS-NETTO, A.M. 2010. Deciphering the Depositional Environment of the Laminated Crato fossil Beds (Early Cretaceous, Araripe Basin, North-eastern Brazil), **Sedimentology**, 57: 677-694.

IDING, M., RINGROSE, P., 2010. Evaluating the impact of fractures on the performance of the in Salah CO2 storage site. **Journal Greenhouse Gas Control** 4, 242–248. https://doi. org/10.1016/j.ijggc.2009.10.016.

DERSHOWITZ, W.S. & HERDA, H.H.. 1992. Interpretation of fracture spacing and intensity. **33th U.S. symposium on rock mechanism**, Santa Fe (1992), pp. 757-766

HOOKER, J.N., GOMEZ, L.A., LAUBAACH, S.E., GALE, J.F.W., MARRETT, R.. 2012. Effects of diagenesis (cement precipitation) during rocks fracture opening on fracture aperture-size scaling in carbonate rocks. **Geological Socity**, Special Publications,. Doi 10.1144/SP370.9.

HOOKER, J.N, LAUBACH, S.E., MARRETT, R.. 2013. Fracture-aperture size – frequency, spatial distribution, and growth processes in strata-bounded and non-strata-bounded fractures, Cambrian Mesón Group, NW Argentina. **Journal of Structural Geology**, v. 54, p. 54-71.

KHAMFOROUSH, M., SHAMS, K, JEAN-FRANÇOIS THOVERT, ADLER, P.M.. Permeability and percolation of anisotropic three-dimensional fracture networks. **Physical Review, Statistical., Nonlinear, and Soft Matter Physics**, [S.l.], v. 77, n. 5, p. 1–10, 2008.

LA POINTE, P. R. 1988. A method to characterize fracture density and connectivity through fractal geometry. **Journal Rock Mechecanic Mineral Science**, 25, pp. 421-429, 10.1016/0148-9062(88)90982-5

LARSSEN, K., SENGER, K., GRUNDVAG, S., 2020. Fracture characterization in Upper Permian carbonates in Spitsbergen: A workflow from digital outcrop to geo-model. **Marine and Petroleum Geology**, 122, 104703. https://doi.org/10.1016/j.marpetgeo.2020.104703

LAVENU, A. P. C., LAMARCHE, J., TEXIER L., MARIÉ, L., GAUTHIER, B. D. M.. 2015. Background fractures in carbonates: inference on control of sedimentary facies, diagenesis and petrophysics on rock mechanical behavior. Example of the Murge Plateau (southern Italy). **Italy Journal Geosciesce**, v. 134, p. 535-555, 2015. Doi: 10.3301/IJG.2014.58).

LEI, Q.; LATHAM, J. P.; TSANG, C. F.. 2017. The use of discrete fracture networks for modelling coupled geomechanical and hydrological behaviour of fractured rocks. **Computers and Geotechnics**, [S.l.], v. 85, p. 151–176.

LEI, Q. & WANG, X.. 2016. Tectonic interpretation of the connectivity of a multiscale fracture system in limestone. **Geophysic**, 43, pp. 1551-1558, 10.1002/2015GL067277

LONG, J. C. S., REMER, J.S., WILSON, C. R., WITHERSPOON, P. A.. 1985. Porous media equivalents for networks of discontinuous fractures. **Water Resource**, 18 (1982), p. 645, 10.1029/WR018i003p00645

MARTINELLI, M., BISTACCHI, A., MITTEMPERGHER, S., BONNEAU, F., BALSAMO, F., CAUMON, G., MEDA, M.. 2020. Damage zone characterization combining scan-line and scan-area analysis on a km-scale Digital Outcrop Model: The Qala Fault (Gozo). **Journal of Structural Geology***, 140*, 104144.

MARQUES, F.O., NOGUEIRA, F.C.C., BEZERRA, F. H. R., DE CASTRO, D. L.. 2014. The Araripe Basin in NE Brazil: An Intracontinental Graben Inverted to a High-Standing Horst. **Tectonophysics**, 630: 251-264.

MARTILL, D.M., FREY, E., 1998. A New Pterosaur Lagerstätte in N. E. Brazil (Crato Formation, Aptian, Lower Cretaceous): Preliminary Observations. **Oryctos**, 1: 79-85.

MARTÍN-MARTÍN, J. D., GOMEZ-RIVAS E., GÓMEZ-GRAS, D., TRAVÉ, A., AMENEIRO, R., KOEHN, D., AND BONS, P. D. 2017. Activation of Stylolites as Conduits for Overpressured Fluid Flow in Dolomitized Platform Carbonates. **Geological Society**, London, Special Publications, 459.

MARTILL, D.M., LOVERIDGE, R., HEIMHOFER, U., 2007. Halite Pseudomorphs in the Crato Formation (Early Cretaceous, Late AptianeEarly Albian), Araripe Basin, Northeast Brazil: Further Evidence for Hypersalinity. **Cretaceous Research**, 28: 613-620.

MARTILL, D. M., LOVERIDGE, R. F., HEIMHOFER, U.. 2008. Dolomite Pipes in the Crato Formation Fossil Lagerstätte (Lower Cretaceous, Aptian), of Northeastern Brazil. **Cretaceous Research**, 29: 78-86.

MARTINELLI, M., BISTACCHI, A., MITTEMPERGHER, S., BONNEAU, F., BALSAMO, F., CAUMON, G., MEDA, M., 2020. Damage zone characterization combining scan-line and scan-area analysis on a km-scale Digital Outcrop Model: The Qala Fault (Gozo). **Journal of Structural Geology**, 104144. doi:10.1016/j.jsg.2020.104144

MASIHI, M. & KING, P.P.. 2008. Connectivity prediction in fractured reservoirs with variable fracture size: analysis and validation. **SPE**, 13 (2008), pp. 12-15, 10.2118/100229-PA

MATOS, R. M. D. 1992. The Northeast Brazilian Rift System. **Tectonics**, 11(4): 766-791.

MATOS R.M.D. 1999. History of the Northeast Brazilian Rift System: Kinematic Implications for the Break-up Between Brazil and West Africa. In: N.R. Cameron, R.H. Bate, V.S. Clure (eds.). The Oil and Gas Habitats of the South Atlantic. **Geological Society**, London, Special Publication, 153: 55-73.

MAZZULLO, S.J., 2004. Overview of Porosity Evolution in Carbonate Reservoirs. **Kansas Geology Society Bulletim**, 79: 20–28.

MIRANDA, T., S.. 2015. Caracterização Geológica e Geomecânica dos Depósitos Carbonáticos e Evaporíticos da Bacia do Araripe, NE Brasil. Tese de Doutorado. 259p.

MIRANDA, T. S., BARBOSA, J. A., GOMES, I. F., NEUMANN, V. H., SANTOS, R. F. V. C., MATOS, G. C., GUIMARAES, L. J. N., FLORENCIO, R. Q., ALENCAR, M. L.. 2012. Aplicação da Técnica de Scanline à Modelagem Geológica/Geomecânica de Sistemas de Fraturamento nos Depósitos Carbonáticos e Evaporíticos da Bacia do Araripe, NE do Brasil. **Boletim de Geociências da Petrobras**, v. 20, p. 305-326,.

MIRANDA, T., BARBOSA, A., GOMES, I., SOARES, A., SANTOS, R., MATOS, G., MCKINNON, E., NEUMANN, V., MARRETT, R.. 2016. Petrophysics and

Petrography of Aptiian Tight Carbonate Reservoir, Araripe Basin, NE Brazil. **78th EAGE Conference & Exhibition**, Vienna, Austria, 30 May,.

MIRANDA, T., STEPHANIE, G. Z., LEWIS, H., FALCÃO, T., SOUZA, J., BARBOSA, J. A., GOMES, I.. 2018. Fracture-Enhanced Permeability in Tight Carbonate Reservoir Analogue. **AAPG Annual AnnualConvention & Exhibition**, p. 20-23,.

MIRANDA, T.S., MAGALHÃES, J.G., BARBOSA, J.A., CORREIA, O.F., ALENCAR, M. L.. 2014a. Araripe Basin, NE Brazil: A Rift Basin Implanted Over a Previous Pull-Apart System? In: **Atlantic Conjugate Margin Conference**, St Jonh's, Canada.

MIRANDA, T. S., BARBOSA, J. A., GALE, J., MARRETT, R., GOMES, I. F., NEUMANN, V. H., MATOS, G. C., CORREIA FILHO, O. J., ALENCAR, M. L.. 2014. Natural Fracture Characterization in Aptian Carbonates, Araripe Basin, NE Brazil. In: **76th EAGE Conference & Exhibition**, Amsterdam. Abstracts book, 88-92.

MIYOSHI, T.; ELMO, D.; ROGERS, S.. 2018. Influence of data analysis when exploiting DFN model representation in the application of rock mass classification systems. **Journal of Rock Mechanics and Geotechnical Engineering**, [S.l.], v. 10, n. 6, p. 1046–1062.

MORAIS NETO J.M. 1999. **As coberturas sedimentares terciáríàs do interior da Paraíba e Rio Grande do Norte e a génese da Antéclise da Borborema.** Universidade Federal de Ouro Preto, Ouro Preto, Dissertação de Mestrado, 170 p

MOTIE, M. & ASSAREH, M., 2020. CO_2 sequestration using carbonated water injection in depleted naturally fractured reservoirs: A simulation study. **Internacional Journal of Greenhouse Gas Control**, 93. https://doi.org/10.1016/j.ijggc.2019.102893

NEUMANN, V. H. & CABRERA, L. 1999. Una Nueva Propuesta Estratigráfica para la Tectonosecuencia Post-Rifte de la Cuenca de Araripe, Noroeste de Brasil. In: Bol. **5º Simpósio Sobre o Cretáceo do Brasil e 1º Simpósio Sobre el Cretácico de América del Sul**. Serra Negra-SP. UNESP, Rio Claro. Pg. 279-285.

NEUMANN, V. H.. **Estratigrafia, Sedimentologia, Geoquimica y Diagenesis de los Sistemas Lacustres Aptiense-Albienses de la Cuenca de Araripe.** Tese de Doutorado. Universidad di Barcelona, 1999

NEUMANN, V. H. & ASSINE, M. L. 2015. Stratigraphic Proposal to the Post-rift I Tectonic-Sedimentary Sequence of Araripe Basin, Northeastern Brazil. In: **2nd International Congress on Stratigraphy**, Graz, Austria.

NEVES, S.P., 2003. Proterozoic history of the Borborema Province (NE Brazil): correlations with neighboring cratons and Pan-African belts, and implications for the evolution of western Gondwana. **Tectonics** 22, 1031, doi:10.1029/2001TC001352.

NEVES, S. P., BRUGUIER, O., SILVA, J. M. R., BOSCH, D., ALCANTARA, V. C., LIMA, C. M., 2009. The age distributions of detrital zircons in metasedimentary sequences in eastern Borborema Province (NE Brazil): evidence for intracontinental sedimentation and orogenesis? **Precambrian Research** 175, 187-205.

NEVES, S.P., BRUGUIER, O., DA SILVA, J.M.R., MARIANO, G., DA SILVA FILHO, A.F., TEIXEIRA, C.M.L.. 2014. From Extension to Shortening: Dating the Onset of the Brasiliano Orogeny in Eastern Borborema Province (NE Brazil), **Journal of South American Earth Sciences***.* doi: 10.1016/j.jsames.2014.06.004.

NEVES, S. P., MARIANO, G. 1999. Assessing the Tectonic Significance of a Large-scale Transcurrent Shear Zone System: the Pernambuco Lineament, Northeastern Brazil. Journal of Structural Geology, 21: 1369-1383.
Neuwerth, R., Suter, F., Guzman, C.A., Gorin, G.E., 2006. Soft-sediment deformation in a tectonically active area: the Plio-Pleistocene Zarzal Formation in the Cauca valley (Western Colombia). **Sedimentary Geology** 186, 67–88. https://doi.org/10.1016/j.sedgeo.2005.10.009.

NOVAK, A. & EGENHOFF, S., 2019. Soft-sediment deformation structures as a tool to recognize synsedimentary tectonic activity in the middle member of the Bakken Formation, Williston Basin, North Dakota. **Marine and Petroleum Geology** 105, 124–140. https:// doi.org/10.1016/j.marpetgeo.2019.04.012.

NYBERG, B.; NIXON, C. W.; SANDERSON, D. J.. 2018. Networkgt: a gis tool for geometric and topological analysis of two-dimensional fracture networks. **Geosphere**, [S.l.], v. 14, n. 4,p. 1618–1634..

OLIVEIRA, R. G.. 2008. **Arcabouço Geofísico, Isostasia e Causas do Magmatismo Cenozóico da Província Borborema e de Sua Margem Continental**. Tese de Doutorado, Universidade Federal de Rio Grande do Norte, Natal., Brasil.

OLIVEIRA, R.G.; MEDEIROS, W. E de. 2012. Evidences of Buried Loads in the Base of the Crust of Borborema Plateau (NE Brazil) from Bouguer Admittance Estimates. **Journal of South America Earth Sciences**, 37:60-76

OLIVEIRA, D.C., WINDLEY, B.F., ARAÚJO, D.B., 2010. The Neoproterozoic Sergipano orogenic belt, NE Brazil: A complete plate tectonic cycle in western Gondwana. **Precambrian Research** 181, 64-84.

OLSON, J. & POLLARD, D.. 1989. Inferring paloestresses from natural fracture patterns: a new method. **Geology**, 17, pp. 345-348, 10.1130/0091-7613(1989) 017<0345

ORTEGA, O.J., MARRETTT, R.A., LAUBACH, S. E.. 2006. A scale-independent approach to fracture intensity and average spacing measurement. **AAPG Bulletin**, v. 90, n. 2, p. 193–208.

OSÉS, G.L., PETRI, S., VOLTANI, C. G., PRADO, G. M. E. M., GALANTE, D., RIZZUTO, M. A., RUDNITZI, I. D., DILVA, E. P., RODRIGUES, F., RANGEL, E. C., SUCERQUIA, P. A., PACHECO, M. L. A. F.. 2016. Deciphering the Preservation of Fossil Insects: a Case Study from the Crato Member, Early Cretaceous of Brazil. **Scientific Reports**, 7(1): 1468. doi: 10.1038/s41598-017-01563-0.

OWEN, G., MORETTI, M., ALFARO, P., 2011. Recognising triggers for soft-sediment deformation: current understanding and future directions. **Sedimentary Geology** 235, 133–140. https://doi.org/10.1016/j.sedgeo.2010.12.010.

PARRINO, N. et al.. 2019. Fluid storage and migration properties of sheared Neptunian dykes. **Marine and Petroleum Geology**, [S.l.], v. 102, p. 521–534, 2019

PEAULVAST, J. P. & BÉTARD, F., 2015. A History of Basin Inversion, Scarp Retreat and Shallow Denudation: The Araripe Basin as a Keystone for Understanding Long-term Landscape Evolution in NE Brazil. **Geomorphology**, 233: 20-40.

PETIT, P. & MATTAUER, M.. 1995. Palaeostress superimposition deduced from mesoscale structures in limestone: the Matelles exposure, Languedoc, France. **Journal Structural Geology**, 17 (1995), pp. 245-256, 10.1016/0191-8141(94)E0039-2

PONTE, F. C. & APPI, C. J. 1990. Proposta de Revisão da Coluna Litoestratigráfica da Bacia do Araripe. In: **Congresso Brasileiro de Geologia**, 36, Natal., Anais, Natal., SBP. 211-226.

PONTE F.C. & PONTE FILHO F.C. 1996. Estrutura Geológica e Evolução Tectônica da Bacia do Araripe. Recife, **DNPM**, 68 p.

PRIEST, S.D. & HUDSON, J.A.. 1981. Estimation of discontinuity spacing and trace length using scanline surveys. **International Journal Rock Mechenic Mineral Science**, 18 (1981), pp. 183-197. http://dx.doi.org/16/0148-9062(81)909736

RACOLTE, R.. 2021. **Redes de fraturas discretas baseadas em modelos digitais e virtuais de afloramentos carbonáticos**. Dissertação de Mestrado. 100 pg

SALVINI, R., MASTROROCCO, G., SEDDAIU, M., ROSSI, D., VANNESCHI, C. 2017. The use of an unmanned aerial vehicle for fracture mapping within a marble quarry (Carrara, Italy): photogrammetry and discrete fracture network modelling. *Geomatics, Natural Hazards and Risk, 8*, 34 - 52. Sanderson, D. J., and Nixon, C. W., 2015, The use of topology in fracture network characterization: **Journal of Structural Geology**, v. 72, p. 55-66.

SANDERSON, D. J., AND NIXON, C. W., 2018, Topology, connectivity and percolation in fracture networks: **Journal of Structural Geology**, v. 115, p. 167-177.

SANTOS, T.J.S., FETTER, A.H. AND NOGUEIRA NETO, J.A., 2008. Comparisons between the northwestern Borborema Province, NE Brazil, and the southwestern Pharusian Dahomey Belt, SW Central Africa. **Geological Society**, London, Special Publications 294, 101-119.

SANTOS, R. F. V. C., MIRANDA, T.S., BARBOSA, J.A., GOMES, I.F., MATOS, G.C., GALE, J., NEUMANN, V.H., GUIMARÃES, L.J. 2015. Characterization of Natural Fracture Systems: Analysis of Uncertainty Effects in Linear Scanline Results. **AAPG Bulletin**, 99(12): 2203-2219. doi: 10.1306/05211514104

SAVASTANO, V.L.M., SCHMITT, R.S., ARAÚJO, M.N.C., INOCÊNCIO, L.C.. 2017. Rift brittle deformation of SE-Brazilian continental margin: Kinematic analysis of onshore structures relative to the transfer and accommodation zones of southern Campos Basin. **Journal of Structural Geology**, v. 94, p. 136-153, 2017.

SEGALL, P. & POLLARD, D.D.. 1983. Joint formation in granitic rock of the Sierra Nevada. **Geology Society America Bulletim**, 94 , p. 563, doi:10.1130/0016-7606

SHANMUGAM, G., 2016. The seismite problem. **Palaeogeography**. 5, 318–362. https://doi. org/10.1016/j.jop.2016.06.002.

SILVA, A. L. & NEWMANN, V.H.. 2002. Estratigrafia Física e Deformação do Sistema Lacustre Carbonático Aptiano-Albiano da Bacia do Araripe. **Boletim do 2º Workshop PRH-ANP/MCT dos Programas de Formação de Recursos Humanos para o Setor de Petróleo e Gás da UFPE**. Recife, p. 15-18.

SILVA, A. L.; NEUMANN, V. H.; CABRERA, L. Fácies. 2002. Carbonáticas Laminadas da Formação Crato (Aptiano), Bacia do Araripe: Litofácies, Microfácies e Microestruturas. In: **6º Simpósio Sobre o Cretáceo do Brasil e 3º Simpósio Sobre el Cretácico de América Del Sur**. São Pedro-SP. UNESP, Rio Claro, p. 37-41.

SMALL, H. L.. 1913. Geologia e Suprimento de Água Subterrânea no Ceará e Parte do Piauí. **Publicação Inspetoria de Obras Contra Secas**, 25:1-80.

SMERAGLIA L, MERCURI M, TAVANI S, PIGNALOSA A, KETTERMANN M, BILLI A, CARMINATI, E.. 2021. 3D Discrete Fracture Network (DFN) models of damage zone fluid corridors within a reservoir-scale normal fault in carbonates: multiscale approach using field data and UAV imagery. **Marine and Petroleum Geology**, 126:104902

STEER, P., BIGOT, A., CATTIN, R., SOLIVA, R.. 2011. In-situ characterization of the effective elasticity of a fault zone and its relationship to fracture spacing. **Journal of Structural Geology**, v. 33, p. 1541-1553,.

TAVANI, S.; GRANADO, P; CORRADETTI, A.; GIRUNDO, M.; IANNACE, A.; ARBUÉS, P.; MUÑOZ, J.A.; MAZZOLI, S.. 2014. Building a virtual outcrop, extracting geological information from it, and sharing the results in Google Earth via OpenPlot and Photoscan: An example from the Khaviz Anticline (Iran). **Computer & Geosciences**, v. 63, p. 44-53.

VAUCHEZ. A., NEVES, S., CABY, R., CORSINI, M., EGYDIO-SILVA, M., ARTHAUD, M., AMARO, V.. 1995. The Borborema Shear Zone System, NE Brazil, 1995. **Journal of South American Earth Science**, 8: 247-266.

VALLE, L.M.; GRIMA, C.; RODRIGUEZ, R.; Llopis, C., 2020. Effect of scCO2-brine mixture on injectivity and storage capacity in rock samples of naturally fractured carbonate formations. **Journal of Natural Gas Science and Engineering**, 81, 103482

VILLARREAL, C. A., ROJAS, J. D., RIOS, C. A., 2020. 3D digital outcrop modelling of the Lower Cretaceous Los Santos Formation sandstones, Mesa de Los Santos region (Colombia): Implications for structural analysis. ***Journal of Structural Geology****, 104214.* doi:10.1016/j.jsg.2020.104214

VILES, H., GOUDIE, A., GRAB, A., LALLEY, J.. 2011. The Use of the Schmidt Hammer and Equotip for Rock Hardness Assessment in Geomorphology and Heritage Science: A Comparative Analysis. **Earth Surface Process Landforms**, v. 36, p. 320-333.

VOLLGER, S. A. & CRUDEN, A.R.. 2016. Mapping fold and fractures in basement and cover rocks using UAV photogrammetry, Cape Liptrap and Cape Paterson, Victoria, Australia. **Journal of Structural Geology**, v. 85, p. 168-187, 2016.

WANG, X.. 2005. **Stereological interpretation of rock fracture traces on borehole walls and other cylindrical surfaces**. Faculty of the Virginia Polytechnic Institute and State Unversity, [S.l.], p. 113.

WATKINS, H., BOND, C.E., HEALY, D., & BUTLER, R.W. 2015. Appraisal of fracture sampling methods and a new workflow to characterise heterogeneous fracture networks at outcrop. **Journal of Structural Geology***, 72*, 67-82.

WENNBERG, O. P., CASINI, G., JONOUD, S., PEACOCK, D. C.P.. 2016. The characteristics of open fractures in carbonate reservoirs and their impact on fluid flow: A discussion. **Petroleum Geoscience**, v. 22, n. 1, p. 91–104.

YIN, T. & CHEN, Q.. 2020. Simulation-based investigation on the accuracy of discrete fracturenetwork (DFN) representation. **Computers and Geotechnics**, [S.l.], v. 121, n. August 2019, p. 103487.

ZEEB, C.. 2013. Evaluation of sampling methods for fracture network characterization using outcrops. **AAPG bulletin**, [S.l.], v. 97, n. 9, p. 1545–1566.

ZIHMS, S. G., MIRANDA, T., LEWIS, H., BARBOSA, J. A., NEUMANN, V. H., SOUZA, J. A. B., CRUZ FALCÃO, DA T.. 2017. Crato Formation laminites – a Representative Geomechanical Pre-salt Analogue? **5th Atlantic Conjugate Margins Conference**, Porto de Galinhas, Pernambuco, brazil, 22th – 25th August 2017.